EUROPEAN LABORATORY FOR PARTICLE PHYSICS

CERN-SPSC-2006-034
SPSC-P-330
November 3, 2006

Proposal

Study of Hadron Production in Hadron-Nucleus and Nucleus-Nucleus Collisions at the CERN SPS

By NA49-future Collaboration
http://na49future.web.cern.ch

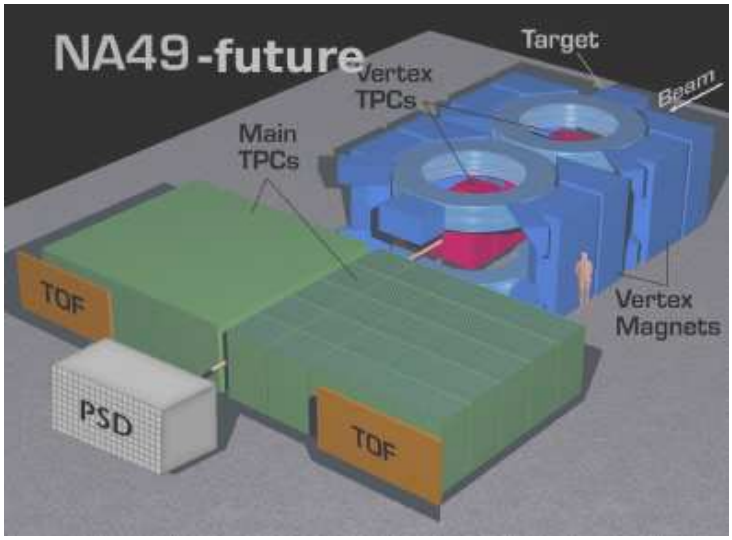

Participating Institutions

University of Athens, Athens, Greece
N. Antoniou, P. Christakoglou, F. Diakonos, A. D. Panagiotou, A. Petridis, M. Vassiliou

University of Bari and INFN, Bari, Italy
F. Cafagna, M. G. Catanesi, T. Montaruli[1], E. Radicioni

University of Bergen, Bergen, Norway
D. Röhrich

KFKI Research Institute for Particle and Nuclear Physics, Budapest, Hungary
L. Boldizsar, Z. Fodor, A. Laszlo, G. Palla, I. Szentpetery, G. Vesztergombi

Cape Town University, Cape Town, South Africa
J. Cleymans

Jagellionian University, Cracow, Poland
J. Brzychczyk, N. Katrynska, R. Karabowicz, Z. Majka R. Planeta, P. Staszel

Joint Institute for Nuclear Research, Dubna, Russia
B. Baatar, V. I. Kolesnikov, A. I. Malakhov, G. L. Melkumov, A. N. Sissakian, A. S. Sorin

Fachhochschule Frankfurt, Frankfurt, Germany
W. Rauch

University of Frankfurt, Frankfurt, Germany
M. Gazdzicki, B. Lungwitz, M. Mitrovski, R. Renfordt, T. Schuster,
C. Strabel, H. Stroebele

University of Geneva, Geneva, Switzerland
A. Blondel, A. Bravar, M. Di Marco

Forschungszentrum Karlsruhe, Karlsruhe, Germany
J. Blumer, R. Engel, A. Haungs, C. Meurer, M. Roth

Świetokrzyska Academy, Kielce, Poland
M. Gazdzicki, R. Korus, St. Mrówczyński, M. Rybczynski, P. Seyboth, G. Stefanek,
Z. Wlodarczyk, A. Wojtaszek

Institute for Nuclear Research, Moscow, Russia
F. Guber, A. Kurepin, A. Ivashkin, A. Maevskaya

LPNHE, University of Paris VI and VII, Paris, France
B. Andrieu, J. Dumarchez

Pusan National University, Pusan, Republic of Korea
K.-U. Choi, J.-H. Kim, J.-G. Yi, I.-K. Yoo

Faculty of Physics, University of Sofia, Sofia, Bulgaria
D. Kolev, R. Tsenov

[1] now at University of Wisconsin, Madison, USA

St. Petersburg State University, St. Petersburg, Russia
A. G. Asryan, D. A. Derkach, G. A. Feofilov, S. Igolkin, A. S. Ivanov, R. S. Kolevatov, V. P. Kondratiev, P. A. Naumenko, V. V. Vechernin

State University of New York, Stony Brook, USA
P. Chung, R. Lacey, A. Taranenko

Institute for Particle and Nuclear Studies, KEK, Tsukuba, Japan
T. Kobayashi, T. Nakadaira, K. Sakashita, T. Sekiguchi

Warsaw University of Technology, Warsaw, Poland
K. Grebieszkow, D. Kikola, W. Peryt, J. Pluta, M. Slodkowski, M. Szuba

University of Warsaw, Warsaw, Poland
A. Aduszkiewicz, W. Dominik, D. Kielczewska, M. Posiadala, E. Skrzypczak

Rudjer Boskovic Institute, Zagreb, Croatia
T. Anticic, K. Kadija, V. Nikolic, T. Susa

spokespersons:
Marek Gazdzicki (marek.gazdzicki@cern.ch) and
Gyorgy Vesztergombi (veszter@rmki.kfki.hu)

the participation of the following groups is under discussion:
-University of Bern, Bern, Switzerland (contact: A. Ereditato),
-INFN Sezione di Milano Bicocca, Milano, Italy (contact: M. Bonesini),
-ETH, Zurich, Switzerland (contact: A. Rubbia)

Contents

1 Introduction and summary

This document presents a proposal of the NA49-future Collaboration to study hadron production in of hadron-proton interactions and nucleus-nucleus collisions at the CERN SPS. It follows the Expression of Interest [1] and the Letter of Intent [2] submitted to the SPS committee in November 2003 and January 2006, respectively.

The proposed physics program consists of three subjects:

- measurements of hadron production in nucleus-nucleus collisions, in particular fluctuations and long range correlations, with the aim to identify the properties of the onset of deconfinement and find evidence for the critical point of strongly interacting matter,

- measurements of hadron production in proton-proton and proton-nucleus interactions needed as reference data for better understanding of nucleus-nucleus reactions; in particular correlations, fluctuations and high transverse momenta will be the focus of this study,

- measurements of hadron production in hadron-nucleus interactions needed for neutrino (T2K) and cosmic-ray experiments (Pierre Auger Observatory and KASCADE).

It is foreseen to take data with proton and pion beams starting from 2007, and with the beams of nuclei (C, Si and In) starting from 2009. The data taking period should end in 2011.
The nucleus-nucleus program has the potential for an important discovery – the experimental observation of the critical point of strongly interacting matter. We intend to carry out for the first time in the history of heavy ion collisions a comprehensive scan in two dimensional parameter space: size of colliding nuclei versus interaction energy. Other proposed studies belong to the class of precision measurements.
The collaboration proposes to perform these measurements by use of the upgraded NA49 apparatus [3]. The most essential upgrades are an increase of data taking and event rate by a factor of 24 and the construction of a projectile spectator detector which will improve the accuracy of determination of the number of projectile spectators by a factor of about 20. The cost of all upgrades and detector maintenance is estimated to be 1.5 MSFR.

Synergy of different physics programs as well as the use of the existing accelerator chain and detectors offer the unique opportunity to reach the ambitious physics goals in a very efficient and cost effective way. Thus the multi-task proposal is considered by the collaboration as a whole and should be treated as such in the CERN decision process. The proposed run schedule is based on the assumption that the proposal is approved not

later than by the end of May.

The NA49 apparatus at the CERN SPS served, during the last 10 years, as a very reliable, large acceptance hadron spectrometer and delivered high precision experimental data over the full range of SPS beams (from proton to lead) [4, 5] and energies (from 20A GeV to 200A GeV) [6, 7]. Among the most important results from this study is the observation [6, 7] of narrow structures in the energy dependence of hadron production in central Pb+Pb collisions. These structures are located at the low CERN SPS energies (30A–80A GeV) and they are consistent with the predictions [8] for the onset of the deconfinement phase transition. The questions raised by this observation serve as a strong motivation for new measurements with nuclear beams in the SPS energy range at the CERN SPS as proposed by us and also envisaged at BNL RHIC [9]. The proposed SPS and RHIC programs are to a large extent complementary mainly due to different collision kinematics: beams on a fixed target at SPS and colliding beams at RHIC.

A report from the Villars meeting on "Fixed-Target Physics at CERN beyond 2005" [10] recognizes that the ion beams at the CERN SPS remain ideal tools to study the features of the phase transition between confined and deconfined states of strongly interacting matter. It notes that an ion program aimed at the identification of the critical point and the study of its properties is likely to be of substantial significance. The NA49-future goals to measure hadron production in hadron-nucleus interactions needed for neutrino and cosmic-ray experiments as well as a search for the critical point in nucleus-nucleus collisions were summarized in the Briefing Book for European Strategy for Particle Physics [11]. Letters supporting the NA49-future physics program are presented in the Appendix.

For the proposal in preparation the NA49 apparatus and two detector prototypes were tested in a 5-day long test run in August 2006 [12]. The performance of the NA49 TPCs has not shown any sign of degradation since the beginning of their operation (1994). In addition, this test clearly demonstrated the ability of the new collaboration to operate the NA49 facility and the feasibility of the proposed concepts of the new detectors.

This document is organized as follows. The physics program and its motivation are discussed in Section 2. The existing NA49 detector and the required upgrades are described in Section 3. In Section 4 the physics performance is discussed. The organization and planning are presented in Section 5.

2 Physics Program

The physics program of the experimental project is presented according to the increasing physics complexity, level of detector upgrades and availability of the SPS beams. It consists of three subjects:

I. measurements of hadron production in hadron-nucleus interactions needed for neutrino (T2K) and cosmic-ray (Pierre Auger Observatory and KASCADE) experiments,

II. measurements of hadron production in proton-proton and proton-nucleus interactions needed as reference data for better understanding of nucleus-nucleus reactions; in particular correlations, fluctuations and high transverse momenta will be the focus of this study,

III. measurements of hadron production in nucleus-nucleus collisions, in particular fluctuations and long range correlations, with the aim to identify the properties of the onset of deconfinement and search for the critical point of strongly interacting matter.

The measurements will be performed in subsequent stages of the experimental program.

In the following all subjects are presented in detail.

2.1 Neutrino and Cosmic-Ray Physics Needs

2.1.1 Neutrino Physics

Physics Issues

The study of neutrino oscillation, or in more general terms, the study of neutrino masses and mixings is at present one of the most challenging topics in neutrino physics [13]. From the recent results of neutrino oscillation and other experiments a clear picture emerges of the phenomenology of neutrino mass and mixing. Mixing between the second and third generation neutrinos are found to be close to maximal, while the one between the first and second is large, but not maximal. For the 1–3 mixing only upper limits are available. Recent experiments indicate unique solutions for the values of the 'atmospheric' mass difference (Δm^2_{23}) and the 'solar' mass difference (Δm^2_{12}) in a range such that there are chances to study CP violation in the neutrino sector in the future, provided the value of θ_{13} is large enough.

High-precision measurements of the other angles will provide insight into the mixing

mechanism. A combination of a new generation of reactor experiments and the long baseline experiments T2K [14] and Nova [15] will address these questions in the near future. The ultimate precision in the measurements of oscillation parameters can be reached by experiments at a neutrino factory. The combination of very intense conventional beams ('super beams') and a 'beta beam' [16], a pure electron(anti)-neutrino beam made by the beta decay of nuclei in a storage ring, can also explore a large range in the parameter space.

As mentioned above, the measurement of the value of θ_{13} is essential to decide if the study of CP violation is within reach at a given facility. A number of experiments are proposed to improve the precision in this parameter. T2K is most probably the first experiment which will probe an entirely new region in this parameter space.

The T2K experiment

The T2K experiment will study oscillations of an off axis neutrino beam between the J-PARC accelerator and the Super-Kamiokande detector [14]. The first phase of the T2K experiment (2009 – 2014) is aimed at a more accurate determination of the *atmospheric* parameters θ_{23} and Δm^2_{23} by measuring the $\nu_\mu \to \nu_x$ disappearance, a measurement of the unknown mixing angle θ_{13} by the observation of the $\nu_\mu \to \nu_e$ appearance signal, and the measurement of neutral current events with more than an order of magnitude better sensitivity compared to any previous experiment.

The neutrino beam is produced from the decays of pions and kaons created in the interactions of the 30 GeV/c J-PARC proton beam on a carbon target. In a second phase the proton beam energy can be increased up to 50 GeV/c. The resulting neutrino flux will be measured in the Super-Kamiokande detector located at a distance of 295 km from the neutrino source. T2K adopts an off axis beam (OAB) configuration, in which the beam axis is displaced by a few degrees from the far detector direction. The OAB method yields a low energy neutrino beam with a narrow energy spectrum and a small high-energy tail. The resulting beam intensity is 3 $\times$ higher compared to a momentum selected on axis beam. By varying the OAB angle the neutrino beam peak energy changes and it can be tuned to the oscillation maximum to maximize the sensitivity to the neutrino oscillation parameters. For the distance of 295 km and $\Delta m^2_{23} \sim 3 \times 10^{-3}$ eV^2 the corresponding peak energy is $\sim$ 0.8 GeV and the angle of the OAB is 2.5 degrees. Figure 1 (left plot) shows the neutrino spectrum as a function of the neutrino energy at the near and far detector locations. A drawback of this method, however, is that the characteristics of the beam change rapidly with angle. Detailed understanding of the beam production and properties are therefore required to minimize the systematic uncertainties.

In a long baseline neutrino oscillation experiment, the neutrino flux is measured in a detector far from the neutrino source (*far* in this context means $L/E \gg 1$, where L is the distance from the source and E the neutrino energy) and compared with a prediction based on the neutrino flux unmodified by oscillations. A deviation in the measured neutrino

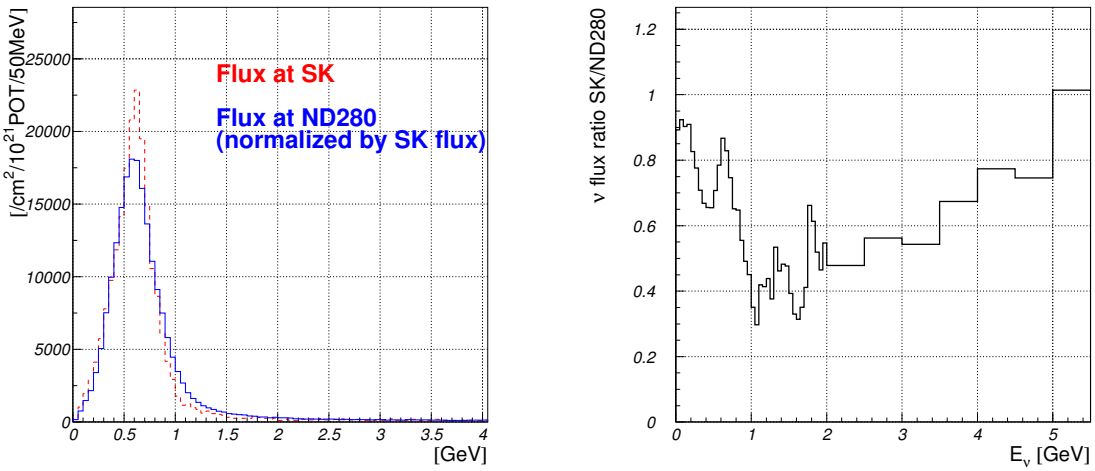

Figure 1: Left: Neutrino fluxes for a 2.5° OAB as a function of neutrino energy E_ν at the near (full line) and the far detector locations (dashed line) predicted by the T2K beam Monte Carlo simulation. The flux peak is shifted to a higher energy in the far detector, which is due to a different solid angle acceptance of the two detectors. Right: the far–to–near flux ratio $\Phi_{\rm far}/\Phi_{\rm near}$.

flux from the predicted one is interpreted as evidence for neutrino oscillation. A well-known technique to predict the neutrino flux at the *far* detector (Super-Kamiokande) is to measure the flux in a *near* detector (ND280 [17]), which intercepts the beam at a distance where the effect of oscillations is negligible. If both detectors are sufficiently far from the neutrino source they will accept the same solid angle. In this case the source can be considered point-like and the ratio of the fluxes in the two detectors is accurately predicted by the squared ratio of the distances from the source and the flux ratio doesn't depend on the neutrino energy. In an ideal case, all systematic uncertainties would cancel out by using the measured spectra in the near detector. In practice, however, the near detector is different from the far detector in terms of solid angle acceptance, materials, and responses. The challenge in understanding the neutrino beam is that only the 'product' of neutrino flux, neutrino cross section and detection efficiency is observable and the details of the production mechanisms of the beam have to be known and understood. The near detector sees the whole length of the pion decay channel under different angles: the closer its location to the decay tunnel the larger the sensitivity to the finite length of the decay tunnel and broader the accepted OAB angle. That leads to a complicated far-to-near spectrum ratio $\Phi_{\rm far}/\Phi_{\rm near}$ shown in Figure 1, right plot. The peak position is shifted to

a higher energy at the far site than at the near site, resulting in a minimum in the flux ratio around 0.6 GeV and the positive slope in the flux ratio up to 1 GeV. Moreover, in the presence of backgrounds, the background subtraction requires the knowledge of the neutrino flux spectrum.

The solution is to understand the beam and the detector responses in detail and correct for the differences. (In a possible second phase an extra detector could be constructed at an intermediate distance, which is sensitive to a neutrino flux with properties much closer to the flux at the far detector.) A beam Monte Carlo is used to predict the neutrino flux unmodified by oscillations at the far detector on the basis of the flux measurements in the near detector. Apart from a full description of the focusing system, the pion production under the conditions of the T2K experiment has to be known with high precision. The current T2K beam Monte Carlo is derived from the K2K beam Monte Carlo. The Monte Carlo is GEANT based and it uses the Calor-Fluka model to describe the beam primary interactions and re-interactions in the target. The uncertainty on the hadro-production cross sections predicted by this model is larger than 20%. Although this Monte Carlo predicted an absolute neutrino flux for K2K with an error better than 20%, the tuning of the beam Monte Carlo to the T2K beam conditions is quite difficult and approximate because of the T2K OAB characteristics.

Since the appearance of electron neutrinos is a key measurement, it is critical to understand the flavor composition of the neutrino beam. ν_e *contamination* of the neutrino is a significant source of background for the ν_e appearance signal and θ_{13} measurement. The subtraction of this background requires a precise prediction of the ν_e energy dependent flux at Super-Kamiokande. The difficulties discussed above for the ν_μ beam, apply also to the ν_e component. The source of the ν_e flux are the decays of kaons (K_{e3} channel), which are the dominant component, and the $\pi \to \mu \to e$ decay chain (see Figure 2, right plot). Therefore, one has to characterize the production of kaons with high accuracy, as well. Note also that the high-energy tail in the ν_μ spectrum originates from kaon decays (see Figure 2).

T2K will not be statistics limited for the ν_μ disappearance measurement. In order to achieve the precision on the neutrino oscillation parameters discussed above, it has been estimated that the far–to–near flux ratio $\Phi_{\rm far}/\Phi_{\rm near}$ has to be known to 2% or better. That requires a high precision measurement of the differential cross section (momentum and polar angle) for pion and kaon production to a 2–3 % level in the phase space and conditions of the T2K beam. For this precision around 500 k fully reconstructed π^+ tracks are required. A similar number of π^- tracks will be required when studying the disappearance of anti-ν_μ's. Likewise, the estimated number of K^+ and K^- tracks needed is around 100 k. The absence of dedicated measurements of hadron production under the specific conditions of the neutrino beam-line introduces a significant systematic error, larger than 10%. For comparison, the error on the flux ratio for the K2K measurement (see later) without dedicated hadro-production measurements was around 7%. Note that there are very few hadron production data available, none in the phase space of the T2K

beam.

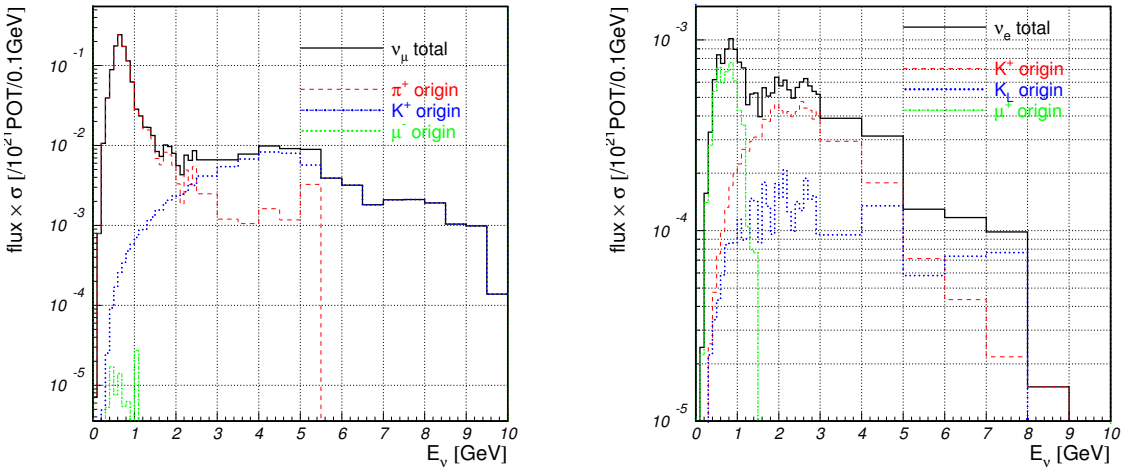

Figure 2: Contributions to the neutrino flux from different parent decays; left: ν_μ parent particle distributions; right: ν_e parent particle distributions. Both plots use the same normalization. The exact composition depends on the relative production cross sections for the parent particles.

HARP Measurement for K2K

The HARP experiment demonstrated that such a precise measurement of the pion yield as a function of momentum and production angle can reduce the component of the experimental uncertainty introduced by the lack of knowledge of the hadron production to a very low level [18, 22, 21]. The HARP measurement was performed for the K2K beam, which is produced by a 12.9 GeV/c proton beam impinging on an aluminum target. Note that the latest K2K publication [22] uses the HARP data. That resulted in the reduction of the systematic error by a factor of two.

The HARP-based prediction has been obtained by substituting the original π^+ production cross-section assumed in the K2K beam Monte Carlo hadronic model with the HARP Sanford-Wang parameterization. All other ingredients of the K2K beam Monte Carlo simulation, such as primary beam optics, pion re-interactions in the aluminum target, pion focusing, pion decay, etc. were not changed. The Sanford-Wang parameterization [19] of the experimental results provides a smooth extrapolation into regions where no measurements are available.

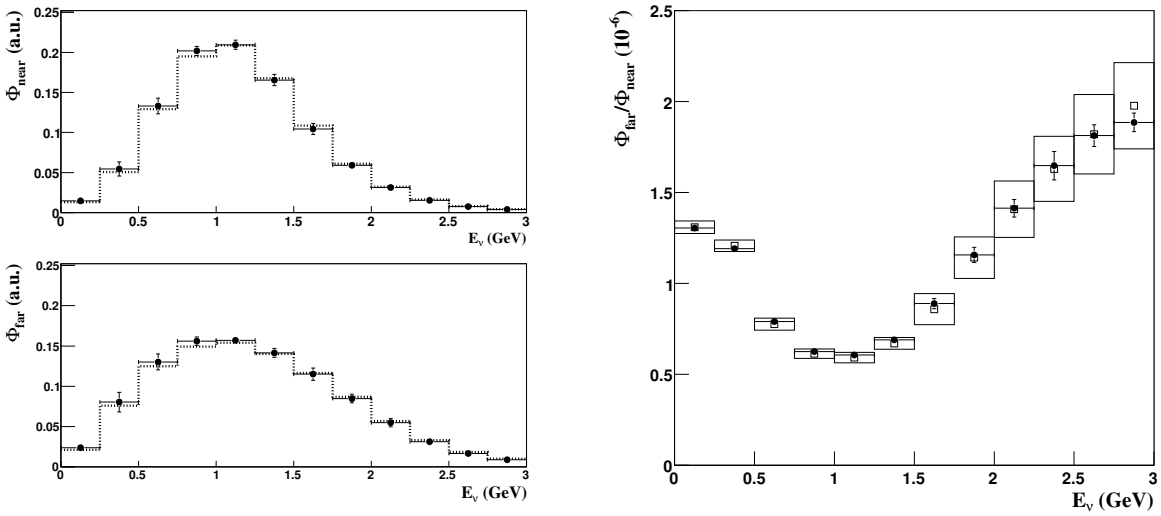

Figure 3: Muon neutrino fluxes in the K2K experiment as a function of neutrino energy E_ν, as predicted by the default hadronic model assumptions in the K2K beam Monte Carlo simulation (dotted histograms), and by the HARP π^+ production measurement (full circles with error bars). The left panel shows unit-area normalized flux predictions at the K2K near (top) and far (bottom) detector locations, $\Phi_{\rm near}$ and $\Phi_{\rm far}$, respectively, while the right panel shows the far–to–near flux ratio $\Phi_{\rm far}/\Phi_{\rm near}$ (empty squares with error boxes show K2K model results). On average, the errors on the flux ratio predicted using the HARP measurement are 2 $\times$ smaller.

The result of the calculation for the K2K beam is shown in Fig. 3. The left panel shows muon neutrino fluxes in the K2K experiment as a function of neutrino energy E_ν, as predicted by the default hadronic model assumptions in the K2K beam Monte Carlo simulation (dotted histograms), and by the HARP π^+ production measurement (full circles). The plots on that panel show unit-area normalized flux predictions at the K2K near (top) and far (bottom) detector locations, $\Phi_{\rm near}$ and $\Phi_{\rm far}$, respectively. The right panel shows the far–to–near flux ratio $\Phi_{\rm far}/\Phi_{\rm near}$ obtained from the K2K Monte Carlo (empty squares with error boxes) and from the HARP measurement (full circles with error bars). The fluxes predicted using the HARP measurement and the K2K model are in good agreement within the errors. This is reflected also in a good agreement in the flux ratios, in particular in the oscillation region (below 1.5 GeV). The error on $\Phi_{\rm far}/\Phi_{\rm near}$ propagating the uncertainties of the HARP measurement is less than 4% [22]. It should be noted however, that part of this uncertainty is also associated with additional uncertainties in the flux calculations. The uncertainty from the HARP measurement itself is 2%. The systematic error attached to $\Phi_{\rm far}/\Phi_{\rm near}$ in the previous K2K analysis was of

the order of 7% [20]. It clearly shows the considerable improvement that was achieved by K2K by using this new measurement.

The recent HARP results are compared in Figure 4 with the collection of π^+ production data from aluminum targets available in the literature prior to the HARP measurement [23, 24, 25, 26]. The comparison is restricted to proton beam momenta between 10 and 15 GeV/c (close to the K2K beam momentum of 12.9 GeV/c), and for pion polar angles below 200 mrad (the range measured by HARP and of relevance to K2K). In order to match pion momenta and angles measured in the different experiments the comparison is based on the HARP Sanford-Wang parameterization. A correction to rescale the HARP Sanford-Wang parameterization at 12.9 GeV/c beam momentum to the momenta in the range 10 GeV/c–15 GeV/c beam momenta of the other Al datasets is applied [27]. Figure 4 shows that it is of enormous importance to measure the full phase-space in a single experiment to avoid the relatively large systematic normalization errors between the different experiments.

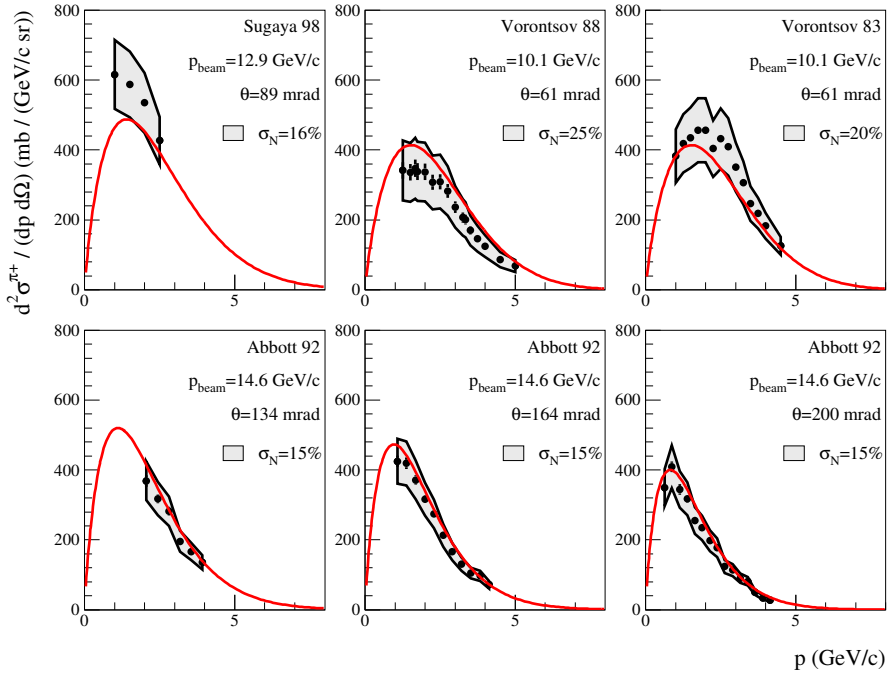

Figure 4: Comparison of the double-differential pion production cross section measured in HARP, and the one measured in past experiments using an aluminum target and 10-15 GeV/c momentum beam protons. The points are the data from the experiments prior to HARP, and the shaded area reflect their normalization uncertainty. The solid line is the HARP Sanford-Wang parameterization rescaled to the beam momentum of past experiments, as discussed in the text.

NA49-future and T2K

Several opportunities to measure the pion and kaon yields for the beam-line of the T2K experiment have been explored: the COMPASS experiment at CERN, the MIPP experiment at Fermilab, and the NA49-future experiment at CERN. The most promising option is the use of the upgraded NA49 detector.

Monte Carlo studies of the NA49 acceptance have shown that this detector has the acceptance and the particle ID capabilities needed for this measurement. The performance of the NA49 detector will be described later in section 4.1. Figure 5 shows the p vs θ distribution of hadrons, which contribute to the neutrino flux in the T2K detectors. Here p and θ are the momentum and polar angle of the outgoing hadrons at their production point, respectively. The relevant π^+ phase space is peaked at low momenta and large angles; momenta as low as 1 GeV/c and angles up to 300 mrad are of interest. The phase space for kaons is shifted to higher momenta and smaller angles due to the characteristics of the beam-line and different lifetimes of the hadrons. In order to avoid too large extrapolations into the unmeasured regions one has to cover all this phase space. The particle ID is crucial over the whole momentum range, since the beam model is sensitive to the relative (ν_μ disappearance) and absolute (ν_e disappearance) kaon content. Particle ID will be based mainly on the ToF measurements.

In order to achieve full coverage of the relevant phase space region (see Figure 5), different configurations of the NA49 apparatus have to be used. At present two settings for the magnetic fields are considered, one with lower fields for the lower momenta and one with higher fields for the larger momenta; and two different locations for the target, upstream of the vertex TPCs and between the vertex TPCs. That is mainly due to the limited acceptance of the existing ToF system. More details are given in section 4.1. A possible extension of the ToF coverage is also under study. The advantage would be that the whole phase space of the T2K beam is covered with one configuration of NA49 only.

Physics Needs

Initially, the T2K beam-line will be operated with 30 GeV/c protons, while upgrades to 40 GeV/c and 50 GeV/c are foreseen. It is planned to use a carbon production target. The first data set will be taken with a 90 cm long carbon target (same length as in T2K). The use of the whole T2K target, including the structure surrounding the target, is also under study. Data with targets of various thicknesses (up to one $\lambda_{\rm I}$) will be needed to control the simulation of secondary interactions, including a thin target (few percent of $\lambda_{\rm I}$) to measure the primary p–C hadron production cross-section. For each configuration (target length and incident proton beam energy) a data set of 500 k π^+'s and π^-'s in the T2K beam phase space will be required. This data sample will include also about 100 k K^+ and K^- tracks.

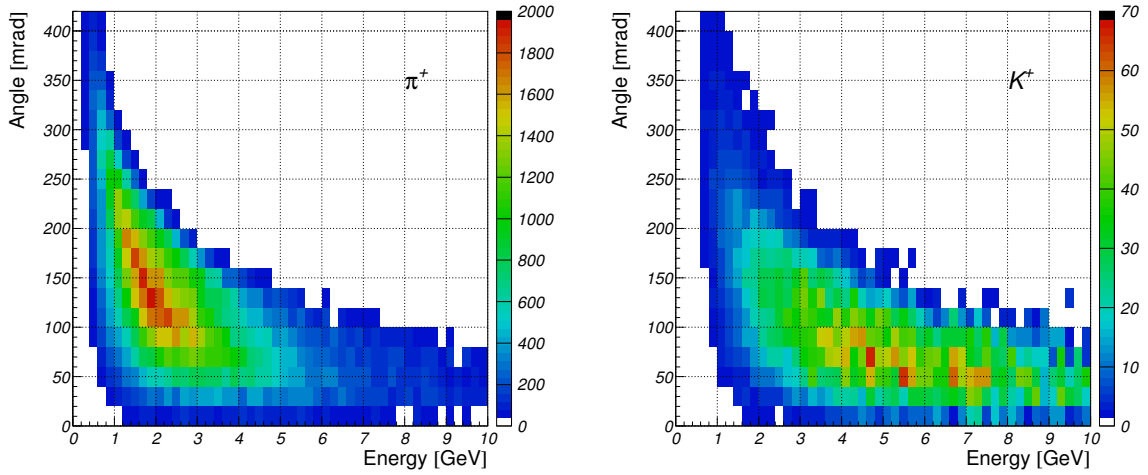

Figure 5: p vs. θ distribution of π^+ mesons (left) and K^+ mesons (right) that contribute to the neutrino flux in the T2K detectors. Here p and θ are the momentum and polar angles at the production point, respectively.

2.1.2 Cosmic-Ray Physics

Physics Questions and Problems

One of the central questions of astroparticle physics is that of the sources and propagation of cosmic rays. Even more than 90 years after the discovery of cosmic rays we still don't know their elemental composition at high energy and also the information on the energy spectrum is very limited [28, 29]. Knowing how the elemental composition of cosmic rays changes with energy is the key information needed for understanding phenomena such as the *knee* – a change in the power-law index of the cosmic ray flux at about 3×10^6 GeV – and the transition from galactic to extra-galactic cosmic rays in the region around 10^9 GeV. Furthermore, composition information is essential for confirming or ruling out models proposed for the sources of ultra-high energy cosmic rays, many of which postulate new particle physics [30].

At energies above 10^5 GeV, the flux of cosmic rays is so low that it cannot be measured directly using particle detectors. Therefore all cosmic-ray measurements of higher energy are based on analyzing secondary particle showers, called extensive air showers, which they produce in the atmosphere of the Earth. To interpret the characteristics of extensive air showers in terms of primary particle type and energy, detailed modeling of the various interaction and decay processes of the shower particles is needed [31]. Modern

high-precision experiments like KASCADE [32] and the Pierre Auger Observatory [33] measure several observables for each shower. The uncertainty in interpreting the data from these experiments is dominated by the uncertainty in predicting hadronic multi-particle production in extensive air showers.

For example, the KASCADE Collaboration use the measured number of electrons and muons at detector level to derive the primary energy and composition of the showers in the knee energy region. Having collected more than 40 million showers it is still not possible to obtain a clear picture of the elemental composition. Applying different hadronic interaction models leads to significantly different fluxes for the elemental groups considered in the analysis [34]. In particular, the fundamental question of having a mass- or rigidity-dependent scaling of the knee positions of the individual flux components cannot be answered.

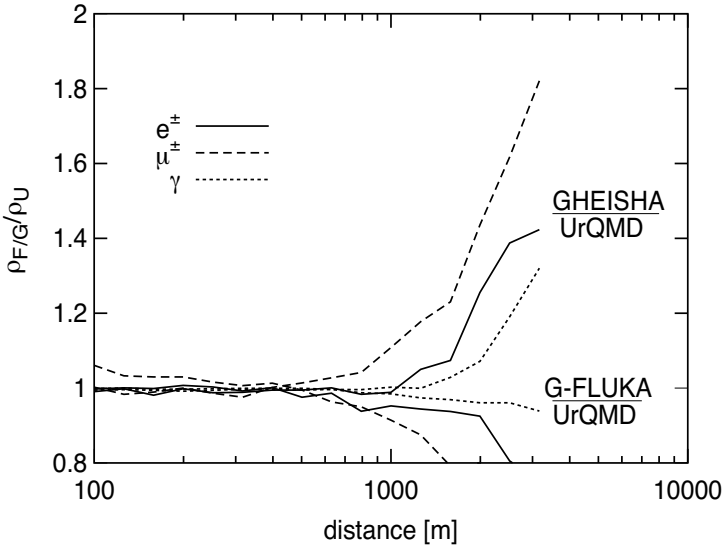

Figure 6: Relative change of the lateral distribution of particles (electrons, photons and muons) in vertical, proton-induced showers of 10^{10} GeV. Interactions at laboratory energies below 80 GeV were simulated with the models G-FLUKA [35], UrQMD [36], and GHEISHA [37]. The model QGSJET [38] was used for simulating high energy interactions. Shown is the ratio of the particle densities relative to the prediction of UrQMD. (from [39])

The dependence on modeling hadronic interactions is also clearly demonstrated by the fact that the Pierre Auger Collaboration finds indications of a 25% discrepancy of the energy that would be assigned to a shower by using either only the Auger surface detector data or the calorimetric measurement of the Auger fluorescence telescopes [40]. In addition, any composition analysis will be hampered by the uncertainty of simulating hadronic interactions. For example, the slope of the lateral distribution of particles in a

shower is a measure of the mass of the primary particle. This slope, however, is also very sensitive to assumptions on hadronic multi-particle production in the energy range up to a few hundred GeV, see Fig. 6.

In the foreseeable future soft multi-particle production will not be calculable within QCD. Therefore the modeling of cosmic-ray interactions will continue to depend strongly on the input from accelerator experiments that is needed to tune phenomenological particle production models.

Role of low-energy hadron production in air showers

Often only the dependence of extensive air shower predictions on the characteristics of hadronic interactions at high energy is considered [41]. Only recently it has been realized that interactions in the energy range up to a few hundred GeV also give rise to large uncertainties. This applies in particular to shower particles measured at large lateral distance from the shower core, as is the case in air shower arrays [42, 43].

In the following we illustrate the role of low-energy interactions by considering muon production in extensive air showers [44]. It should be kept in mind that the ratio of muon to electron numbers in a shower is one of the best composition-sensitive observables. The simulations are done for proton showers of 10^6 GeV but the results apply also to showers of higher energy and other hadronic primary particles. The competing processes of pion interaction and decay in an air shower lead to a relatively energy-independent typical energy below which pions decay and produce muons.

In Fig. 7 (left) the energy distribution of hadronic interactions, in which at least one meson was produced that in turn decayed to a muon that reached sea level, is shown. The maximum of the energy distribution falls in the range between 80 and 200 GeV. Most of the interactions are induced by pions (70%) and nucleons (20%). The shortcomings of the simulation of hadronic interactions are clearly visible as a discontinuity between the energy region of the high- and low-energy models applied in this simulation.

The rapidity distribution of secondary particles, measured relative to the rapidity of the particle that initiated the interaction ($y_{\rm beam} = 5.8$ for $p_{\rm beam} = 160\,{\rm GeV}$), is shown in Fig. 7 (right). The constraint on the muon energy in air showers (low-energy muons decay before reaching the detector level) leads to a strong preference for high energy pions in air showers (filled histogram). Details about the simulation and further phase space comparisons can be found in [44].

The comparison of the secondary particle distribution in p-C and p-Air interactions shown in Fig. 7 (right) demonstrates that particle production on a carbon target is very similar to that on air (mean mass number 14.5). This similarity allows one to tune interaction models without depending on assumptions on the target mass dependence of particle production.

There is a lack of measurements covering the aforementioned energy range and secondary particle phase space. A compilation of available measurements for proton projec-

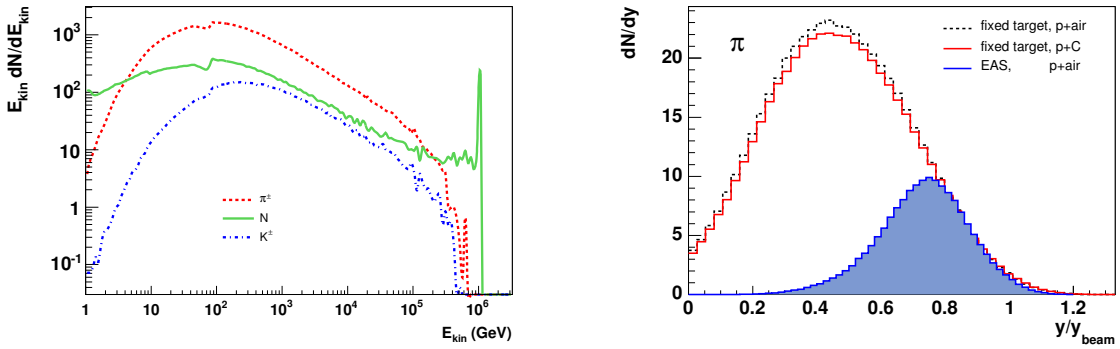

Figure 7: Left panel: Energy distribution of interactions in a shower which produce a meson that in turn decays into an observable muon. The discontinuity at 80 GeV (where the hadronic interaction model is switched from GHEISHA to QGSJET) reflects shortcomings in the hadronic interaction models. The three curves show the relative importance of pion, kaon and nucleon interactions. Right panel: Rapidity distribution (relative to beam rapidity) of secondary pions which produce muons that are detected in air shower experiments. The minimum-bias pion distribution is shown for reference and compared to that of proton-carbon interactions. (from [44])

tiles and light nuclear targets is shown in Figs. 8 and 9. Many measurements are available for beryllium as target, however, the most important phase space regions are not covered by these data sets (see Fig. 8). Recently two new data sets of pion production on carbon became available. These new data sets (HARP data at 12 GeV [46] and NA49 data at 158 GeV [47]) cover at their respective energies the secondary particle phase space relevant to air shower simulations, see Fig. 9. A first comparison of the NA49 data with high-energy interaction models is shown in Fig. 10, illustrating the discriminative power of low-energy measurements.

There exist no data for pion projectiles with good phase space coverage for light target nuclei. The only data set of relevance is Barton et al. [45] covering only a very limited range of the relevant phase space. Given the fact that more than 80% of all hadronic interactions in air showers are initiated by pions, the main uncertainty in modeling air showers stems from the lack of pion-nucleus data.

As can be seen from the proton-carbon data analysis [47], both the energy as well as the secondary particle phase space accessible with the NA49 detector setup are of great importance for air shower physics. In particular the excellent forward acceptance and particle identification are unique features needed for performing measurements that can be used in air shower simulations.

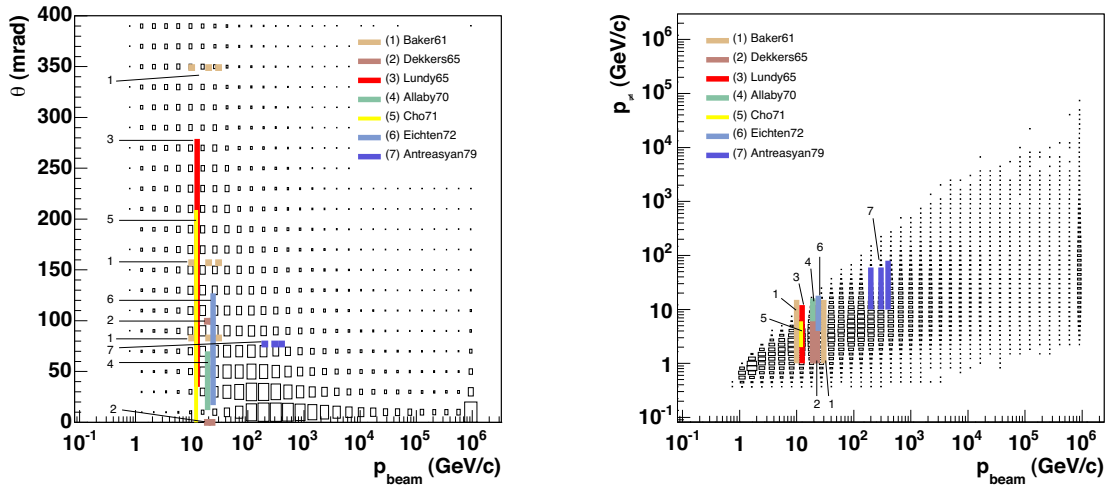

Figure 8: Compilation of existing data on pion production in proton-beryllium collisions [45]. The covered secondary particle phase space is indicated by the shaded regions. The box histogram shows the relative importance of the beam energy and secondary pion angle (left) and momentum (right) for muon production in extensive air showers.

Physics Needs

Regarding cosmic-ray physics, the most important projectile-target combinations would be pion-carbon at beam energies as high as possible, but 50 GeV would already reduce model uncertainties considerably. In addition a measurement of pion and kaon production in proton-carbon interactions would be important. All the data have to be taken with minimum bias trigger and thin targets. The analysis of NA49 min. bias proton-carbon data at 158 GeV can be used to estimate the required statistics. For a data sample of 400k inelastic events for each setting, one can expect a statistical error of less than 10% in the relevant kinematic range of secondaries. The following beam energies would be of particular interest

- p-C: 30, 100, 250, 400 GeV
- π^+-C: 30, 100, 250 GeV
- π^--C: 30, 250 GeV.

It should be noted that proton-proton and partially also pion-proton data is available at 100, 250 and 400 GeV.

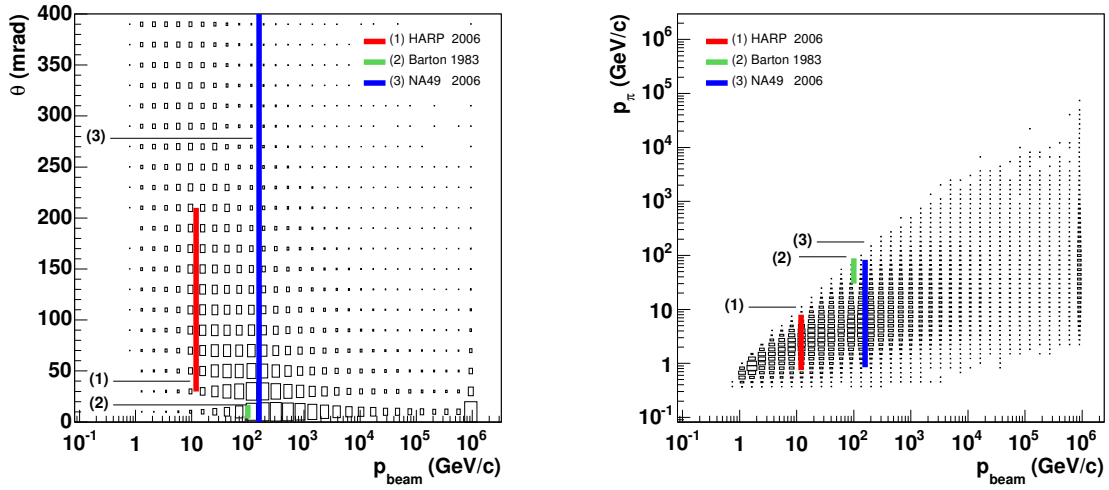

Figure 9: Compilation of existing data on pion production in proton-carbon collisions [45, 46, 47]. The covered secondary particle phase space is indicated by the shaded regions. The box histogram shows the relative importance of the beam energy and secondary pion angle (left) and momentum (right) for muon production in extensive air showers.

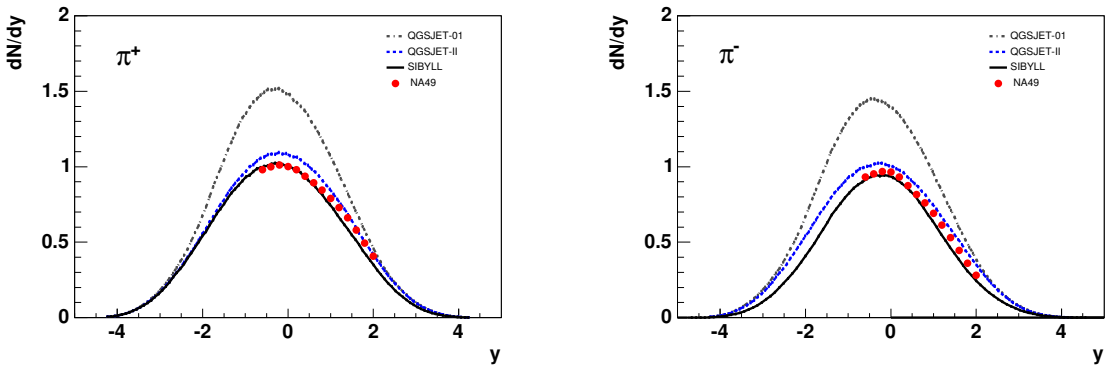

Figure 10: Comparison of rapidity distributions of positive (left) and negative (right) pions in proton-carbon interactions at 158 GeV. NA49 data [47] are compared to model predictions [46]. Both QGSJET II [48] and SIBYLL 2.1 [49] describe the data reasonably well whereas the old version of QGSJET overestimates the central pion production.

2.2 Reference p+p and p+A data

An interpretation of the rich experimental results on nucleus-nucleus collisions at high energies (see e.g. Section 2.3 in this document) relies to a large extent on a comparison to

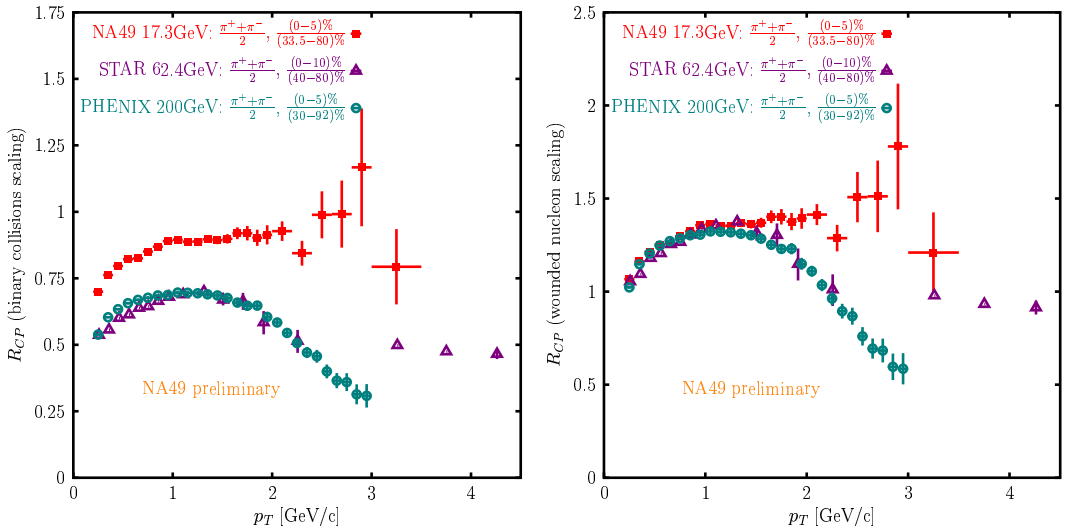

Figure 11: The ratio (R_{CP}) of pion transverse momentum spectra of central to peripheral Pb+Pb interactions at 158A GeV as measured by NA49 [50] scaled by the number of binary collisions (left) and wounded nucleons (right).

the corresponding data on p+p and p+A interactions. However, the available p+p and p+A results concern mainly basic properties of hadron production and they are sparse. Many needed data on fluctuations, correlations and, in particular, particle production at high transverse momenta are missing. Thus the measurements of hadron production in p+p and p+A reactions are necessary and should be performed in parallel to the corresponding measurements for A+A collisions. In the following this general requirement is illustrated by an important example, the inclusive spectra of identified hadrons at high transverse momentum, p_T.

One of the most striking features observed at BNL-RHIC is the suppression of high p_T hadron production in central A+A collisions relative to peripheral A+A collisions or p+p interactions. This is generally interpreted as a sign of parton energy loss in hot and dense hadronic matter created at the early stage of nucleus-nucleus collisions. This interpretation implies that the suppression should disappear at low energies where the energy density is not enough for creation of the deconfined state of matter. Numerous results on energy dependence of hadron yields and spectra indicate that the onset of deconfinement is located at the low SPS energies (see Section 2.3). Thus it is crucial to extend the study of the energy dependence to high p_T production, in particular in the CERN SPS energy range, to search for onset phenomena in the high p_T region.

The NA49 and other CERN SPS experiments measured identified hadron production in Pb+Pb collisions at 158A GeV up $p_T \approx$ 3-4 GeV/c [50]. The first results expressed in terms of the ratio of the p_T spectra measured in central and peripheral collisions (R_{CP})

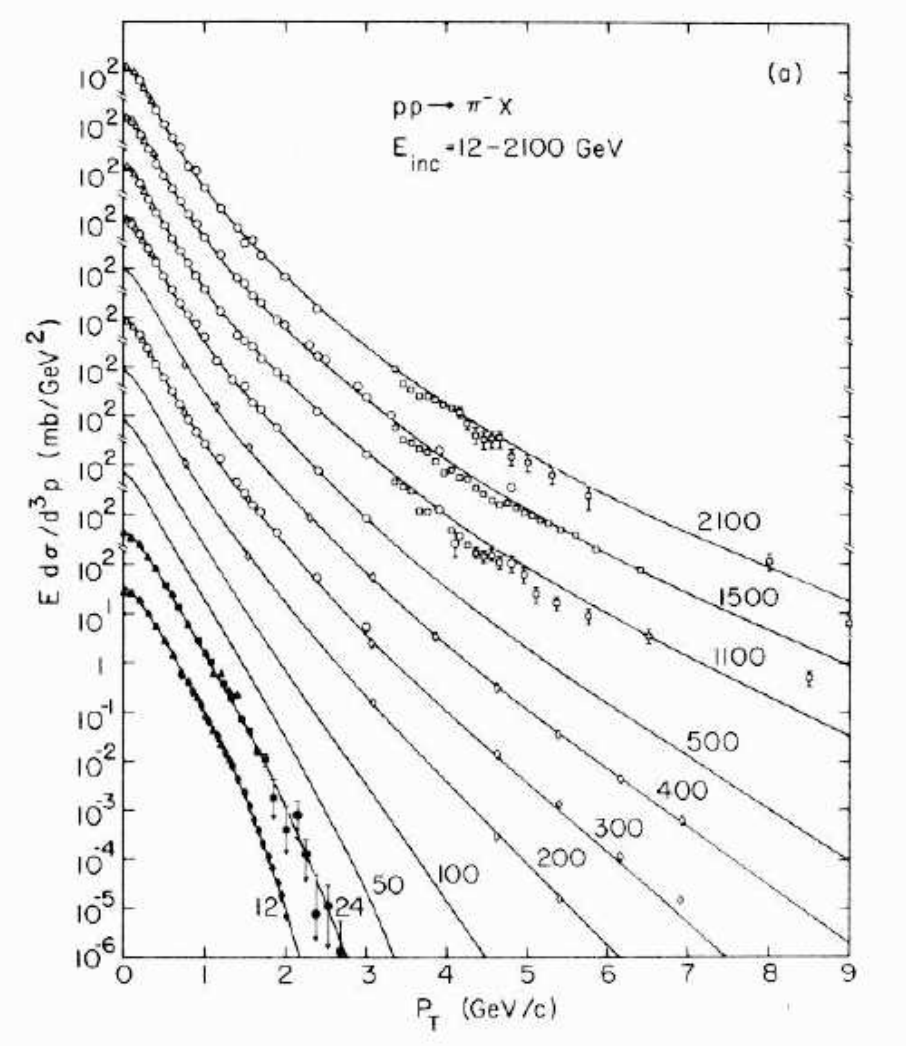

Figure 12: A compilation of the transverse momentum spectra of negatively charged pions produced in p+p interactions at different collision energies [52]. The energy values are given in the laboratory system. There are no data points between 24 GeV and 200 GeV.

are shown in Fig. 11 where the corresponding results at RHIC energies are also plotted for comparison. The suppression seems to weaken gradually with decreasing collision energy. The key measure in this study is, however, the ratio between p_T spectra measured in central Pb+Pb collisions and p+p interactions, R_{AA}. Thus precision p+p data [51] are crucial for an interpretation of the A+A results.

A compilation of the p_T spectra of pions produced in p+p interactions (excluding NA49 data) is shown in Fig. 12 which suggests a strong energy dependence of the high

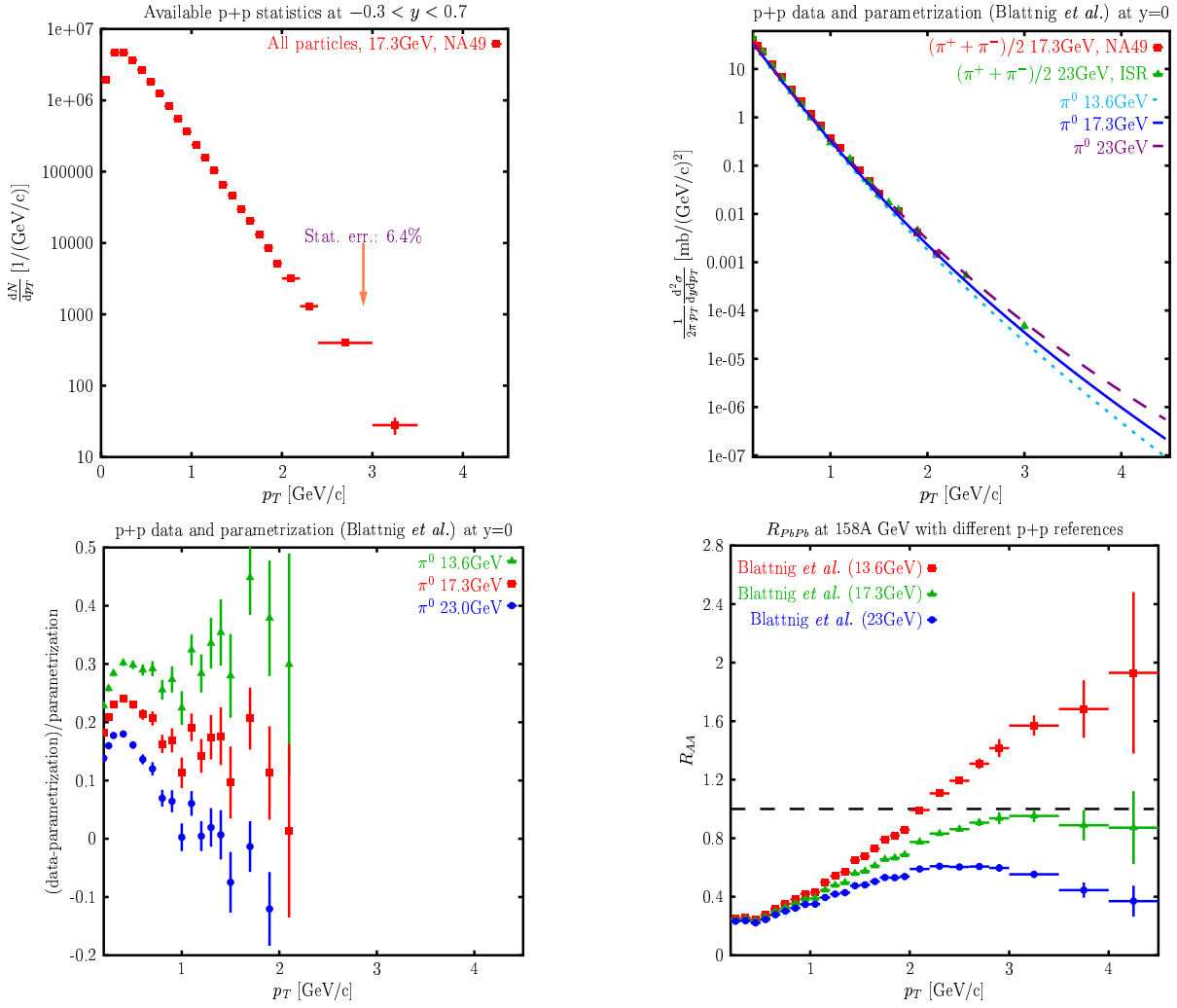

Figure 13: Top/left: Uncorrected transverse momentum spectrum of all charged hadrons as registered by NA49 in $4 \cdot 10^6$ p+p interactions at 158 GeV. Top/right: Data points show the corrected p_T spectra of pions produced in p+p interactions at energies close to 158 GeV (the top SPS energy for Pb+Pb collisions) in comparison to curves depicting the Blattnig et al. [53] parameterization calculated for three slightly different values of the energy parameter, corresponding to the present uncertainty in the extrapolation of existing p+p data. Bottom/left: The deviations of the measured p_T spectrum at 158 GeV from the Blattnig et al. parameterizations. Bottom/right: The R_{AA} ratio calculated for central Pb+Pb collisions at 158A GeV using different values of the energy parameter in the Blattnig et al. parameterization of the p+p data.

p_T tail over the SPS energy range, where the data points are missing. The statistics of

the NA49 p+p published data ($\approx 3 \cdot 10^6$ events) at 158 GeV is presented in Fig. 13, it ends at about 2.6 GeV/c. All this leads to a large systematic uncertainty of the estimate of the high p_T tail of the p+p spectrum based on an extrapolation of the existing data, see Fig. 13 for an illustration.

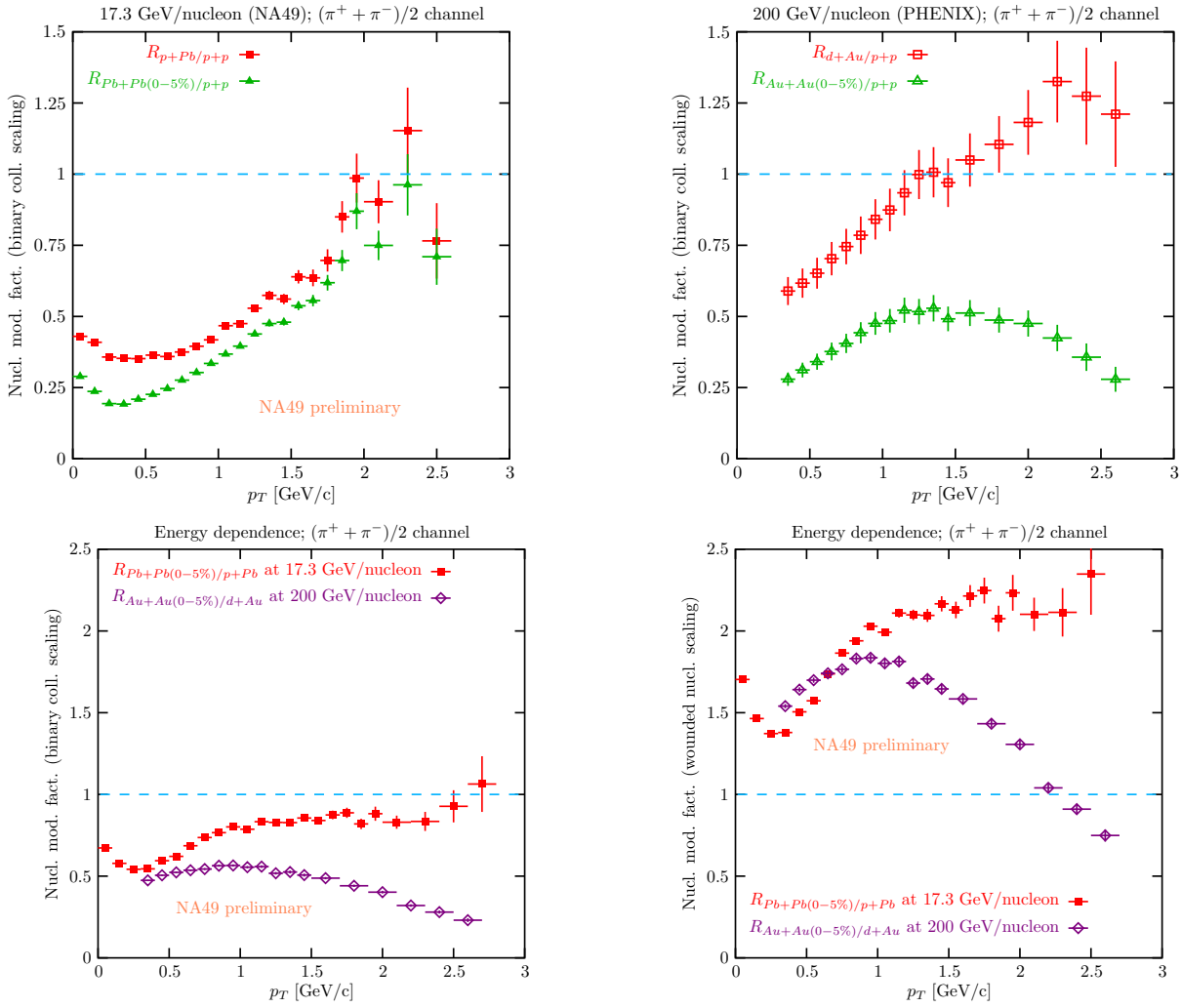

Figure 14: Top/left: Preliminary nuclear modification curves for $(\pi^+ + \pi^-)/2$ yields in the case of p+Pb and Pb+Pb collisions at 17.3 GeV/nucleon c.m. energy (NA49). Top/right: Published RHIC nuclear modification curves for $(\pi^+ + \pi^-)/2$ yields in the case of d+Au and Au+Au collisions at 200 GeV/nucleon c.m. energy (PHENIX). Bottom/left: A comparison of the modification curves $R_{A+A/p+A}$ (binary collision scaling) measured at the top SPS and RHIC energies. Bottom/right: A comparison of the modification curves $R_{A+A/p+A}$ (wounded nucleon scaling) measured at the top SPS and RHIC energies.

The detailed (preliminary) reanalysis of the existing p+p and p+Pb data already provides some results on the behavior of the nuclear modification factors $R_{Pb+Pb/p+p}$, $R_{p+Pb/p+p}$ and $R_{Pb+Pb/p+Pb}$, up to about 2.6 GeV/c, which is just the beginning of the region of interest in question. The results are shown in Fig. 14. It can be clearly seen that the modification factor curve of Pb+Pb (central) relative to p+p closely follows the modification factor curve of p+Pb relative to p+p (which shows a remarkable Cronin effect). However, at 200 GeV, there is a strong suppression in the case of A+A (central) collisions. The question is: do the two closely following curves depart from each other above 2.6 GeV/c, i.e. do we also measure a suppression for A+A (central) reactions? In other words: does the seemingly constant plateau of the modification factor curve $R_{Pb+Pb/p+Pb}$ extend to higher transverse momenta, or will we get a suppression (or an enhancement)?

The above example clearly shows a need for high statistics and high precision measurements of identified hadron production in p+p and p+A collisions at SPS energies. An increase of event statistics by a factor of above 10 would extend the p_T coverage to about 4 GeV/c.

2.3 Onset of deconfinement and critical point in A+A collisions

2.3.1 Key questions

One of the key issues of contemporary physics is the understanding of strong interactions and in particular the study of the properties of strongly interacting matter in equilibrium. What are the phases of this matter and how do the transitions between them look like are questions which motivate a broad experimental and theoretical effort. The study of high energy nucleus-nucleus collisions gives us a unique possibility to address these questions in well-controlled laboratory experiments.

Onset of Deconfinement

Recent results on the energy dependence of hadron production in central Pb+Pb collisions at 20A, 30A, 40A, 80A and 158A GeV coming from the energy scan program at the CERN SPS serve as evidence for the existence of a transition to a new form of strongly interacting matter, the Quark Gluon Plasma (QGP) in nature. Thus they are in agreement with the indications that at the top SPS [54] and RHIC [55] energies the matter created at the early stage of central Pb+Pb (Au+Au) collisions is in the state of QGP.

The key results and their comparison with models are summarized in Fig. 15. Energy dependence of the mean pion multiplicity per wounded nucleon, of the $\langle K^+ \rangle / \langle \pi^+ \rangle$ ratio and of the inverse slope parameter T of the transverse mass spectra of K^+ mesons measured in central Pb+Pb (Au+Au) collisions compared to results from p+p($\overline{p}$) reactions

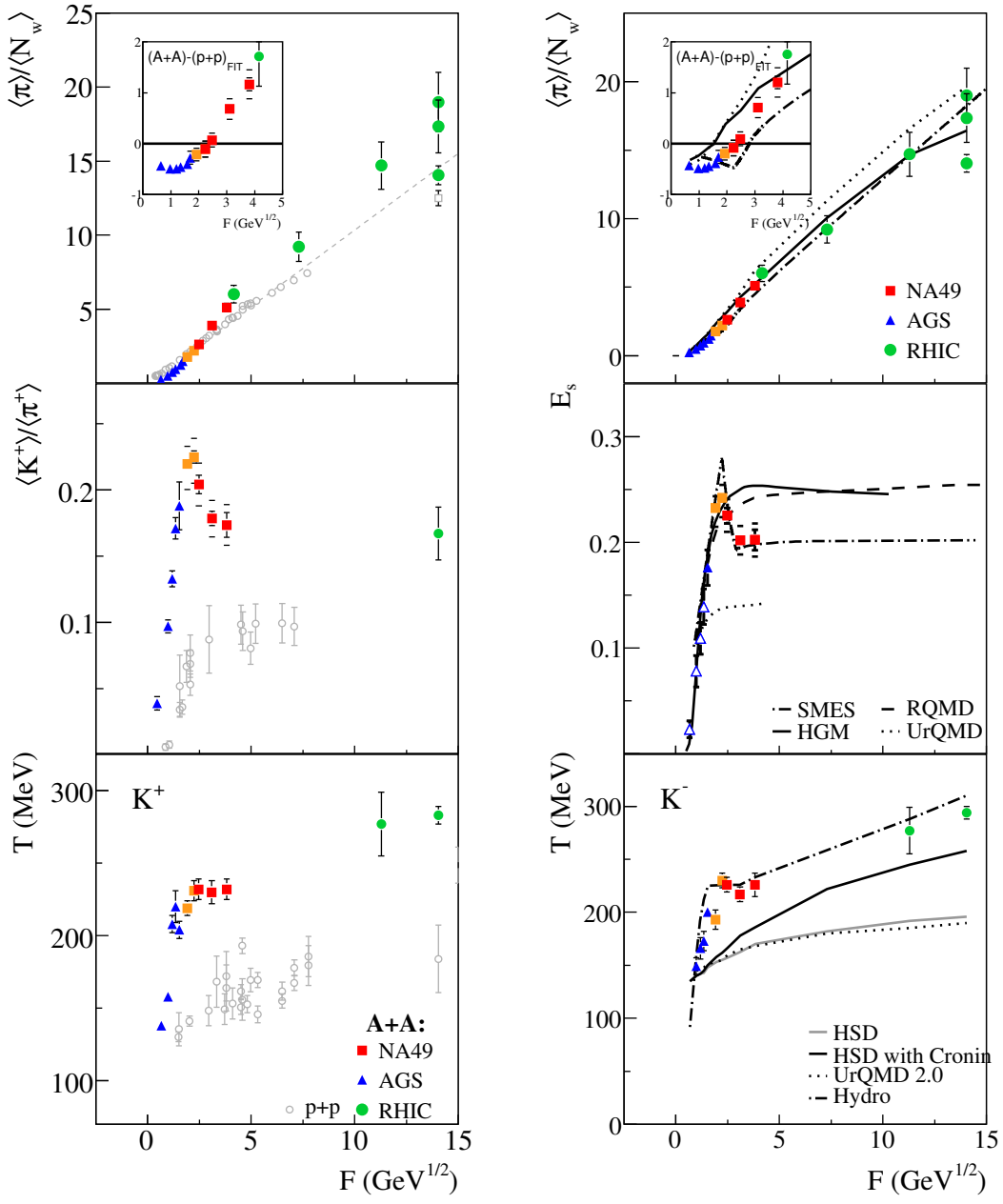

Figure 15: Left: Energy dependence of hadron production properties in central Pb+Pb (Au+Au) collisions (closed symbols) and p+p interactions (open symbols). Right: The results for Pb+Pb (Au+Au) reactions are compared with various models. For details see text.

are shown in Fig. 15 (left). The rapid changes in the SPS energy range (solid squares) suggest the onset of a new physics in heavy ion collisions at the low SPS energies. Energy dependence of the mean pion multiplicity per wounded nucleon, the relative strangeness production measured by the E_S ratio and the inverse slope parameter of m_T–spectra of K^- mesons measured in central Pb+Pb (Au+Au) collisions are compared with predictions of various models in Fig. 15 (right). The models which do not assume the deconfinement phase transition (HGM [56], RQMD [57], UrQMD [58] and HSD [59]) fail to describe the data. The introduction of a 1^{st} order phase transition at the low SPS energies (SMES [8] and hydro [60, 61]) allows to describe the measured structures in the energy dependence.

The energy dependence of the same observables measured in p+p interactions (open symbols in Fig. 15 (left)) is very different than that measured in central Pb+Pb (Au+Au) collisions and it does not show any anomalies.

There are attempts to explain the results on nucleus-nucleus collisions by (model dependent) extrapolations of the results from proton-nucleus interactions [62, 63]. As detailed enough p+A data exist only at the top AGS and SPS energies the extrapolations are limited to these two energies and thus there are no predictions concerning energy dependence of the quantities relevant for the onset of deconfinement (see Fig. 15). The underlying models are based on the assumption that particle yield in the projectile hemisphere is due to production from excited projectile nucleon(s). This assumption is, however, in contradiction to the recent results at RHIC [64] and SPS [65] energies which clearly demonstrate a strong mixing of the projectile and target nucleon contributions in the projectile hemisphere. Furthermore, qualitative statements on similarity or differences between p+A and A+A reactions may be strongly misleading because of a trivial kinematic reason. The center of mass system in p+A interactions moves toward the target nucleus A with increasing A, whereas its position is A-independent for A+A collisions. For illustration several typical examples are considered. The baryon longitudinal momentum distribution in A+A collisions gets narrower with increasing A and, of course, it remains symmetric in the collision center of mass system. In p+A collisions it shrinks in the proton hemisphere and broadens in the target hemisphere (for example see slide 5 in [62]). Thus a naive comparison would lead to the conclusion that A+A collisions are qualitatively similar to p+A interactions if the proton hemisphere is considered, or that they are qualitatively different if the target hemisphere is examined. One encounters similar difficulty in a discussion of the A-dependence of particle ratios in a limited acceptance. For instance the kaon/pion ratio is independent of A in p+A interactions if the total yields are considered [66], it is however strongly A-dependent in a limited acceptance (e.g. see slides 10 and 11 in [62]). Recent string-hadronic models ([57, 58, 59]) take all trivial kinematic effects into account and parametrize reasonably well p+p and p+A results. Nevertheless they fail to reproduce the A+A data (see e.g. Fig. 15).

Further progress in understanding effects which are likely related to the onset of deconfinement can be done only by a new comprehensive study of hadron production in proton-nucleus and nucleus-nucleus collisions.

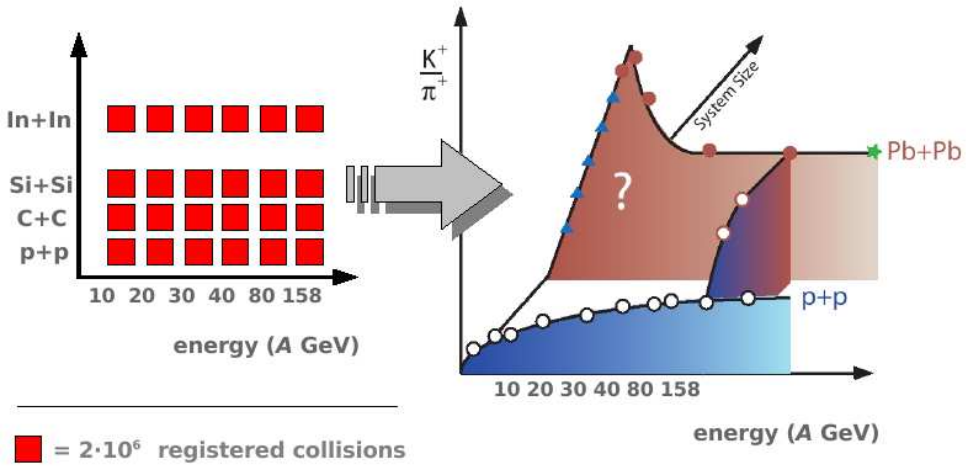

Figure 16: An illustration of the impact of the new measurements (of central collisions) on clarifying the system size dependence of the K^+/π^+ anomaly observed in central Pb+Pb collisions at the low SPS energies.

The two most important open questions are:

- **what is the nature of the transition from the anomalous energy dependence measured in central Pb+Pb collisions at SPS energies to the smooth dependence measured in p+p interactions?**
- **is it possible to observe the predicted signals of the onset of deconfinement in fluctuations [69] and anisotropic flow [70]?**

The qualitative progress in the experimental situation which will be achieved by the proposed new measurements is illustrated in Fig. 16 using as an example the K^+/π^+ ratio. A detailed discussion of the requested reactions is given below.

Critical Point

In the letter of Rajagopal, Shuryak, Stephanov and Wilczek addressed to the SPS Committee one reads: *... Recent theoretical developments suggest that a key qualitative feature, namely a critical point (of strongly interacting matter) which in a sense defines the landscape to be mapped, may be within reach of discovery and analysis by the SPS, if data is taken at several different energies. The discovery of the critical point would in a stroke transform the map of the QCD phase diagram which we sketch below from one based only on reasonable inference from universality, lattice gauge theory and models into one with a solid experimental basis. ...* More detailed argumentation is presented below.

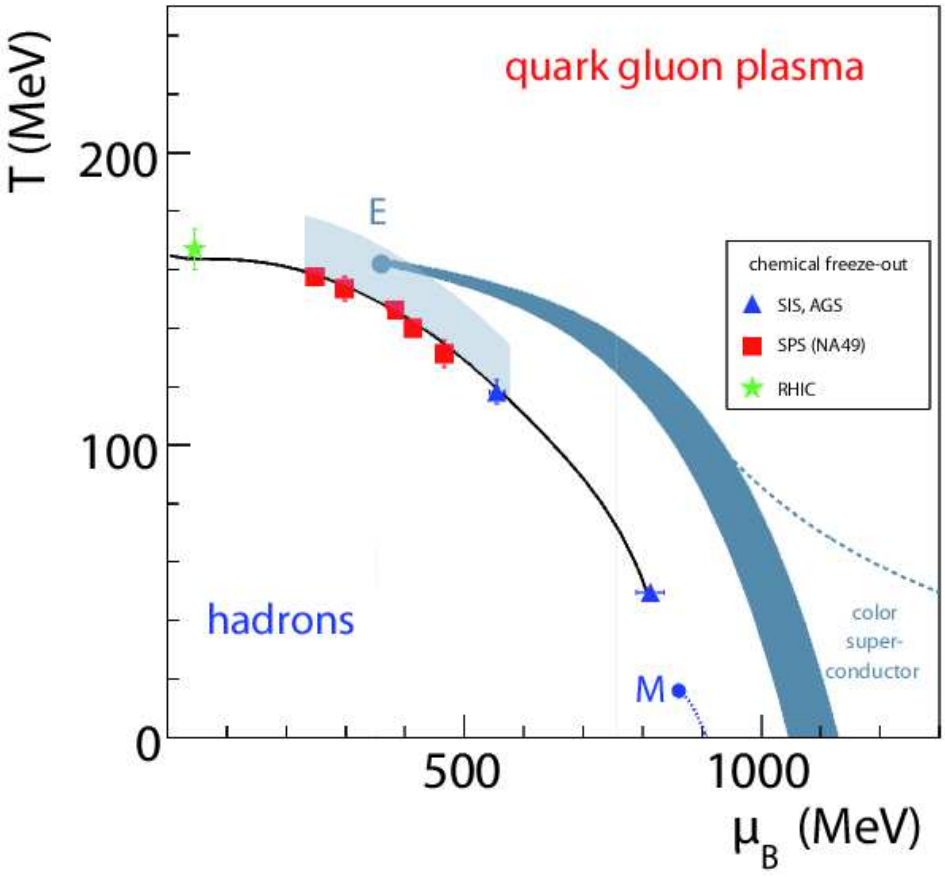

Figure 17: The hypothetical phase diagram of strongly interacting matter in the plane temperature, T, and baryonic chemical potential, μ_B. The end point **E** of the first order transition strip is the critical point of the second order. The chemical freeze-out points extracted from the analysis of hadron yields in central Pb+Pb (Au+Au) collisions at different energies are plotted by the solid symbols. The region covered by the future measurements at the CERN SPS is indicated by the gray band.

Rich systematics of hadron multiplicities produced in nuclear collisions can be described reasonably well by hadron gas models [71, 72, 73]. Among the model parameters fitted to the data are temperature, T, and baryonic chemical potential, μ_B, of the matter at the stage of freeze-out of the hadron composition (the chemical freeze-out). These parameters extracted for central Pb+Pb collisions at the CERN SPS energies are plotted in the phase diagram of hadron matter, Fig. 17, together with the corresponding results for higher (RHIC) and lower (AGS, SIS) energies. With increasing collision energy the

chemical freeze-out parameter T increases and μ_B decreases. A rapid increase of temperature is observed up to mid SPS energies, then from the top SPS energy ($\sqrt{s_{NN}} = 17.2$ GeV) to the top RHIC energy ($\sqrt{s_{NN}} = 200$ GeV) the temperature increases only by about 10 MeV.

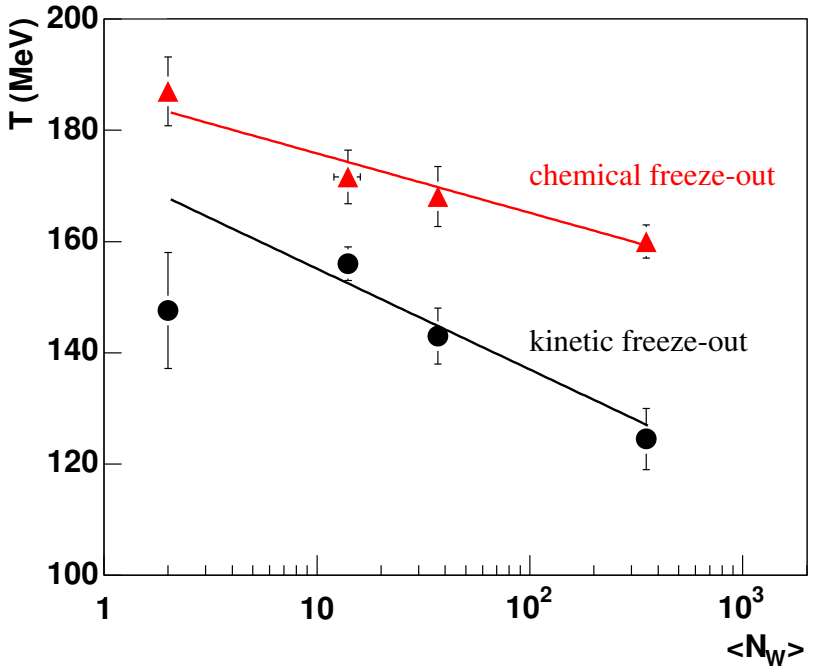

Figure 18: The dependence of the chemical and kinetic freeze-out temperatures on the mean number of wounded nucleons for p+p, C+C, Si+Si and Pb+Pb collisions at 158A GeV.

Fig. 17 also shows a sketch of the phases of strongly interacting matter in the (T, μ_B) plane as suggested by QCD-based considerations [75, 76]. To a large extent these predictions are qualitative, as QCD phenomenology at finite temperature and baryon number is one of the least explored domains of the theory. More quantitative results come from lattice QCD calculations which can be performed at $\mu_B = 0$. They suggest a rapid crossover from the hadron gas to the QGP at the temperature $T_C = 170 - 190$ MeV [77, 78], which seems to be somewhat higher than the chemical freeze-out temperatures of central Pb+Pb collisions ($T = 150 - 170$ MeV) [79] at the top SPS and RHIC energies.

The nature of the transition to QGP is expected to change with increasing baryo-chemical potential. At high potential the transition may be of the first order, with the end point of the first order transition domain, marked E in Fig. 17, being the critical point of the second order. Recently even richer structure of the phase transition to QGP was discussed within a statistical model of quark-gluon bags [80]. It was suggested that the line of the first order phase transition at high μ_B is followed by a line of second order phase transition at intermediate μ_B, and then by lines of "higher order transitions" at low μ_B. A characteristic property of the second order phase transition (the critical point or line) is a divergence of the susceptibilities. Consequently an important signal of a second-order phase transition at the critical point are large fluctuations, in particular an enhancement of fluctuations of multiplicity and transverse momentum are predicted [74]. A characteristic feature of the second order phase transition is the validity of appropriate power laws in measurable quantities related to critical fluctuations. Techniques associated with such measurements in nuclear collisions are under development [81] with emphasis on the sector of isoscalar di-pions (σ-mode) as required by the QCD conjecture for the critical end point in quark matter [75]. Employing such techniques in a study of nuclear collisions at different energies at the SPS and with nuclei of different sizes, the experiment may test not only the existence and location of the critical point but also the size of critical fluctuations as given by the critical exponents of the QCD conjecture.

Thus when scanning the phase diagram a maximum of fluctuations located in a domain close to the critical point (the increase of fluctuations can be expected over a region $\Delta T \approx 15$ MeV and $\Delta\mu_B \approx 50$ MeV [82]) or the critical line should signal the second order phase transition. The position of the critical region is uncertain, but the best theoretical estimates based on lattice QCD calculations locate it at $T \approx 158$ MeV and $\mu_B \approx 360$ MeV [83, 84] as indicated in Fig. 17. It is thus in the vicinity of the chemical freeze-out points of central Pb+Pb collisions at the CERN SPS energies.

Pilot data [4] on interactions of light nuclei (Si+Si, C+C and p+p) taken by NA49 at $40A$ and $158A$ GeV indicate that the freeze-out temperature increases with decreasing mass number, A, of the colliding nuclei, see Fig. 18. This means that a scan in the collision energy and mass of the colliding nuclei allows us to scan the (T, μ_B) plane in a search for the critical point (line) of strongly interacting matter [74].

The experimental search for the critical point by investigating nuclear collisions is justified at energies higher than the energy of the onset of deconfinement. This is because the energy density at the early stage of the collision, which is required for the onset of deconfinement is higher than the energy density at freeze-out, which is relevant for the search for the critical point. The only anomalies possibly related to the onset of deconfinement are measured at $30A$ GeV ($\sqrt{s_{NN}} \approx 8$ GeV) (see Fig. 15). This limits a search for the critical point to an energy range $E_{lab} > 30A$ GeV ($\mu_B(CP) < \mu_B(30A\text{GeV})$).

Fortunately, as discussed above and illustrated in Fig. 17, the best theoretical predictions locate the critical point in the (T, μ_B) region accessible in nuclear collisions in this energy range (at about $80A$ GeV). There are, however, large and difficult to estimate

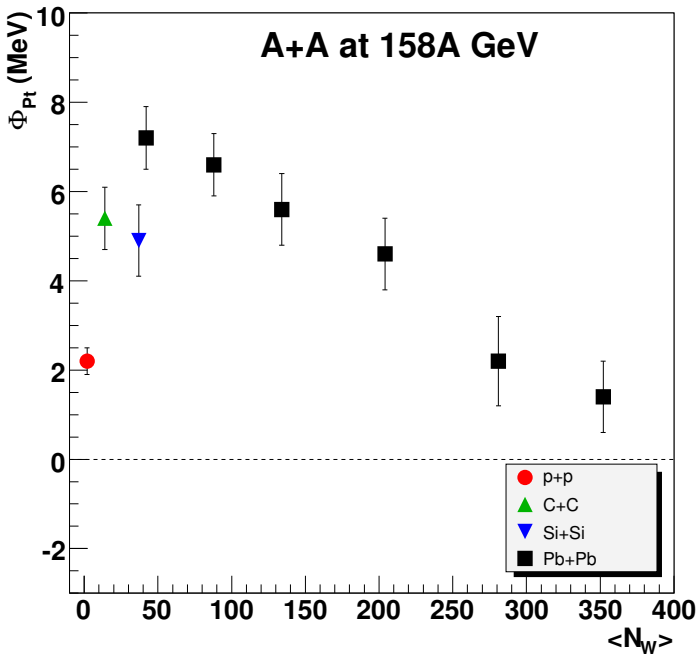

Figure 19: The measure of transverse momentum fluctuations Φ_{p_T} versus mean number of interacting nucleons $\langle N_W \rangle$ for nuclear collisions at 158A GeV. The results for all charged hadrons are presented. Only statistical errors are plotted, the systematic errors are smaller than 1.6 MeV.

systematic errors in these predictions.

Under the minimal assumption that the critical point is located with equal probability at $\mu_B(CP) < \mu_B(30A\text{GeV})$ one can estimate a probability of 0.5 that it is reachable in the SPS energy range.

One of the first proposed signals of the critical point of strongly interacting matter was a maximum of the transverse momentum fluctuations in the (collision energy)-(system size) plane [74]. NA49 performed the system size scan at 158A GeV and, in fact, a maximum was observed for collisions with a number of interacting nucleons of about 40 [85]. Qualitatively similar results were obtained by CERES [86]. The experimental results of NA49 are shown in Fig. 19, where the intensive fluctuation measure, Φ_{P_T} is plotted against the mean number of interacting nucleons. The magnitude of the observed fluctuations, $\Phi_{P_T} = 7 \pm 2$ MeV, is in approximate agreement with the predictions for the critical point, $\Phi_{P_T} \approx 10$ MeV [87].

Onset of deconfinement and the critical point are also expected to lead to anomalies in the multiplicity fluctuations [69, 74]. The dispersion of the multiplicity distribution

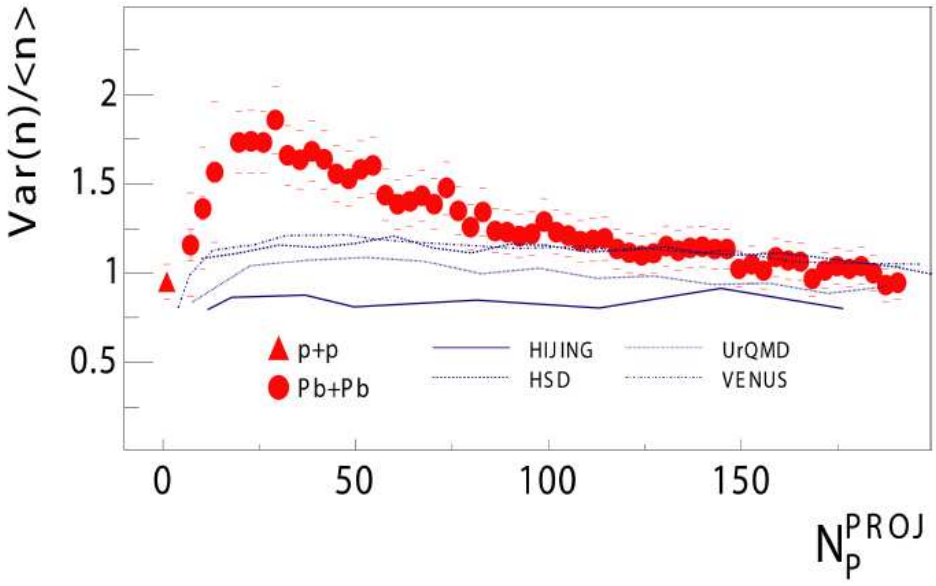

Figure 20: Scaled variance of the multiplicity distribution for negatively charged hadrons as a function of the number of projectile participants for Pb+Pb collisions at 158A GeV. The systematic errors due to a poor resolution in the measurement of the number of projectile spectators are indicated by the horizontal bars. The lines show predictions of string-hadronic models.

should increase by about 10-20% when crossing the energy domain in which the onset of deconfinement is located [69]. The scaled variance of the multiplicity distribution is expected to increase by about 10% in the vicinity of the critical point [74]. The identification of these effects is however non-trivial. This is mainly because the measured multiplicity fluctuations are directly sensitive to the fluctuations in the number of interacting nucleons caused by event-by-event changes in the collision geometry.

First results from NA49 on the scaled variance of the multiplicity distribution as a function of the number of interacting nucleons from the projectile nucleus are shown in Fig. 20. The measurements show an increase towards peripheral collisions similar to that seen for Φ_{P_T}. This increase is not present in existing string-hadronic models [88]. It was recently suggested [89] that the large fluctuations for peripheral collisions may be caused by equilibration (mixing) of particle sources from the projectile and target nuclei. It is clear that clarification of the origin of the observed large increase of multiplicity fluctuations in peripheral collisions is a necessary first step in a search for the fluctuation signals of the critical point or onset of deconfinement. This requires new high precision comprehensive data on multiplicity fluctuations and an improved forward calorimeter to

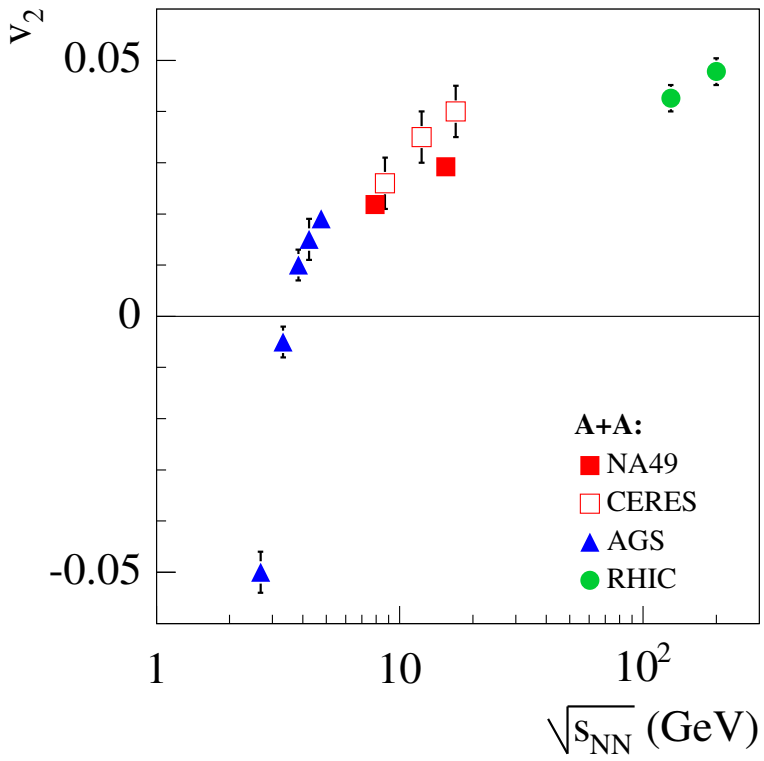

Figure 21: The energy dependence of elliptic flow of charged pions at mid-rapidity in Pb+Pb (Au+Au) collisions for mid-central events.

reduce uncertainties in the determination of the collision geometry.

Whether the measured p_T and multiplicity fluctuations signal the vicinity of the critical point (line) remains an open question. This is mainly because systematic data on the energy and collision system size dependence of these fluctuation observables are missing. Only an observation of a maximum (or an onset) in the energy dependence will serve as a strong indication for the critical point (line).

The energy dependence of anisotropic flow is considered to be sensitive to both the onset of deconfinement [70] and the critical point [90]. The two can be distinguished by separate measurements of the flow for mesons and baryons. In the case of the onset of deconfinement the flow of both mesons and baryons should be reduced [91], whereas the critical point should lead to a decrease of the baryon flow and an increase of the meson flow [90]. However, the existing data [92] are inconclusive on whether the expected effects are present in the CERN SPS energy range. The main experimental results are summarized in Figs. 21 and 22. The energy dependence of the v_2 parameter for pions in Pb+Pb (Au+Au) collisions is shown in Fig. 21. A rapid increase observed at low energies seems

to weaken in the SPS energy range. In Fig. 22 the rapidity dependence of the elliptic flow parameter, v_2, of pions and protons is plotted for Pb+Pb collisions at 40A GeV. The results from the standard analysis suggest the reduction of v_2 for protons at mid-rapidity. This effect is, however, not observed in the results from the cumulant analysis and the 40A GeV data from NA49 are the only data on proton flow at low SPS energies. Thus the present data suggest the possibility of anomalies in the energy dependence of elliptic flow of mesons and baryons at the SPS energies, but they are too sparse to allow any firm conclusion.

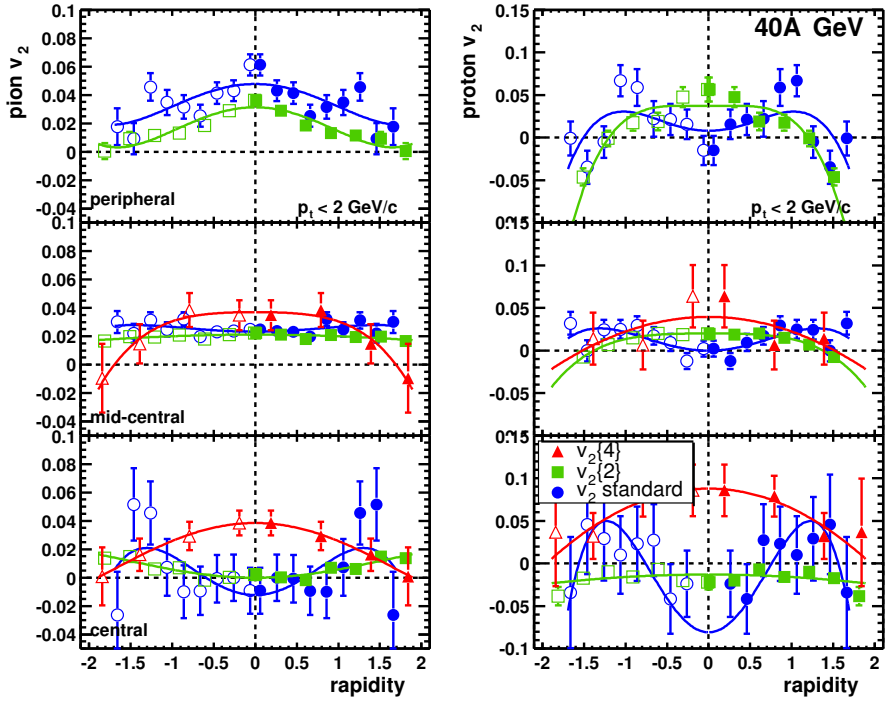

Figure 22: Elliptic flow of charged pions (left) and protons (right) obtained from the standard (v_2 standard) and cumulant ($v_2\{2\}$) methods as a function of the rapidity in Pb+Pb collisions at 40A GeV for three centrality bins. The open points have been reflected with respect to mid-rapidity. The solid lines are from polynomial fits.

It is thus clear that only the new measurements at the CERN SPS can answer the important question:

- **does the critical point of strongly interacting matter exist in nature and, if it does, where is it located?**

The qualitative progress in the experimental search which will be achieved by the proposed new measurements is illustrated in Fig. 23. The critical point is expected to

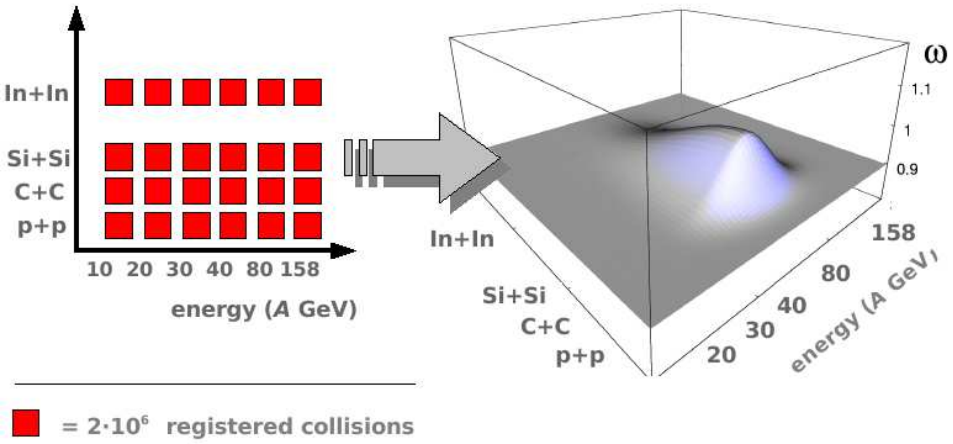

Figure 23: An illustration of the impact of the new measurements of central collisions on the search for the critical point of strongly interacting matter.

manifest itself by a maximum of fluctuations of e.g. of the scaled variance ω of the produced particle multiplicity distribution. A detailed discussion of the requested reactions is given below.

In conclusion, the recent experimental and theoretical findings strongly suggest that a further study of nuclear collisions in the CERN SPS energy range is of particular importance. The new measurements will dramatically improve the current experimental situation and they should allow to answer the key questions concerning the nature of the onset of deconfinement and the existence and location of the critical point.

2.3.2 General requirements

The physics goals of the new experimental program with nuclear beams at the CERN SPS presented in the previous section require a comprehensive energy scan in the whole SPS energy range (10A-200A GeV) with light and intermediate mass nuclei. The NA49-future collaboration intends to register p+p, C+C, Si+Si and In+In collisions at 10A, 20A, 30A, 40A, 80A, 158A GeV and a typical number of recorded events per reaction and energy of $6 \cdot 10^6$. Quantitative justification of this request will be given in Section 4.3.

The data sets recorded by NA49 and those planned to be recorded by NA49-future are shown in Fig. 24. It is clear that the new measurements will lead to a very significant experimental progress.

It is important to underline that collisions of medium size and light nuclei can not be replaced by centrality selected collisions of heavy (e.g. Pb+Pb) nuclei. This point is

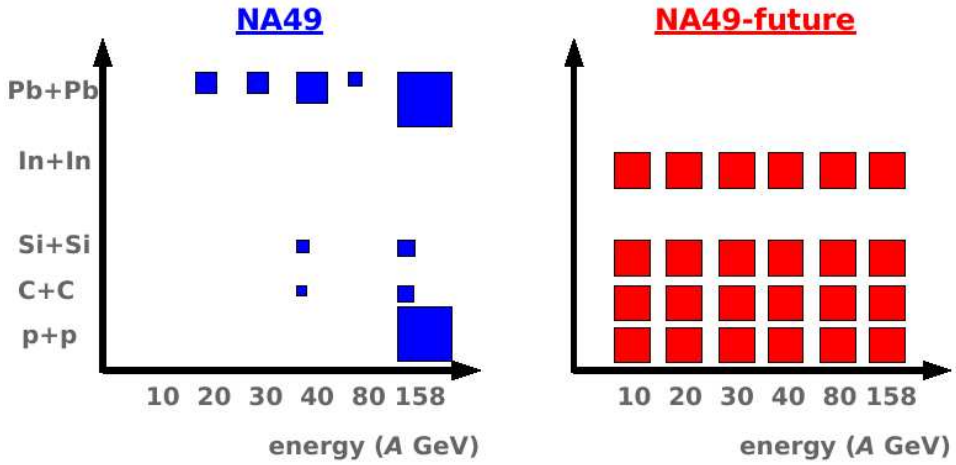

Figure 24: The data sets recorded by NA49 and those planned to be recorded by NA49-future. The area of the boxes is proportional to the number of registered central collisions, which for NA49-future will be $2 \cdot 10^6$ per reaction.

illustrated in Fig. 25, where a large difference between hadron production properties in central collisions of light nuclei and peripheral Pb+Pb (Au+Au) interactions is clearly seen. This conclusion is valid both for mean values (Fig. 25 (left)) and for fluctuations (Fig. 25 (right)). Furthermore it has to be stressed that a hadronic final state produced in central collisions is much closer to the chemical and thermal equilibrium than a corresponding final state produced in peripheral collisions. Thus, for the planned study of the properties of the onset of deconfinement and the search for the critical point central collisions are of primary interest.

The future analysis should focus on the study of fluctuations and anisotropic flow. The first NA49 results on these subjects [92, 85, 93, 94] suggest, in fact, the presence of interesting effects for collisions with moderate number of participant nucleons and/or low collision energies. However, as discussed above, a very limited set of data and resolution limitations do not allow firm conclusions.

Several upgrades of the current NA49 apparatus are necessary to reach the physics goals.

1. The event collection rate should be significantly increased in order to allow a fast collection of sufficient statistics for a large number of different reactions (A, $\sqrt{s_{NN}}$).

2. The resolution in the event centrality determination based on the measurement of the energy of projectile spectator nucleons should be improved. This is important for high precision measurements of event-by-event fluctuations.

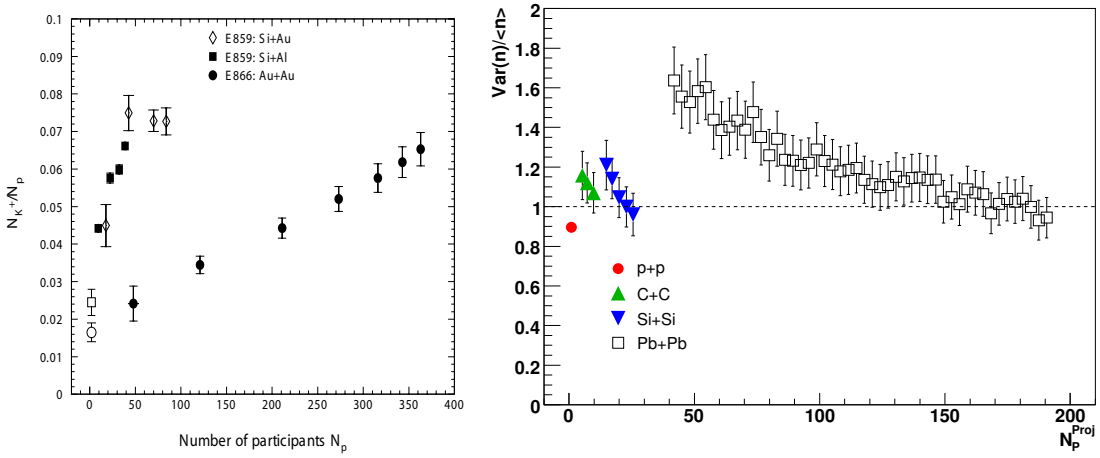

Figure 25: Left: The mean number of K^+ mesons per participant nucleon is plotted as a function of the number of participants for for Si+Al, Si+Au and Au+Au collisions at the top AGS energies (10A-14A GeV). Right: The scaled variance of the multiplicity distribution of negatively charged hadrons in the projectile hemi-sphere for p+p, C+C, Si+Si and Pb+Pb interactions is plotted versus the number of projectile participants.

3. It is desirable to increase the acceptance for the measurements of charged hadrons.

In the following sections we propose hardware upgrades of the NA49 apparatus and discuss the resulting improvements of its physics performance.

2.3.3 Experimental landscape

The SPS energy range is of particular importance for the study of nucleus-nucleus collisions for two reasons. Firstly, at the low SPS energies anomalies in the energy dependence of hadron production properties are observed. They are attributed to the onset of deconfinement. Secondly, at high SPS energies the critical point of strongly interacting matter can be discovered. This expectation is based on the recent estimate of the location of the critical point from lattice QCD and the freeze-out parameters determined from measured hadron yields using the hadron-resonance gas model.

Among other existing heavy ion accelerators only RHIC at BNL can potentially run in the SPS energy range. In March 2006 a RIKEN BNL workshop "Can the QCD critical point be discovered at the BNL RHIC" took place, where it was decided to start preparations for a low energy RHIC program. The first tests of the accelerator complex were performed in June 2006. Proton beams of 11 GeV/c ($\sqrt{s_{NN}} = 22$ GeV) were successfully injected, circulated and collided at RHIC. The magnet currents for this test correspond

to those required for Au+Au running at $\sqrt{s_{NN}} \approx 8.8$ GeV, or equivalently with fixed target running at about 40A GeV. Tests at lower energies using ion beams are foreseen in 2007. The physics run with Au beams at several energies which correspond to the NA49 settings may be scheduled for 2009. The performance of the STAR and PHENIX detectors matches, in general, the physics requirements of running at low RHIC energies.

The SPS program proposed here and the suggested new RHIC program are to a large extent complementary. This is due to different collision kinematics and different priorities in data taking.

NA49-future at the SPS will take data in the fixed target mode. First, this gives the unique possibility to measure the number of projectile spectators for each collision, which, in turn, allows a precise study of event-by-event fluctuations, in particular, fluctuations of extensive quantities like multiplicity. Second, the NA49-future acceptance for identified hadrons covers a large part of the projectile hemi-sphere. This allows measurement of almost the full rapidity spectrum and total multiplicities of produced hadrons. NA49-future intends to perform the energy scan for collisions of light and medium size nuclei (p+p, C+C, Si+Si and In+In).

In contrast, it is planned to start the low energy RHIC program with the energy scan for Au+Au collisions. STAR and PHENIX at the RHIC will take data in the collider mode. This allows to perform measurements with full and uniform azimuthal angle acceptance and forward–backward symmetry with respect to mid-rapidity. This is crucial for a precise measurement of azimuthal flow and other measures of azimuthal correlations.

Starting from 2015 the study of nucleus-nucleus collisions at lower SPS energies (10A-40A) will be continued by the CBM experiment at SIS-300 (FAIR, Darmstadt). Low cross-section processes, like di-lepton as well as open and hidden charm hadron production will be the focus of these measurements.

Furthermore there is a discussion of the possibility to construct a heavy ion collider at JINR, Dubna, which would also cover the low SPS energy range.

3 Experimental Apparatus and Software

The future measurements will be performed with the upgraded NA49 apparatus. The total cost of the existing equipment can be estimated to be about 20M SFR. The cost of upgrades will be about 1.5M SFR.

In the following a brief description of the existing NA49 facility and software is given and the planned upgrades are presented.

3.1 NA49 detector

The NA49 experiment was a large acceptance hadron spectrometer at the CERN-SPS for the study of the hadronic final states produced by collisions of various beam particles (p, Pb from the SPS and C, Si from the fragmentation of the primary Pb beam) with a variety of fixed targets. The main tracking devices were four large volume Time Projection Chambers (TPCs) (Fig. 26) which were capable of detecting 70% of the approximately 1500 charged particles created in a central Pb+Pb collision at 158A GeV. Two of them, the vertex TPCs (VTPC-1 and VTPC-2), were located in the magnetic field of two superconducting dipole magnets (1.5 and 1.1 T, respectively) and two others (MTPC-L and MTPC-R) were positioned downstream of the magnets symmetrically to the beam line. The NA49 TPCs allowed precise measurements of particle momenta p with a resolution of $\sigma(p)/p^2 \cong (0.3 - 7) \cdot 10^{-4}$ (GeV/c)$^{-1}$. The set–up was supplemented by two time of flight (TOF) detector arrays with a time measurement resolution σ_{tof} ≈60 ps and a set of calorimeters. The targets used in the NA49 program were C (561 mg/cm^2), Si (1170 mg/cm^2) and Pb (224 mg/cm^2) for ion collisions and a liquid hydrogen cylinder (length 20 cm) for elementary interactions, were positioned about 80 cm upstream from VTPC-1.

Pb beam particles were identified by means of their charge as seen by a helium gas-Cerenkov counter (S2') and p beam particles by a 2 mm scintillator (S2). Both of these were situated in front of the target. The study of C+C and Si+Si reactions was possible through the generation of a secondary fragmentation beam which was produced in a primary target (1 cm carbon) in the extracted Pb-beam. With the proper setting of the beam line magnets a large fraction of all $Z/A = 1/2$ fragments were transported to the NA49 experiment. On-line selection based on a pulse height measurement in a scintillator beam counter (S2) was used to select particles with $Z = 6$ (carbon) and $Z = 13, 14, 15$ (Al, Si, P). In addition, a measurement of the energy loss in beam position detectors (BPD-1,2,3 in Fig. 26) allowed for a further selection in the off-line analysis. These detectors consisted of pairs of proportional chambers and were placed along the beam line. They also provided a precise measurement of the transverse positions of the incoming beam particles.

For p beams, interactions in the target were selected by an anti-coincidence of the incoming beam particle with a small scintillation counter (S4) placed at the beam axis between the two vertex magnets. For p+p interactions at 158A GeV this counter selected a (trigger) cross section of 28.5 mb out of 31.6 mb of the total inelastic cross section. For Pb beams, an interaction trigger was provided by an anti-coincidence with a helium gas-Cerenkov counter (S3) directly behind the target. The S3 counter was used to select minimum bias collisions by requiring a reduction of the Cerenkov signal by a factor of about 6. Since the Cerenkov signal is proportional to Z^2, this requirement ensured that the Pb projectile had interacted with a minimal constraint on the type of interaction. This setup limited the triggers on non-target interactions to rare beam-gas collisions, the fraction of which proved to be small after cuts, even in the case of peripheral Pb+Pb

collisions.

The centrality of the nuclear collisions was selected by use of information from a downstream calorimeter (VCAL), which measured the energy of the projectile spectator nucleons. The geometrical acceptance of the VCAL calorimeter was adjusted in order to cover the projectile spectator region by the setting of the collimator (COLL).

Details of the NA49 detector setup and performance of tracking software are described in [3].

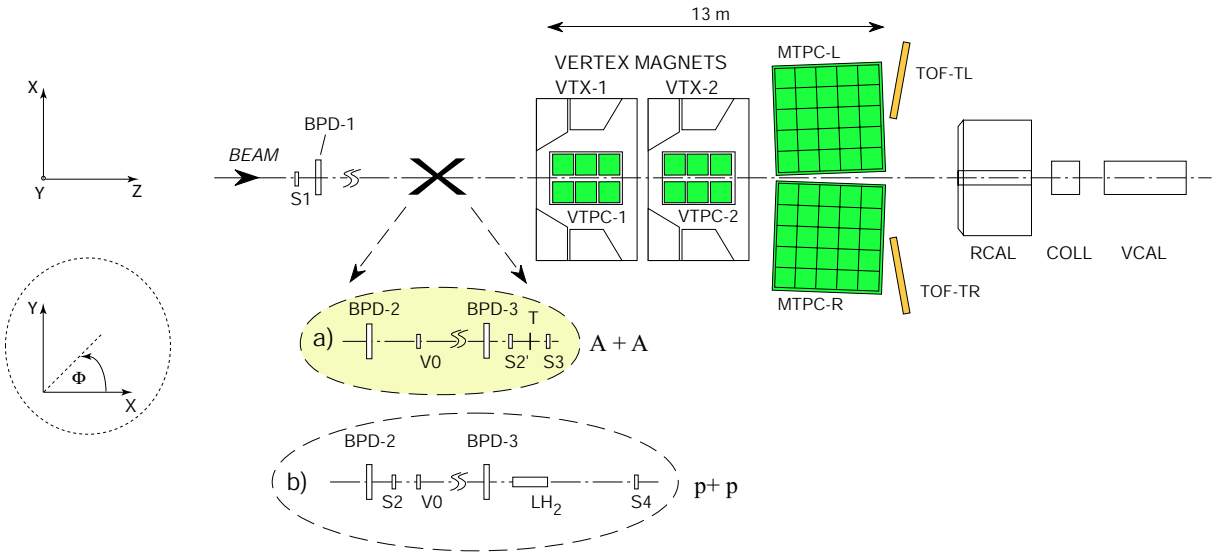

Figure 26: The experimental set–up of the NA49 experiment [3] with different beam definitions and target arrangements.

3.2 NA49 software

The NA49 off-line software consists of tools which provide a framework for data reconstruction, DST production, MC simulation and physics analysis. The main component of the software is the DSPACK package prepared to process data from large HEP experiments. DSPACK provides a simple technique of passing data between the program and the data manager. The interface is identical for FORTRAN and C programs. The basic information about the experiment like: geometry of detectors, magnetic field map, calibration factors and simulation parameters are stored in the NA49 database. The NA49 database is based on the HEPDB package which is part of the CERN software library, has a FORTRAN interface and supports remote access through TCP/IP or AFS. It uses ZEBRA direct access files internally. The database resides on CERN machines and consists of entries:

- DE - geometry database with parameters of MTPCs and VTPCs relevant to reconstruction software
- RU - run database, containing run sheets
- MF - magnetic field, calculated official NA49 field map
- SI - simulation database with parameters of NA49 relevant to GEANT detector simulation.

The interface to HEPDB, based on the DSPACK package, is through the dbman utility for interactive examination and creation of database entries and NA49DB interface , a set of C and FORTRAN callable subroutines to retrieve data. The DSPACK program is usually used in server-client mode especially during the reconstruction process although it can be also used in a local mode. The main purpose of the reconstruction software is to read raw data, reconstruct events and write output in DSPACK format. The reconstruction chain is a collection of several client programs which are run sequentially as a chain. These client programs are used for: cluster finding (DIPT), local tracking (MTRACK PATREC), global tracking (MPAT), momentum fitting (MTRACK, R3D), merging split tracks (REFORM) and finding V0 decays. Samples of raw data files as well as reconstructed events in DSPACK format are stored on disks using the CERN storage manager (CASTOR). DSPACK software is used in the data reconstruction process as well as in the analysis although the user can convert the output from DSPACK into ROOT mini-DST. The conversion makes possible an analysis of experimental data using a modular Object Oriented Framework (ROOT system) with previously prepared NA49 analysis classes . The off-line software contains also two NA49 libraries: T49DST which contains classes that are used for storing DSTs in mini-DST trees and T49ANA which provides all kind of tools to be used in the analysis of mini-DSTs.

The NA49 simulation environment is a collection of several programs which are run sequentially as a chain. The simulation input may be a file in ASCII format from a simple event generator or an output from any model like Venus, UrQMD, Fritiof and others. The geometry of the detector and the transport of particles through the detector use the CERN-developed GEANT 3.21 software. The TPC simulation program MTSIM reads in the output from the NA49 GEANT software, takes TPC MC points and produces digitized data based on the properties of the TPC gas and readout electronics. A simulated event can be superimposed on an actual event by the GTEMBED program for checking the reconstruction efficiency. The reconstruction chain is in principle identical to the one used in the standard reconstruction of raw data. The reconstructed data, in the form of the TPC points and tracks are compared to the GEANT MC data to determine which of the originally generated MC particles were actually reconstructed. This matching procedure produces final MC data.

All parts of the off-line software work on CERN LXPLUS machines under the Scientific Linux system (current version 3.0.6). Data analysis, simulation and other NA49 jobs are usually submitted to LXBATCH, the CERN Public Batch Service. Depending on the load and resource requirements, programs are running on one of 1500 batch farm machines.

The NA49 off-line software has been used for nearly ten years. It proved its usefulness and stability in every stage of preparation of NA49 data and physics results. The NA49-future collaboration plans to use the same off-line software with only minor changes required due to the new detectors added in the experimental setup. It is also planned to use the Central Data Recording (CDR) system for the transfer of raw physics data from the on-line data acquisition system to a mass storage system (CASTOR) instead of writing them on tapes.

3.3 Upgrades for 2007 T2K run

For the first stage of data taking the following modifications or replacements of obsolete equipment of the existing NA49 facility are planned.

3.3.1 TPC and its infrastructure

The Time Projection Chambers are the main components of the NA49 experimental apparatus. There are four TPC modules: two modules, called VTPC1 and VTPC2, are located in line in the magnetic field downstream of the target, two big TPCs, called MTPC-l and MTPC-R, are located behind the magnet on each side of the beam. The operation of a Time Projection Chamber requires filling with an appropriate gas mixture, not containing electronegative additives like oxygen. The level of naturally occurring impurities should be controlled. The system providing the controlled gas mixture to the TPC should assure stability of the gas mixture composition with sufficient purity over long running periods. The gas mixtures selected for the whole NA49 experimental period were: Ne+CO_2 (90:10) for VTPCs and Ar+CO_2+CH_4 (95:5:5) for the MTPCs [3]. The use of the three-component gas mixture was dictated by the need to minimize the charge loss over the long drift distance in the MTPCs. As the charge loss rate in the presence of oxygen traces is proportional to the content of the CO_2, the CO_2 amount was lowered to 5% and methane was added to strengthen the quenching power of the gas. Adding methane was driven by the intention of gaining an additional safety factor in the wire chamber operation. The applied drift fields of 200 V/cm (175 V/cm) correspond to drift velocities of 1.4 cm/s (2.4 cm/s) in the VTPCs and MTPCs, respectively. In this range, drift velocities are unsaturated, i.e. they change almost linearly with electric field. The exact measurement and control of drift velocity and its correction for pressure and temperature variations therefore becomes a key issue to achieve a high quality level of experimental data.

During the whole NA49 experiment (1994-2002) all TPCs performed very well with a very low failure rate. The automated gas mixing/filling system, the drift velocity and gas gain stability monitoring system were well designed and made with high quality. The NA49-future experimental team gained the necessary expertise on the technical aspects of the TPC operation and the TPC gas and high voltage supply systems during the recent test period.

The whole system was made operational in August 2006 for the first time after four years in stand-by. The full gas mixing system was used in all designed modes of operation and using all functions:

- purge with the selected and controlled gas mixture,
- recirculation with the TPC bypass and through the TPC,
- recirculation with automatic control of gas overpressure in the TPCs,
- recirculation with filtering (for the run filters were not regenerated after their last use in 2002),
- monitoring of Oxygen level and humidity in all TPCs,
- activation of the drift velocity monitor (for MTPC-L and VTPC2 only).

During the run period methane was not used because gas flammability monitoring was not available. All TPCs were filled with a two-component gas mixture. The following gas mixtures were employed:

- Ar+CO_2 (90:10) for VTPCs,
- Ar+CO_2 (95:5) for MTPCs.

The nominal drift voltages were applied to all TPCs: 19 kV and 13 kV for MTPC and VTPC, respectively. The applied drift field provided drift velocities which allowed charge collection from the whole TPC depth, thus the whole volume of each TPC was active. The performance of each TPC was measured with three sets of voltages on the wire chambers: low HV, medium HV and high HV. All TPCs performed well for all voltage levels; even for the highest applied voltages the TPCs demonstrated stable medium-term operation (limited by the duration of the test only). For each set of voltages the pulse amplitude and the cluster size were sufficient to obtain good reconstruction quality. The main practical result of the test, which may contribute to the definition of the system parameters for the NA49-future experiment, is that the MTPCs may be successfully operated without methane. Using the two-component (Ar+CO_2) gas mixture gives several advantages: Limited safety problems as no flammable additives are used, a two component gas mixture may be better stabilized over long experimental runs, and the aging of the wire chambers

should be slowed down as methane is not used. The following work has to be done for the 2007 running period.

Although no major upgrade of the gas system is needed, additional parameters should be monitored via the slow-control system, namely:

- oxygen and humidity content,
- gas flow,
- compressor status,
- overpressure in the TPC.

This requires better understanding of the existing slow-control system (both hardware and software) and integration of the readout of the above mentioned parameters into the slow-control system upgrade (see below).

Full revision and servicing of all elements of the gas system is needed. The main items to be processed are discussed in the following. Four compressors need to be serviced, the spare one will be repaired or replaced by a new one. 10 units of gas flow meters/controllers providing the control of the working gas mixture will be re-calibrated (work will be done by the CERN gas service group). Two oxygen sensors will be cleaned; purchasing a spare oxygen sensor should be considered. Two existing oxygen control units will be calibrated. Functionality of the humidity control units should be understood and verified; purchasing of new control units with remote monitoring should be considered. All six gas filters have to be regenerated to provide oxygen cleaning capabilities; the work will be done in the existing NA49 gas cage as the stand for the filter regeneration exists there and is operational. Resources needed: one man month of work, 30 standard bottles of Ar+H_2 (cost of gas about 6000 SFR). Five drift velocity detectors exist and will be used, 3 of them need repair (replacement of broken wire in the single wire counter, two charge amplifiers should be fixed). The status of the gas gain monitor (8 double units) has to be checked. There is a good chance that no intervention will be needed; eventual intervention should not cause technical problems and should be easy to make using existing resources.

Safety issues: One should consider the connection of the gas exhaust of the gas lines of all TPCs to a common system venting the gas outside of the experimental hall. A gas flammability control system should be installed, unless the decision of not using methane for the working gas mixture will be taken.

Laboratory measurements of the drift velocity in Ar+CO_2 mixtures as a function of drift field should be performed for various CO_2 concentrations. This will allow to optimize the TPC operational parameters in the case of the decision of using non-flammable gas in all TPCs.

3.3.2 Slow control and monitoring

The Slow Control system (SC) of the NA49 experiment was developed more than 10 years ago as a set of separate NI LabVIEW v.4.1 based applications. Among them one can distinguish:

- a program for low voltage control and temperature monitoring in TPCs,
- a general program for monitoring TPC related parameters,
- a program for control of the TOF detector,
- a program for monitoring of Beam Position Detectors, Veto Proportional Chamber (VPC), scalers, beam fragmentation, VETO, Ring Calorimeters and Centrality Detector.

It is proposed to base the NA49-future SC system on EPICS2 (Experimental Physics and Industrial Control System). EPICS is a set of open source software tools, libraries and applications developed during more than 10 years. Probably, it is the most mature and reliable platform for detector control system (DCS) development. A two step upgrade procedure is suggested.

First, for the 2007 run it is planned to deploy a new DCS based on EPICS, but with existing LabVIEW applications integrated with it. This integration requires porting of all applications to LabVIEW v.8.x running on PCs with Linux, change of the communication modules to reflect hardware replacements (see below) and addition of network capabilities. This way we keep the existing applications in a new architecture saving at the same time considerable efforts needed for replacing the LabVIEW code with a new one, written in C/C++. Without such an approach it might not be possible to develop new DCS software before the first run planned for October 2007.

Second, for the 2008 run the LabVIEW applications will be coded in C/C++ and will be included into the general EPICS architecture as IOC (Input Output Controllers). The following hardware changes are necessary:

- Replace all MacIntosh computers by one (may be two) powerful PC with 2 processors, running Linux,
- replace CAMAC crate controllers and the VME embedded controller (as they use MICRON dedicated to MacIntosh Nubus) by the modern CAMAC Ethernet Controller C111C manufactured by CAEN and a VME embedded computer with PPC processor (manufactured by CES),
- add to the system a GPIB card by National Instruments.

The total cost of the hardware upgrade is estimated to be 33 kSFR. All necessary work will be done by the group from Warsaw University of Technology.

3.3.3 DAQ

The original NA49 data acquisition system [95] is still functional as was demonstrated in the running period in August 2006. Because the previously used data recording facility based on a SONY DIR-1000 tape drive is no longer available, data will be transferred to the CERN central data recording facility (CDR, CASTOR) instead. Unfortunately, direct access from the data acquisition system to the CDR is not possible because no OS9 software for CASTOR is available.

For the running period in 2007 it is planned to overcome this bottleneck by two minor upgrades of the present network setup.

1. A fast Ethernet connection from the CERN network to the NA49 counting house will be asked for. According to the network group at CERN this is no major operation, because a high-speed connection not far from NA49 already exists.

2. The present FDDI network of NA49 will be extended by an IBM-compatible PC running LINUX. This PC will have two network connections, one for the FDDI network, and the other to the CERN backbone. The FDDI connection can be realized either by using an FDDI network card for the PCI-bus or by using an FDDI to fast Ethernet switch and a standard fast Ethernet network card. The software for receiving data from the OS9-based DAQ system, presently running under AIX, can be easily ported to Linux, because the access to the network layer software is done through TCP/IP sockets. The data transfer to the CDR will be realized through the other network card. Because Linux has no file size limitation unlike AIX and because inexpensive, large-capacity disks are readily available for PCs, a lot of data can be buffered. Therefore it is relatively simple to decouple the reading of data from the DAQ system and the writing of it to the CDR.

Both these upgrades are minor in terms of cost and manpower and will be implemented in summer 2007 by the Fachhochschule Frankfurt group.

The TOF system is read out with the old Aleph Event Builder (AEB) processor. It is too slow for the expected higher event rate in 2008. It also limits the event rate in the 256 time bin mode of TPC running which is planned to be used in the 2007 run. The actual readout time is around 70 ms. With new electronics the TPC readout time will be around 3 ms (see below) and the TOF readout time must be reduced accordingly. This is possible using a copy of the BUDAwall (GTOF) readout system [96]. The TOF and GTOF systems are using the same FASTBUS ADC and TDC units, only the readout part is different. Without block transfer the readout time of the GTOF is 4 ms. Taking into account the largest number of channels and using the block transfer readout mode we can achieve the 3 ms readout time. The required hardware modification of the system consists of replacing the old AEB processor by VME based FIC processors, and changing

the interface cards in the FASTBUS and in the VME crates. The same software as in GTOF with only a small modification can be used.

The required hardware is: one LDA9212 unit and for each of the six FASTBUS creates one FADAP9212 and one FVSB9210 unit.

3.3.4 Beam Position Detectors

The Beam Position Detectors (BPDs) determine the transverse positions of the incoming beam particles. These counters are small (3x3 cm^2) proportional counters with cathode strip readout and are described in reference [3]. The Cracow group is taking responsibility for all tasks related to the preparation and maintenance of the BPDs in the NA49-future project. R&D on a new generation of BPDs and fast FEE readout will be carried out by the Cracow group.

The BPDs were not used in the NA49-future test run. One of four existing BPDs was placed in the beam line. However, this detector was not able to hold HV (due to a broken wire) and was disconnected. So, the present status of the BPDs will be discussed based on their performance during NA49 runs and the results of the laboratory survey.

The performance of the BPDs during the NA49 runs confirmed the validity of the design and the construction. Accuracy of about 100 μm was achieved in the transverse position determination. The FEE matches well to this detector at present beam intensity. The cathode strips show indications of aging.

In order to prepare the BPDs for 2007 running it is necessary to replace the cathode strip planes and perform a source test of the detectors.

In order to prepare the BPDs for running at a factor 24 higher beam intensity it is necessary to:

- investigate the performance of the existing BPDs at higher beam intensities
- study an alternative construction of the BPDs (e.g. GEM detectors)
- perform R&D on new readout electronics to reach the required speed

3.4 TPC readout upgrade in 2008

In order to achieve the event rates and statistics required for the physics program we have to modify the TPC readout electronics. In the present electronics the front end cards are read out in serial mode, 24 cards consecutively. It is possible to change the readout logic to parallel mode. In such a scheme we keep the front end cards and the properties of the chamber readout, using the same sampling and digitization clock frequency. With new electronics after the front end we can achieve the 160 Hz readout rate.

The original electronics was developed 12 years ago. In the meantime technology has changed, now offering larger bandwidth. The modification of the TPC readout control

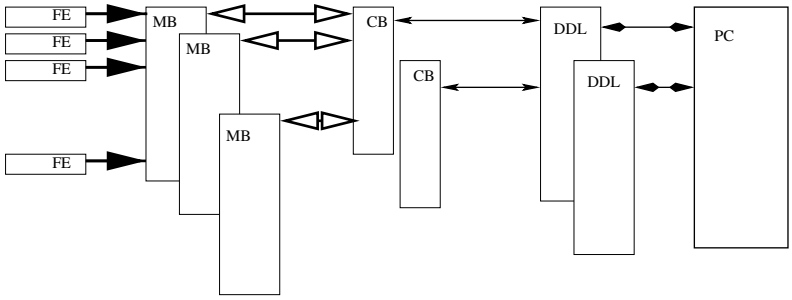

Figure 27: The logical scheme of the proposed TPC readout. FE: Front-end electronics card comprising amplifier, shaper, and digitization. MB: Motherboard. CB: Control board. DDL: Data link.

	kb/event	zero suppressed	Huffman coded
FE card	32*0.5 = 16		
motherboard	24*16 = 384	48	24
control board	10*384 = 3840	480	240
DDL	2*3840 = 7680	960	480
PC	2*7680 = 15360	1920	960
total	5*15360 = 76800	9600	4800

Table 1: Data volume at successive stages of data acquisition from the TPCs.

system necessitates the change of the whole downstream DAQ system (also for the other detector components), because we will be using the same data flow everywhere in the data acquisition system.

	zero suppressed	Huffman coded
motherboard	7.7	4.8
control board	76.8	38.4
DDL	153.6	76.8
PC	307.2	154.0
total	1536.0	768.0

Table 2: Bandwidth in the outputs of successive data acquisition stages at 160 Hz event rate.

We plan to use the system developed for ALICE (see Fig. 27) [97]. We can use the

data transfer system (DDL) from detector to counting house without any change. Our data rate allows us to reduce the number of DDL connections. We can concentrate the data with a small control card, in a way which is totally transparent for the data. This control card contains the connections to the motherboards on the TPCs and to a RCU unit communicating with the card on the PC through a glass fiber. The communication between the control card and motherboard is a standard serial line connection. The motherboards organize the readout, and build the data structure. One motherboard reads out 24 FE cards in parallel, resulting in a gain of a factor of 24 in the readout speed. In the old system 2 or 3 FE cards were connected by the same cable to the motherboard. For the parallel readout we have to change these connections, because of the addressing of the FE cards in a one card to one cable configuration. However, we have to keep in mind, that we may run into some trouble with the re-cabling of the FE cards. Therefore we want to keep the possibility, to use the old configuration and only parallelize the readout of the existing connection cables. This way we can gain a factor of 8 or 12 on the readout speed. Additionally we could reduce the number of the measured time slices from 512 to 256 by halving the clocking rate. This procedure was already used in previous heavy-ion runs of NA49 without significant loss of data quality. The rest of the system will be designed for the maximum speed and event size.

Unit	pieces	price for one unit (SFR)	price (SFR)
new cables to FE			20000
motherboard	183+7(spare)	1750	332500
serial cables	183	30	5490
control board	20+2(spare)	1500	33000
RCU in DDL	20+2(spare)	750	16500
optical fiber	20+4(spare)	160	3840
DDL PCI board	10+2(spare)	1700	20400
PC	5		
total price			431730

Table 3: Cost estimate of the TPC readout upgrade without the PCs

For the planned higher event recording rate we can not store the events in buffers on the boards as was done in the old system. Therefore we have to have the same bandwidth in the full DAQ line. Only after the PC - when writing data to the disk storage - we can profit from the spill structure. The motherboard will perform pedestal subtraction, zero suppression and Huffman coding. In a special mode of operation it can measure the time dependent pedestals.

A sketch of the proposed new system for the TPC readout is shown in Fig. 27.

The Hungarian group is ready to develop and produce the new motherboard and control card. They have the expertise for this job because the same group produced the DDL units for ALICE. For the development a maximum of half a year is required after the go-ahead decision and another 6 months at maximum for the full production after successful testing of the prototypes. We plan to equip one of the MTPC sectors with the new readout for the run in 2007.

The expected data volume at subsequent stages of DAQ is shown in the Table 1, and the expected bandwidth requirement in Table 2. All the used bandwidths are less then the capability of the channels.

The cost of the upgrade is shown in Table 3.

3.5 Upgrades for 2009 ion run

3.5.1 Projectile Spectator Detector

The Projectile Spectator Detector (PSD) will measure the number of non-interacting nucleons from a projectile nucleus in nucleus-nucleus collisions on an event-by-event basis which in turn allows to determine the number of nucleons participating in a reaction. The latter quantity is of key importance in the study of event-by-event fluctuations which are the focus of the future experimental searches for the critical point of strongly interacting matter and of the analysis of the properties of deconfinement.

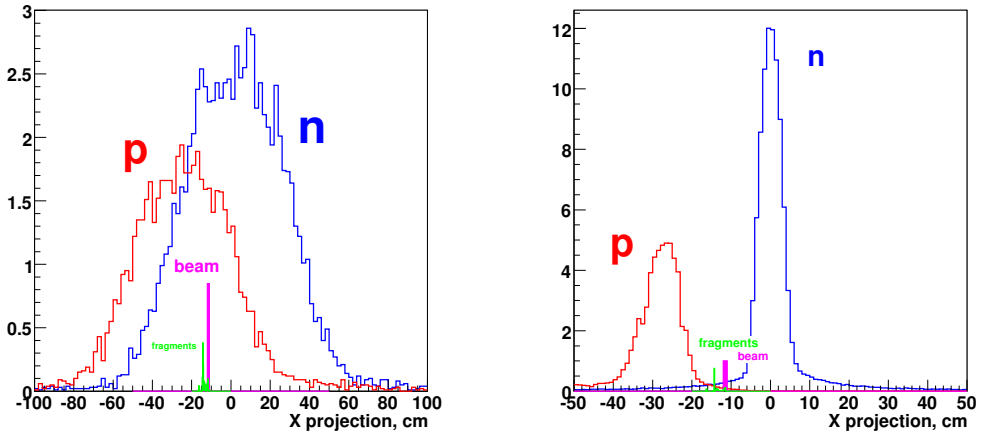

Figure 28: Spectator spot 20 m downstream of the interaction target: projection onto the (horizontal) X-axis for collision energies 10A GeV (left) and 100A GeV (right). The magnetic field is scaled proportional to the beam momentum.

The proposed PSD has two main features which distinguish it from the Zero Degree Calorimeters (ZDCs) commonly used by current heavy ion experiments at CERN and

RHIC. First, it is the large size of the detector which is determined by the spectator spots at the detector position in the required energy range, 10A-158A GeV. As seen in Fig. 28, the dimensions of the spectator spots increase strongly with decreasing energy due to an increasing spread caused by Fermi motion of the projectile spectators. This demands a large front (transverse) size ($\approx$ 2x1 m^2) calorimeter in contrast to compact ZDCs used at higher beam energies. Second, it is the required energy resolution which must be much better than the typical resolution of ZDCs due to the challenging task of a precise measurement of the number of participants.

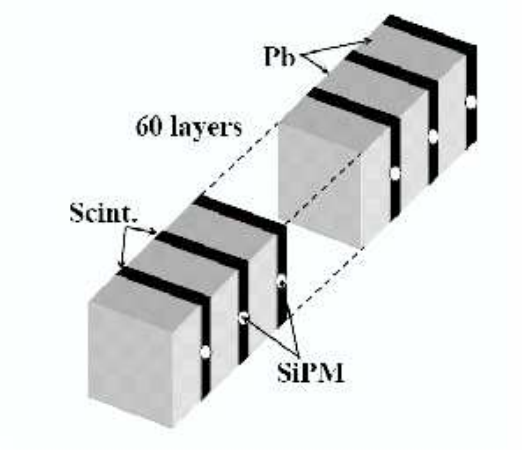

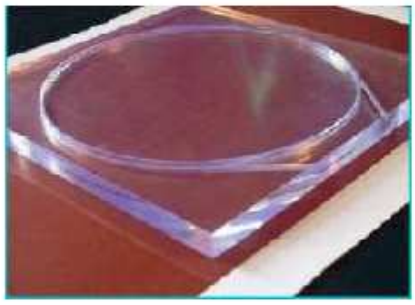

Figure 29: Top: PSD module: Pb:lead absorber; Scint.:scintillator plate with WLS fiber tile; SiPM: silicon photo-multiplier. Bottom: Photo of scintillator plate/WLS-fiber tile unit. The WLS-fiber is inserted in the circular groove and one fiber end is read out by the silicon photo-multiplier.

The main properties of the required detector are:

- a high resolution for measurement of the total energy of the projectile spectators

$(\sigma(E)/E < 50/\sqrt{(E)})$ in a very broad energy range from 10 GeV to 30 TeV which should lead to a low uncertainty in the determination of the number of interacting nucleons even for peripheral collisions of heavy nuclei at low energies (below 10% for Pb+Pb collisions with 20 participant nucleons),

- a modular design, which should allow to optimize the detector geometry in accordance with the requirements defined by the collision energy as well as the target-PSD distance and the magnetic field used in the experiment, and provide the necessary reduction of systematic errors due to non-uniformity and leakage,
- a high granularity of the energy measurement, which will enable the separation of different contributions (protons, neutrons, fragments) and should allow the determination of the event reaction plane.

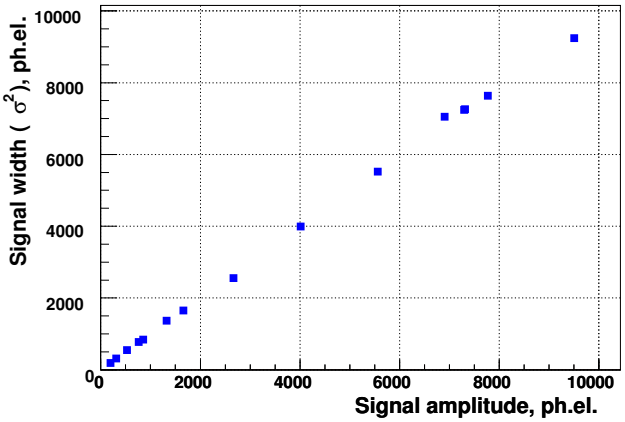

Figure 30: The dependence of the signal width in number of photo-electrons on the signal amplitude. In case of linear response the square of the signal width (square of sigma) must be equal to the signal amplitude if both parameters are measured in terms of the number of photoelectrons. A MAPD with size 3x3 mm^2 and number of pixels 10^5 was used in this measurement.

Challenging energy resolution, transverse uniformity as well as linearity and Gaussian shape of the detector signal are the critical parameters for the appropriate detector design. These requirements mandate a specific type of PSD, namely, the compensating hadron calorimeter. The concept of compensating calorimetry was intensively developed during the last years based on the understanding of the physical processes inside the hadron shower. The hadron shower in an absorber consists in reality of two components, one electromagnetic (e) and the other pure hadronic (h). The former originates from neutral pions produced in nuclear interactions and is the dominant source of the fluctuations.

The energy sharing between the e and h components can be very different from event to event and depends mainly on the nature of the first interaction, which will produce (or not produce) π^0s. The equalization of the calorimeter response to the e and h components ($e/h = 1$ or compensation concept) eliminates one of the dominant sources of the energy fluctuation and hence improves the energy resolution of the calorimeter. The other advantages of compensating calorimeters are the linearity and the Gaussian shape of the detector signal. This concept was initially applied to uranium calorimeters and then generalized. Now this approach is successfully applied to calorimeters with iron and/or lead absorbers [98]. It was shown, that the compensating condition ($e/h = 1$) depends on the relative absorber/active medium thickness ratio and equals Fe:Scintillator=20 for iron absorber and Pb:Scintillator=4 for lead absorber. The lead/scintillator calorimeter is rather attractive due to the smaller compensating ratio and consequently smaller sampling fluctuation of the shower.

These general considerations were confirmed experimentally during the last few years. At present, there exist a few compensating lead/scintillator calorimeters with rather promising energy resolution [99, 100]. These designs together with preliminary Monte Carlo simulations indicate that the compensating lead/scintillator calorimeter meets all the requirements of our project and might be cheap enough in spite of the rather large required size.

The above considerations allow us to summarize the parameters of PSD modules as follows:

- energy resolution $< 50\%/\sqrt{(E)}$,
- transverse non-uniformity of the light collection $< 5\%$,
- full functionality in the energy range 10-30000 GeV,
- transverse dimensions of a single PSD module: 10x10 cm^2,
- longitudinal segmentation: 60 layers of lead and scintillator,
- lead thickness of one layer 16 mm,
- scintillator thickness of a single layer 4 mm,
- total length of a single module 120 cm (6 nuclear interaction lengths).

The sketch of one PSD module is shown in Fig. 29. About 200 modules are required to fully cover the spectator spot at 10A GeV beam energy. The necessary number of modules are about 2 times less at beam energy larger than 15 GeV.

The key challenge in the development of the PSD detector is to devise a reliable method of light readout. Traditional use of WLS plates and/or fibers coupled to PMTs has a couple of problems, namely: Cherenkov radiation in plates/fibers, nuclear counting

effect in PMTs, and problems with light transport over a long distance (attenuation length, radiation effect, mechanical instability, etc.). Presently, the most advanced technique is the use of scintillator tiles with embedded WLS-fibers. This ensures uniformity of light collection across the scintillator within a few percent. Direct light readout could be done by Micro-pixel Avalanche Photo-Diodes (MAPDs) coupled to the end of the fiber where it exits the scintillator tile. MAPDs are rather novel devices with very promising properties [101]. They are avalanche photo-diodes working in Geiger mode with internal gain up to $\approx 10^6$. MAPDs have very compact dimensions, typically a few millimeters. Due to the pixel structure, MAPDs have no nuclear counting effect, are sensitive to the single photo-electron signal and have remarkable energy resolution even for a few photo-electron signal. The technology of MAPD production and their parameters have rapidly improved. Presently there are a few experimental setups that use MAPDs for the light readout [102] including the hadron calorimeter prototype for the future International Linear Collider project.

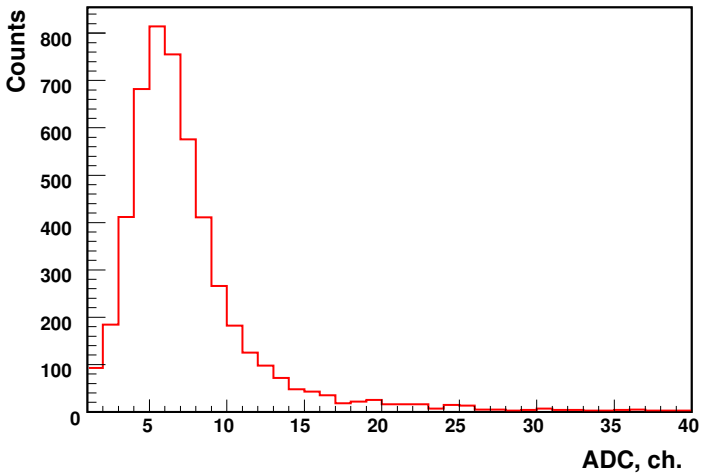

Figure 31: Typical ADC spectrum from muon signals in one section of the PSD prototype module.

One of the serious problems in using MAPDs for calorimetric purposes is the limited dynamical range of these devices that is determined by the pixel structure. If the number of the photons is compared with the number of pixels, then the probability to hit one pixel with two or more photons increases with intensity, while the amplitude of the output signal depends only on the number of fired pixels. This leads to the nonlinear MAPD response (signal saturation) at large amplitudes. As follows from theoretical considerations, the degree of nonlinearity depends on the ratio of the number of photons to the number of pixels. The non-linearity problem is successfully solved with MAPDs having a pixel

density of about $10^4/mm^2$. For a MAPD of 3x3 mm^2 size, the number of pixels reaches 10^5 ensuring the appropriate dynamical range even for high energy calorimetry. The linearity of such a MAPD was measured by irradiating it by light from a diode with variable intensity. As seen in Fig. 30, the linearity is preserved up to 10^4 photons.

To check the performance and reliability of the proposed concept of the PSD calorimeter, a first module prototype was assembled at INR, Moscow. The PSD module is longitudinally divided into 10 sections with individual readout by Micro-pixel Avalanche Photo Diodes (MAPDs). Each section consists of 6 lead/scintillator layers with thickness of about 0.6 nuclear interaction length.

In August 2006 the first beam test of the PSD prototype was performed at the CERN SPS. During the beam test the calibration of each readout channel was done with the muon beam. The typical ADC spectrum obtained from muon signals in one section is shown in Fig. 31. The peak of the ADC spectrum corresponds to a light yield of about 10 photo-electrons/MIP/section or 2 photoelectrons per MeV.

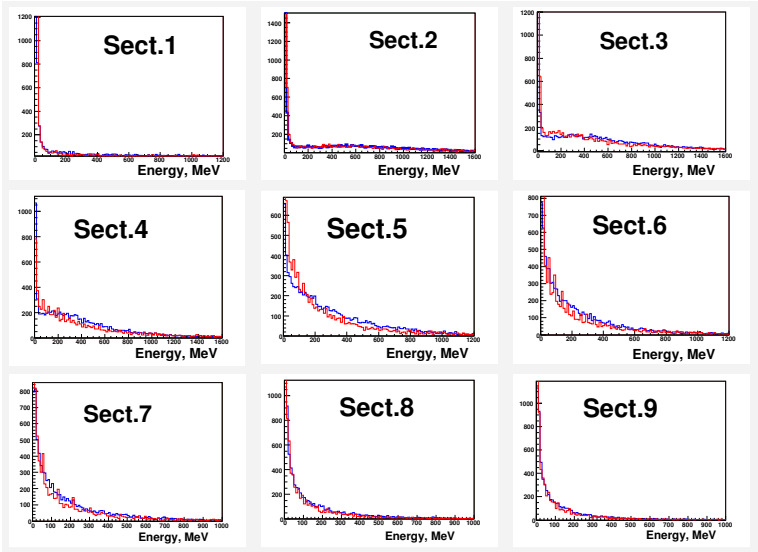

Figure 32: Energy spectra in different sections of the PSD prototype module. Red line: experimental distribution for 150 GeV pions, blue line: Monte Carlo simulation for 150 GeV pions.

After calibration, the energy deposition from pions was determined in each section. The signal amplitudes reflect the longitudinal profile of the hadron shower. Fig. 32 presents the energy spectra in different sections of the PSD module. As seen, the shapes of the energy distributions are in good agreement with the MC predictions.

Fig. 33 shows the total deposited energy in the PSD module for a few beam energies. In this case, the energy depositions in all sections were summed up with the appropriate

normalization coefficients obtained from the calibration with muon beam. The beam profile at the module face affects strongly the shape of the deposited energy distributions. This effect is not yet taken into account in the MC simulation.

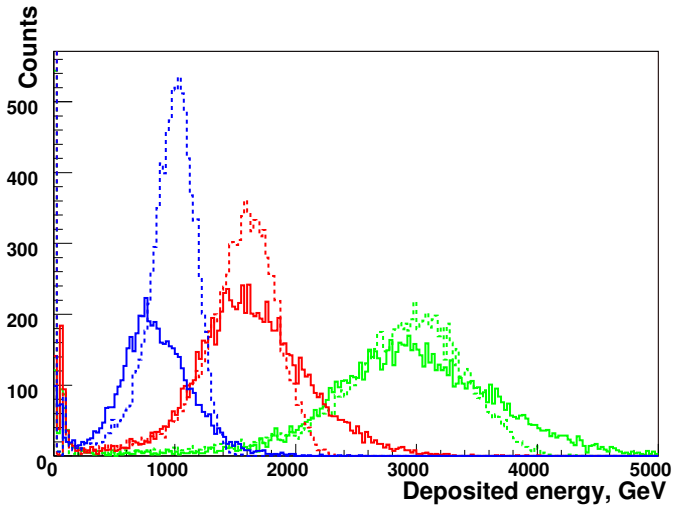

Figure 33: Spectra of deposited energies (sum of longitudinal sections) in the PSD module for different pion beam energies. Solid histograms show experimental distributions, dashed histograms the MC predictions. Colors distinguish the different pion beam energies: green corresponds to 150 GeV, red to 80 GeV, blue to 50 GeV. Beam profile at the module face is not taken into account in the MC simulation.

Further development of the PSD needs detailed simulation including realistic beam conditions, detector geometry and hadron shower propagation in the calorimeter. The optimization of the detector dimensions as well as of the longitudinal module segmentation must be done. In principle, the readout of the PSD module might be performed by a single PMT reducing the cost of the detector by a factor of about 1.5. In this case the nuclear counter effect in the PMTs must be studied additionally. Also, the lack of longitudinal segmentation narrows the possibility of hadron shower reconstruction and separation of secondary particles in the PSD. In summary, the proposed concept of the PSD as a full compensating lead/scintillator calorimeter seems to be realistic and satisfies all the requirements of our project.

3.5.2 He beam pipe

Introduction

Channeling of the high intensity heavy ion beam through the gas volume of the VTPCs has limitations when compared to the proton beam. δ-electrons produced in the gas volume

between the two separated drift field cages inside the VTPCs from beam-gas interactions could easily "leak" into the active area, forming a fluctuating background. The NA49 studies show that this background, if high enough, leads to a significant distortion of measurements of event-by-event fluctuations. A typical Pb beam intensity used by NA49, 10k ions per second, is still acceptable for the fluctuation measurements.

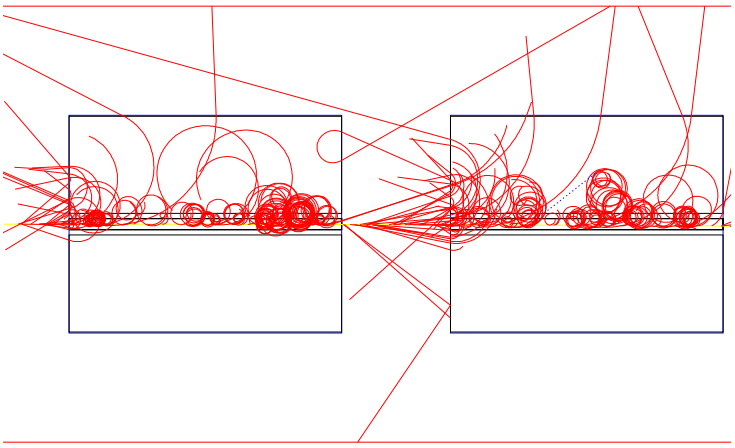

Figure 34: Tracks of δ-electrons produced by a single In ion at 10A GeV traveling along the beam line through the NA49 VTPCs.

In order to saturate the high speed DAQ of NA49-future an increase of ion beam intensity by about a factor of 20 will be necessary. Therefore a corresponding reduction of the δ-electron yield is obligatory. This can be achieved by the introduction of a low mass beam pipe. For illustration of the problem δ-electron tracks originating from a single In nucleus of 10A GeV traversing the NA49 VTPCs are shown in Fig. 34. In NA49 the VTPCs were filled with Ne/CO_2 gas mixture and were separated by an air-gap. A schematic NA49 magnetic field map was used for the simulation.

Two options for a self-supported beam pipe are briefly discussed:

- vacuum glass fiber (kevlar) rigid beam pipe,
- helium/nitrogen filled mylar beam pipe.

Both pipes are assumed to be placed in the gap between the separate field cages inside the VTPCs. They are similar in their design and mounting procedure and are using the same interface to the VTPC gas envelope. Basic properties of the rigid glass fiber beam pipe with 2 mylar (input and output) windows are:

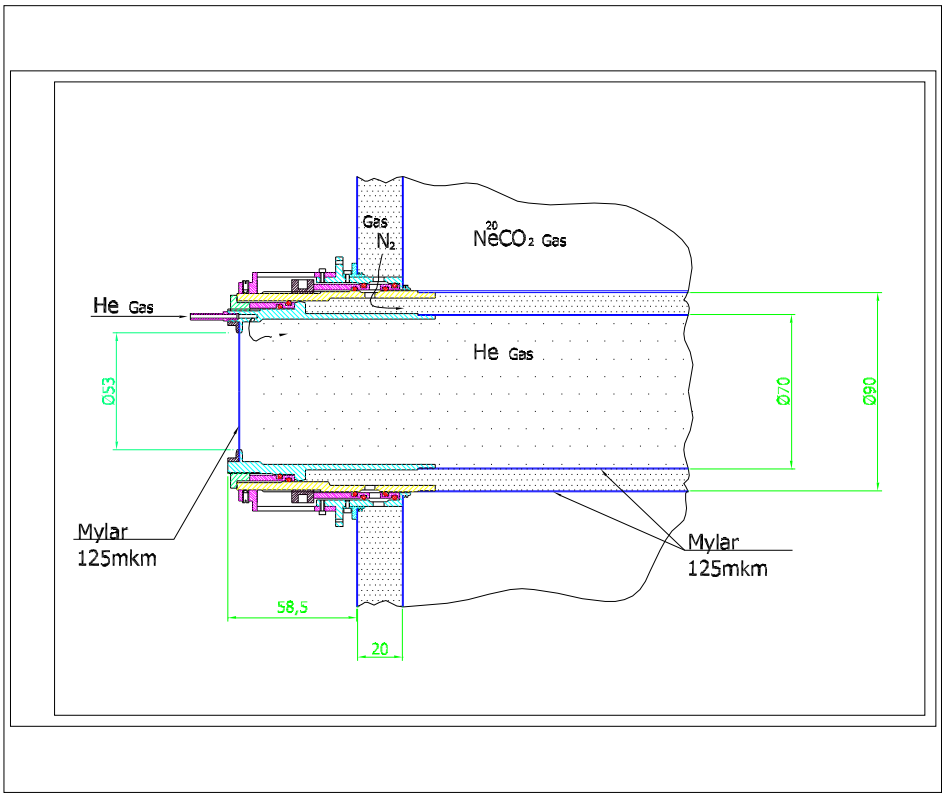

Figure 35: The interface unit of the helium/nitrogen beam pipe.

- GEANT simulations show the required reduction of δ-electron yield for 0.1 bar pressure inside the tuber; thus rather poor vacuum is sufficient,
- an insulated glass fiber tube does not influence the VTPC performance (no distortions of the drift field, no contamination of the VTPC gas),
- the mechanical stability of the beam pipe requires (even for the poor vacuum) 2 mm wall thickness for the beam pipe of 70 mm diameter.

The helium/nitrogen filled (normal pressure) thin wall self-supported pipe has the

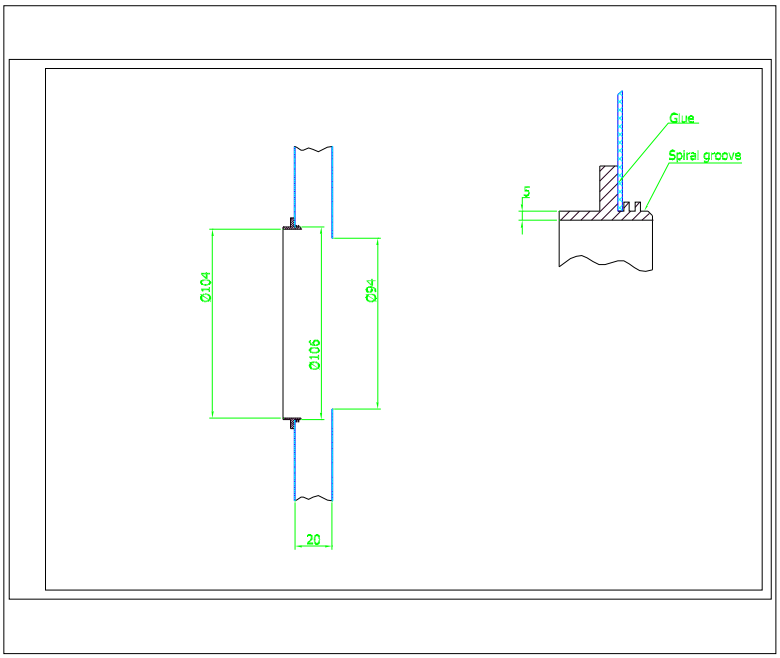

Figure 36: The beam-pipe/gas-envelope interface unit and gas input manifold for the 70 mm helium/nitrogen beam-pipe.

following features:

- an inner helium filled pipe is surrounded by a protective layer of nitrogen,
- a very low mass; 125 μm mylar walls are enough,
- a relatively simple design and construction.

Due to significantly lower mass it is suggested to construct the helium/nitrogen beam pipe. Furthermore it is planned to introduce an additional helium pipe in the gap between VTPC1 and VTPC2.

The design of the main interface unit of the helium/nitrogen pipe is shown in Fig. 35. The main inner beam pipe is formed by the ultrasonic welding of 125 μm mylar sheet. The ends of the pipe are then glued to short low-mass glass-fiber cylinders with mylar

windows. These input/output windows for the beam particles provide also the hermetic volume for the helium gas. The beam-pipe/gas-envelope interface unit (see Fig. 36) is the multi-functional module that provides a number of important functions: low-mass support and beam pipe fixation, separation of gases, hermetic sealing. An important feature of the proposed design is that it foresees the use of the same N_2 gas supply as for the VTPC gas envelope.

The beam pipe assembly and integration with the VTPCs will consist of the following main steps:

- cutting a circular window in the external mylar VTPC wall and gluing of the first interface ring to this wall,
- slight pressurizing of the VTPCs to meet "clean room" conditions during this and all next in-site procedures listed below,
- fixing of the first interface ring to the corners of the VTPC frame by using 4 fishing lines,
- gluing of the second interface ring of this "entrance" beam-pipe/gas-envelope interface unit to the the inner VTPC mylar wall,
- testing hermeticity of glued joints of the beam-pipe/gas-envelope interface unit with the use of dummy end-caps inserted instead of the beam pipe,
- assembly of the mylar inner beam pipe for helium and the outer mylar pipe for N_2 protective gas and hermeticity tests of the unit,
- insertion of the beam pipe in the working position (the diameters of "the entrance" and "the exit" beam-pipe/gas-envelope interface units are slightly different in order to allow easy insertion of the beam pipe from one side of the VTPC,
- fixation of the end-units of the beam pipe and their hermetization using viton o-rings,
- final tests of hermeticity.

Geant simulations were performed for the δ-electron tracks produced by a single In ion at $10A$ and $158A$ GeV for several relevant configurations. The results are summarized in Table 4. As one can see, the helium/nitrogen beam pipe reduces the δ-electron load of the VTPCs by a factor of about 10. The results for the vacuum beam pipe (0.1 bar pressure), not shown in Table 4, are found to be very similar to and not significantly better than the results for the helium/nitrogen beam pipe (normal pressure). This suggests that the better choice is the helium/nitrogen beam pipe as, in addition, it is a very low mass solution.

Note that the number of δ-electrons per In ion in NA49-future will be lower by a factor of about 17 in comparison to the corresponding number in NA49 per Pb ion. The additional factor of 1.7 is due to the lower charge of In ions.

Gas in BP+G	E=160A GeV			E=10A GeV		
	Beam pipe	VTPC1	VTPC2	Beam pipe	VTPC1	VTPC2
Ne+Air	133	8	10	125	41	50
He+Air	51	5	7	12	16	49
Ne+He	95	3	4	90	33	40
He+He	16	1	1	15	5	6

Table 4: The mean number of δ-electron tracks contained in the volume of the beam pipe ("Beam pipe") and reaching the active volume of one of the VTPCs ("VTPC1" and "VTPC2") produced by a single In ion at 160A and 10A GeV traversing the detector. The results are obtained using GEANT simulation and assuming different gases in the beam pipe ("BP") and in the gap between the VTPCs. The standard NA49 running conditions correspond to "Ne+Air", whereas the proposed helium/nitrogen beam pipe to "He+He".

3.5.3 Enlargement of the tracking acceptance

Although the acceptance of the NA49 TPCs is rather large (about 2π below 2 GeV/c transverse momentum), upgrades aiming to increase the acceptance in NA49-future runs are under discussion. The upgrades of the acceptance in the forward and backward hemi-spheres (in the c.m. system) are considered separately due to different track density and topology.

The NA49 TPCs covered a large fraction of the forward hemi-sphere, whereas their acceptance is poor in the backward hemi-sphere, where a detector covering a large solid angle is needed. Together with the CERN PH DT2 detector group the NA49-future collaboration started R&D of such detector with the final goal to increase the acceptance in the backward region. A minimum solution is a single layer detector for a measurement of charged particle multiplicity. The prototype of such a detector was successfully tested in the test run in August 2006. It is a semi-cylinder surface shaped GEM detector shown in Fig. 37, and represents the first prototype of a drift chamber with non-planar GEM readout. Such a semi-cylindrical detector surrounding the target can measure the multiplicity of produced particles in the event, and can provide a specific energy loss value for each particle. A multi-layer detector can be considered for measurements of particle charge and momentum.

An increase of the azimuthal acceptance can be achieved by reducing the gap between the sensitive volumes of the left and right readout chambers of the VTPC-1 and VTPC-2

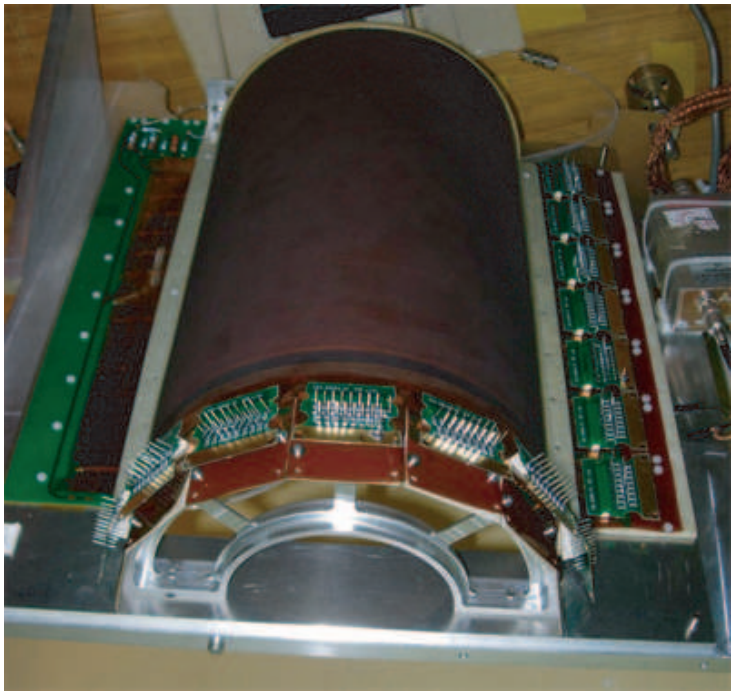

Figure 37: The semi-cylindrical GEM prototype detector tested in the NA49-future test run in August 2006.

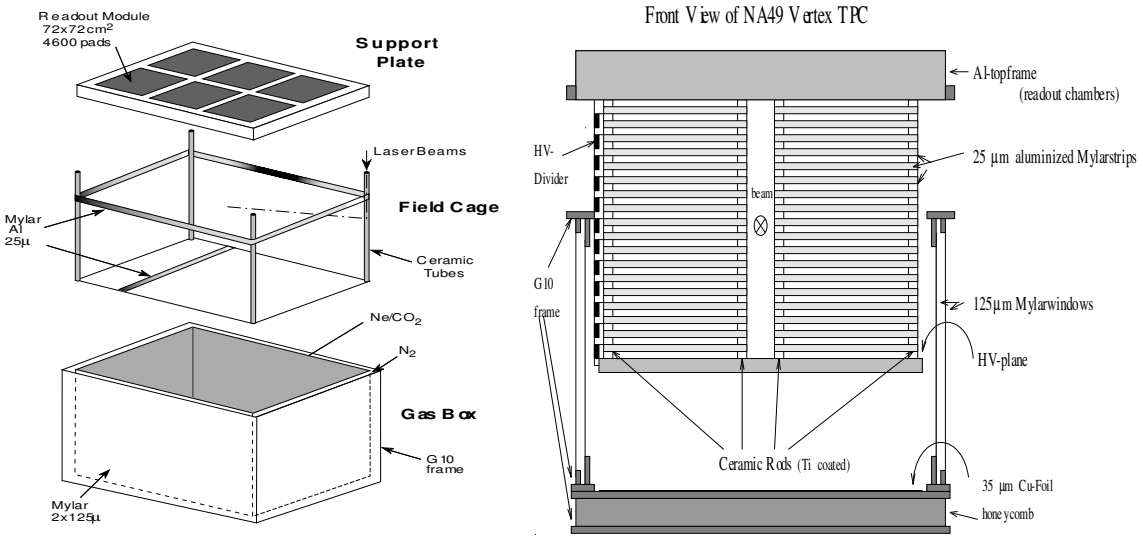

Figure 38: Schematic view of the Vertex TPCs mechanical construction.

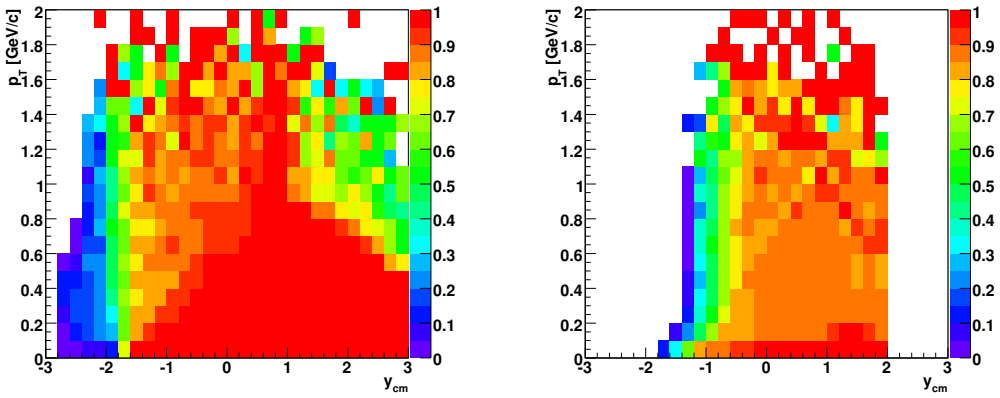

Figure 39: Geometrical acceptance in transverse momentum and rapidity of the TPCs after modifications of the geometry for collisions at 158A GeV (left) and 20A GeV (right). The beam and target rapidities are ± 2.91 and ± 2.08 at 158A and 20A GeV, respectively. The fraction of accepted vertex pions increases in comparison to the NA49 TPC configuration by $\approx$20% at 158A GeV and by $\approx$50% at 20A GeV.

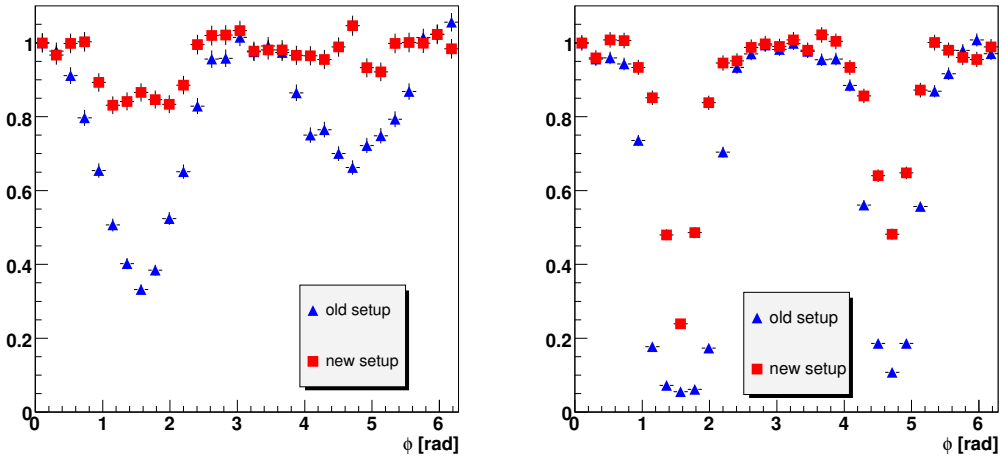

Figure 40: Geometrical acceptance in azimuthal angle for the rapidity interval $-1 < y < 0$ after (squares) and before (triangles) modification of the TPC geometry for collisions at 158A GeV (left) and 20A GeV (right).

detectors (see Fig. 38 for details of the vertex TPC construction) from about 25 cm to 9 cm and moving the target closer to VTPC-1 (by about 60 cm). This requires a significant

mechanical effort. The geometrical acceptance for charged vertex pions resulting from this modification is shown in Figs. 39 and 40 for collisions at 20A and 158A GeV. In Fig. 40 the new acceptance is compared with the acceptance of the standard NA49 setup. The fraction of registered vertex pions will be ≈75% and ≈90% for collisions at 20A and 158A GeV, respectively.

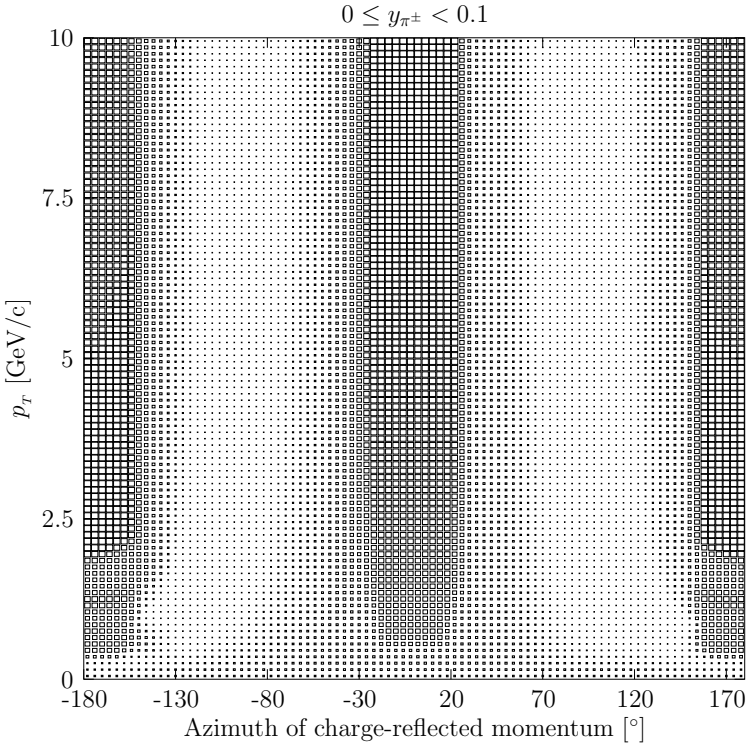

Figure 41: Number of points left in the detector by particles as a function of momentum (around mid-rapidity), for collisions at 158A GeV. The maximum box size corresponds to 234 points. The missing (or poor) azimuthal domain is well visible.

Another possibility to increase the acceptance in azimuthal angle is to introduce a new detector: e.g. a small TPC chamber (possibly with GEM readout), which would be situated between VTPC1 and VTPC2 or in front of VTPC1 to fill the vertical acceptance gap. The chamber may consist of two halves, placed below and above the beam-line.

The upgrading of the forward hemisphere would also be important for the p+p/p+A physics: by extending the available azimuthal domain at high transverse momentum, one could gain more statistics for the p+p and p+A reference data. The need for such a detector can be demonstrated by the acceptance at mid-rapidity, shown in Fig. 41. It can be observed, that it would be desirable to improve the azimuthal coverage at high transverse momentum.

4 Physics Performance

4.1 Neutrino and Cosmic-Ray Physics Needs

In NA49 the TPCs perform the task of measuring the trajectories of particles and contribute to the particle identification (PID) by dE/dx measurements. A time-of-flight (TOF) measurement system supplements the PID. In particular, the TOF provides a good measurement of the PID in the non-relativistic regime where the dE/dx versus p curves of pions, protons, and kaons cross.

The acceptance of the Main TPCs and TOF detectors of the NA49 facility in the $p - \theta$ plane is shown in Fig. 42 for the magnetic field configuration used in running at 40A GeV. The identification of charged pions, kaons and protons by use of the dE/dx measurements in the MTPCs is possible for $p >$ 3 GeV/c. At lower momenta ($1 < p <$ 3 GeV/c) the identification is performed on the basis of the TOF information. Comparing the acceptance needed for neutrino physics shown in Fig. 5 with the NA49 acceptance (Fig. 42), one notes that the NA49 TPC is very well suited for the reference measurements required by the neutrino program. Full coverage of the T2K phase space by the TOF at low momenta and large angles can be achieved by lowering the magnetic fields in the two magnets and/or moving the target between the two vertex TPCs. These different options are being considered including the possibility of extending the TOF coverage by adding additional TOF scintillator bars.

The acceptance needed for the measurements motivated by the cosmic-ray physics is shown in Fig. 7. It is almost fully located in the forward hemisphere, $y > 0$, where y denotes the pion rapidity in the center of mass system. In Fig. 49 (below) the rapidity spectra of identified hadrons measured at the SPS energies (20A-158A GeV) are presented. For all hadrons and at all energies the NA49 acceptance matches requirements of the cosmic-ray experiments.

Running Time

With the present performance of the NA49 DAQ the maximum number of events which can be recorded per spill is about 60. Using a typical duration of 18 s for the cycle length of the SPS, the requirement of 2×10^6 triggers per setting, and an efficiency of the SPS of about 80% one requires about 10 days to obtain the statistics for one setting. After the stage II TPC DAQ upgrades the running time for a single configuration will be reduced to 1-2 days.

As the initial T2K runs are foreseen with 30 GeV/c protons we propose to start our measurements in 2007 by a one month run at 30 GeV/c. This will allow to collect basic data with two different target thicknesses. It will also include a setting-up period, and runs needed to study calibration and backgrounds. The further data on proton and pion interactions on carbon target required by cosmic-ray (at 30-400 GeV/c) and neutrino (at

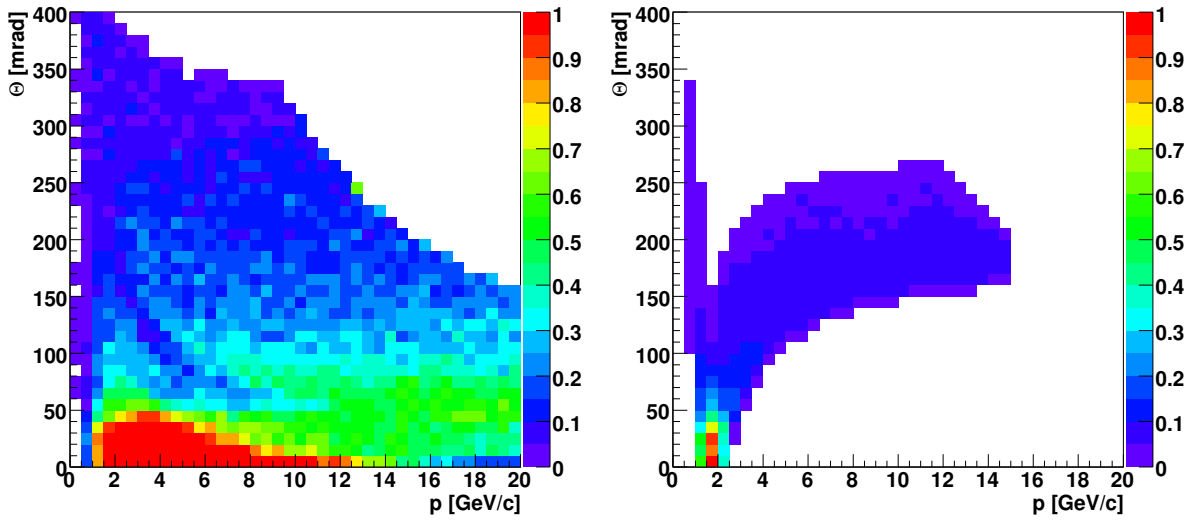

Figure 42: The acceptance of NA49 TPC (left) and TOF (right) detectors in the p,θ plane for hadrons for the 40A GeV magnetic field configuration. The color shading indicates the relative acceptance of the detector at a given point in phase space.

40 and 50 GeV/c) physics will be taken in 2008 after the increase of the event collection rate.

Conclusions

The NA49 detector is well suited to measure with high precision the identified hadron yields under conditions relevant for the T2K beam line as well as for the cosmic-ray experiments. The measurements can be performed with only minor additions to the existing detector. There is a significant overlap between the data required by the neutrino and cosmic-ray experiments. The time scale is such that these measurements can be available at the start-up of T2K. These measurements would form an important contribution to the T2K (neutrino) as well as KASCADE and Pierre Auger Observatory (cosmic-ray) experiments. They would provide a valuable addition to the present European efforts, *e.g.* the construction of the near detector (T2K) and the construction and running of the cosmic-ray experiments.

4.2 Reference p+p and p+A data

The detector upgrades planned for the stage II of data taking will result in an increase of the event rate by a factor of about 24 compared to the standard NA49 data rate. Thus

within one month of p+p running at 158 GeV about $60 \cdot 10^6$ events will be registered. This will extend the p_T coverage for identified hadrons to $\approx$4 GeV/c. Furthermore it will be possible to perform the energy scan with p+p and/or p+A collisions (6 energies as in the case of ion running) within 4 weeks of proton running (about $6 \cdot 10^6$ events per energy).

4.3 Onset of deconfinement and critical point

The performance of the fully upgraded (after stage III upgrades) NA49-future experiment with respect to physics of nucleus-nucleus collisions will be qualitatively improved in comparison to the performance of NA49. The increase of data taking and event rate by a factor of 24 will allow for a comprehensive two-dimensional scan in collision energy and mass of the colliding nuclei. The construction of the projectile spectator detector will increase the accuracy of determination of the number of projectile spectators by a factor of about 20.

In the following the NA49-future performance with respect to the event samples and statistics, centrality determination as well as acceptance will be presented.

Event samples and statistics

Three runs with ion beams are planned in the subsequent three years (2009-2011). Collisions of In+In (first year), Si+Si (second year) and C+C (third year) at 10A, 20A, 30A, 40A, 80A and 158A GeV will be registered. Each run will be 30 days long. Thus there will be 5-day long running time for a given reaction (energy and system size).

The 5-day long sub-runs will be organized as follows. The first day will be devoted to the proper (energy dependent) configuration of the PSD as well as to setting-up the beam and trigger. The second day will be used to take calibration data, target-out events and beam-trigger events. $2{\cdot}10^6$ of the 5% most central events selected by the PSD energy will be registered during the third day. The remaining two days will be used to collect $4{\cdot}10^6$ minimum bias events.

The statistical error on the measure of transverse momentum fluctuations, Φ_{p_T} is shown in Fig. 43 as a function the collision energy and the system size. The expected number of $2{\cdot}10^6$ events for each reaction was assumed. The statistical errors measured by NA49 were propagated using the known dependence on the number of particles and events. For 10A GeV a smooth extrapolation from higher energies was used. The expected errors are about 0.1 MeV and thus much smaller than the predicted increase of Φ_{P_T} in the vicinity of the critical point [87].

The scaled variance of the multiplicity distribution is expected to increase by about 10 % [74] in the vicinity of the critical point. The expected statistical errors of the scaled variance for the 1% most central collisions (as used in the multiplicity fluctuation analysis by NA49) is smaller than 0.5 %.

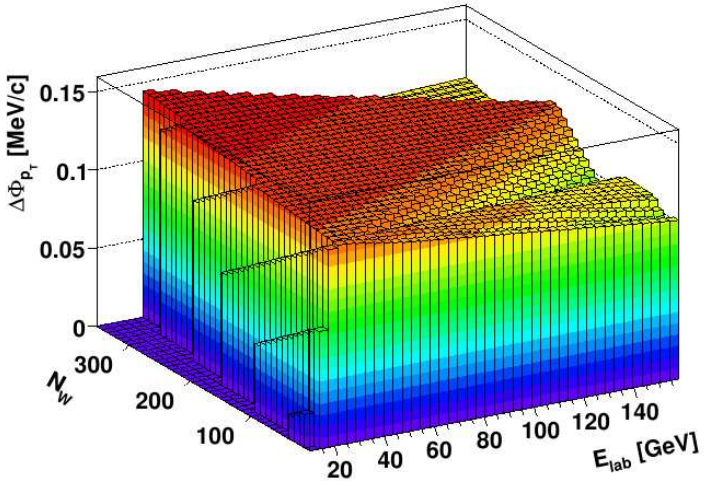

Figure 43: Expected statistical error of the Φ_{p_T} measure of fluctuations for $2{\cdot}10^6$ events as a function of the collision energy and system size.

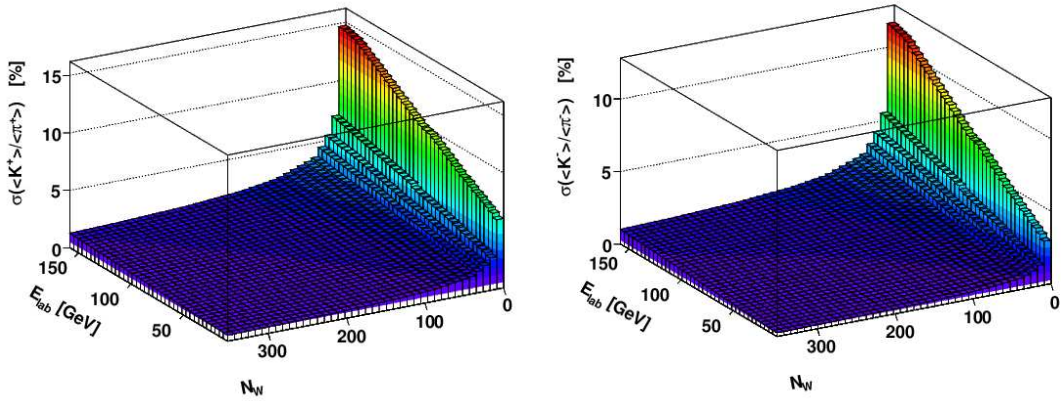

Figure 44: Expected statistical error of the $\langle K^+\rangle/\langle\pi^+\rangle$ (left) and $\langle K^-\rangle/\langle\pi^-\rangle$ (right) ratios for $2{\cdot}10^6$ events as a function of the collision energy and system size.

The expected statistical error of the $\langle K^+\rangle/\langle\pi^+\rangle$ and $\langle K^-\rangle/\langle\pi^-\rangle$ ratio for the 5% most central collisions is shown in Fig. 44 as a function of the collision energy and system size. The errors measured by NA49 were propagated to the domain of the NA49-future measurements. The assumed number of events is $2{\cdot}10^6$. The magnitude of the "horn"-like

structure in the $\langle K^+ \rangle / \langle \pi^+ \rangle$ ratio measured by NA49 is about 30 %, which is significantly larger than the statistical error of the future measurements. Note that the requested number of p+p interactions is $6{\cdot}10^6$ per energy and thus the statistical error for these reactions will be smaller by a factor of about 1.7 than the error shown in Fig. 44.

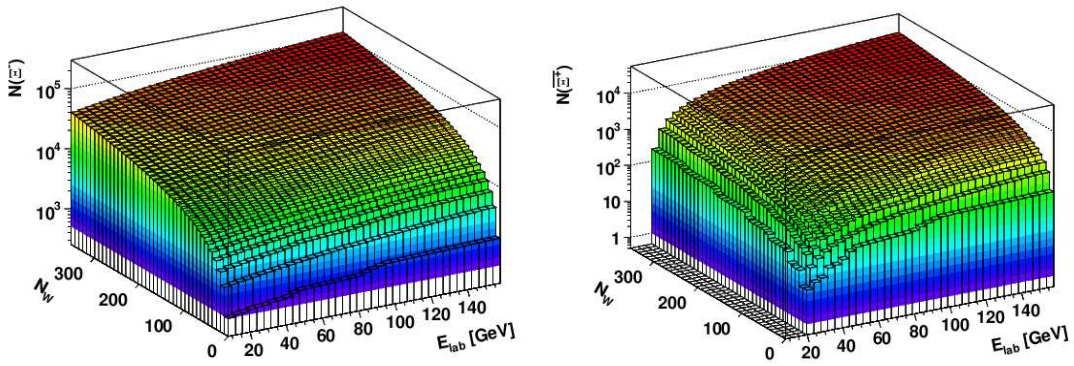

Figure 45: The expected number of reconstructed decays of Ξ^- (left) and $\overline{\Xi}^+$ (right) hyperons for $2{\cdot}10^6$ events as a function of the collision energy and system size.

The expected number of reconstructed decays of Ξ^- and $\overline{\Xi}^+$ hyperons for the 5% most central collisions is given in Fig. 45 as a function of the collision energy and system size. Again the numbers measured by NA49 were extrapolated to the NA49-future domain assuming $2{\cdot}10^2$ events for each reaction. The measurements of Ξ^- and $\overline{\Xi}^+$ hyperons is essentially background free and thus the number of counts directly determines the statistical error. The plots demonstrate the feasibility of measuring Ξ^- production for all considered reactions. However, measurements of $\overline{\Xi}^+$ production will be possible only inside the "island" of large systems and energies (see Fig. 45 right).

Future measurements of In+In collisions at 10-158A GeV should allow to establish the energy dependence of elliptic flow for mesons (charged pions and K^0_S mesons) and baryons (protons and Λ hyperons). The statistical resolution will be increased by a factor of about 2 in comparison to the NA49 results at 40A GeV and the systematic error will be reduced due to lower track multiplicity and lower background. In order to quantify the significance of the expected data the NA49 results on Λ elliptic flow obtained from a high statistics ($3 \cdot 10^6$ events) sample of Pb+Pb collisions at 158A GeV were used (see Fig. 46). The Λ multiplicity in In+In collisions is expected to be about half of that in Pb+Pb interactions, and approximately energy independent in the SPS energy range like in Pb+Pb collisions. Thus the expected Λ multiplicity in $2 \cdot 10^6$ In+In events will be close to the Λ multiplicity in $1 \cdot 10^6$ Pb+Pb collisions. The results obtained from this statistics are also plotted in Fig. 46 to illustrate the feasibility of the Λ hyperon flow measurements in the future study.

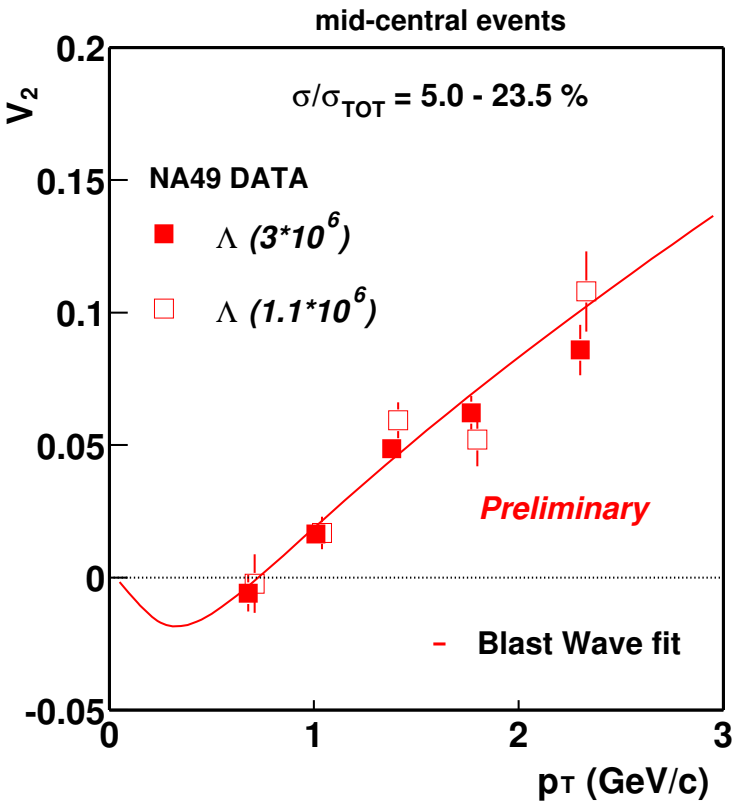

Figure 46: Elliptic flow of Λ hyperons as a function of the transverse momentum in mid-central Pb+Pb collisions at 158A GeV obtained using the full event sample of NA49 ($3 \cdot 10^6$) events and a reduced event sample ($\approx 1 \cdot 10^6$) which yields the same Λ hyperon statistics as expected in the future measurements.

Centrality determination

A crucial experimental goal in the study of multiplicity fluctuations is to understand the influence of fluctuations in the number of interacting nucleons. The NA49 results suggest a large increase of the multiplicity fluctuations with decreasing centrality of Pb+Pb collisions [93]. In Fig. 47 the scaled variance of the multiplicity distribution is plotted as a function of the number of interacting nucleons from the projectile nucleus. The results were corrected as much as possible for the fluctuations in the number of interacting projectile nucleons, which cannot be avoided in the collision centrality selection procedure using the NA49 Veto calorimeter. The following steps were taken to minimize and estimate the corrections [93]. First, the energy of the projectile spectator nucleons was measured for each event by the Veto calorimeter. The scaled variance was then calculated in narrow bins of the measured energy and thus only reduced fluctuations of the number

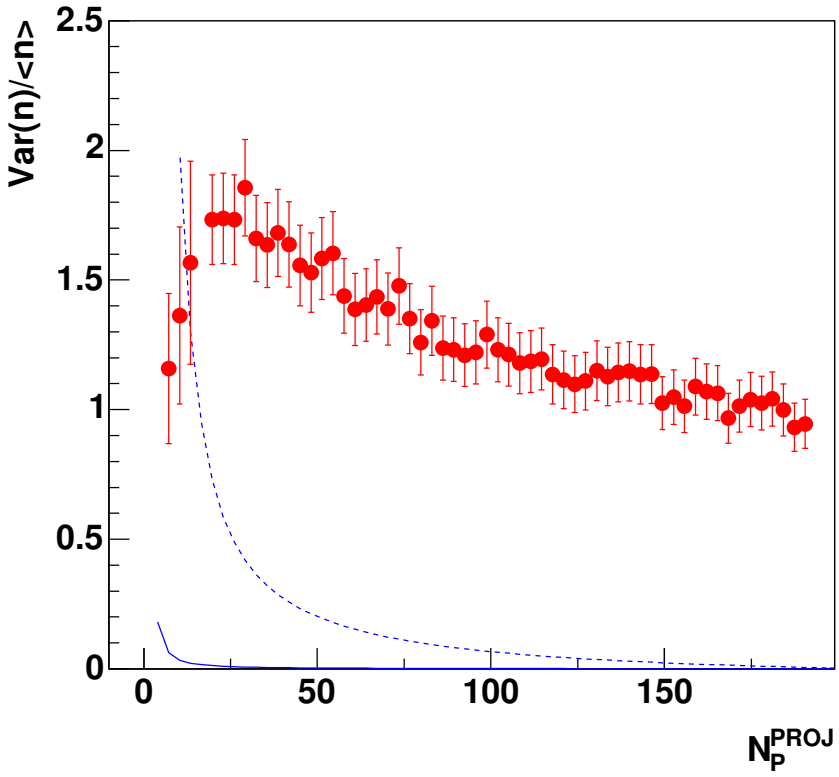

Figure 47: Scaled variance of the multiplicity distribution for negatively charged hadrons as a function of the number of projectile participants for Pb+Pb collisions at 158A GeV. The dashed line shows the correction factor for the resolution of the NA49 Veto calorimeter. This correction is poorly known and and its uncertainty dominates the shown total error of the measurements. The solid line indicates the corresponding correction estimated for the future Projectile Spectator Detector. The PSD detector will allow to establish the behavior of the scaled variance for peripheral collisions where a maximum is suggested by the present data.

of interacting nucleons are present in the event sub-samples selected in this way. Secondly, calibration measurements and simulations were used to determine corrections for the remaining fluctuations of the number of interacting projectile nucleons caused mainly by interactions of the projectile spectator nucleons in the detector material and the resolution of the Veto calorimeter. Unfortunately these two corrections are poorly known

and lead to a large systematic error on the scaled variance for peripheral collisions. The correction factor of the scaled variance is shown in Fig. 47 by a dashed line.

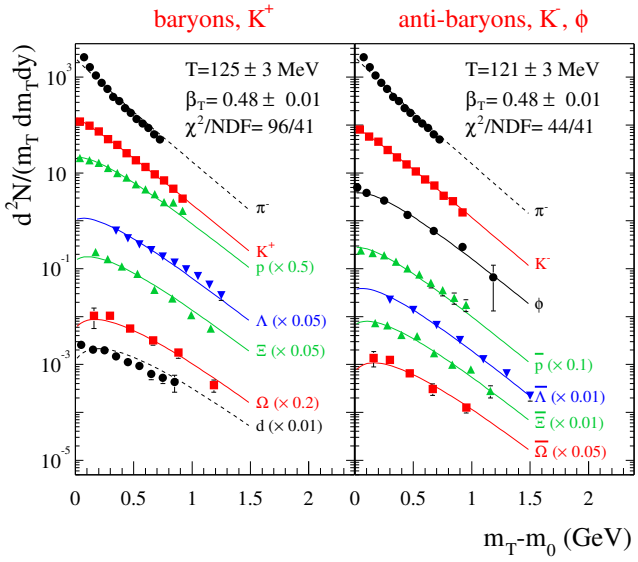

Figure 48: The transverse mass spectra of identified hadrons produced in central Pb+Pb collisions at 158A GeV [103]. Only statistical errors are plotted, the systematic errors are in the range 5-10%.

The large systematic error is caused mainly by an interplay between the strong non-uniformity of the Veto calorimeter response and the poorly known physics of the nuclear fragmentation processes. This error will be significantly (by a factor of about 20) reduced in the future measurements by use of the Projectile Spectator Detector and by a reduction of the material between the target and PSD due to the introduction of the He beam pipe. The correction factor for the scaled variance expected for the future measurements is shown in Fig. 47 by a solid line. In the region of the maximum in multiplicity fluctuations suggested by the NA49 data (see Fig. 47) the correction will be significantly below 10%. The about 10% increase of the scaled variance is predicted in the vicinity of the critical point [74].

Acceptance and resolution

The acceptance and resolution (momentum, dE/dx and TOF measurements) in NA49-future will remain the same as in NA49.

In order to illustrate the quality of the expected new results on inclusive spectra of identified hadrons, the transverse mass and rapidity distributions measured by NA49 in central Pb+Pb collisions at the SPS energies are shown in Figs. 48 and 49.

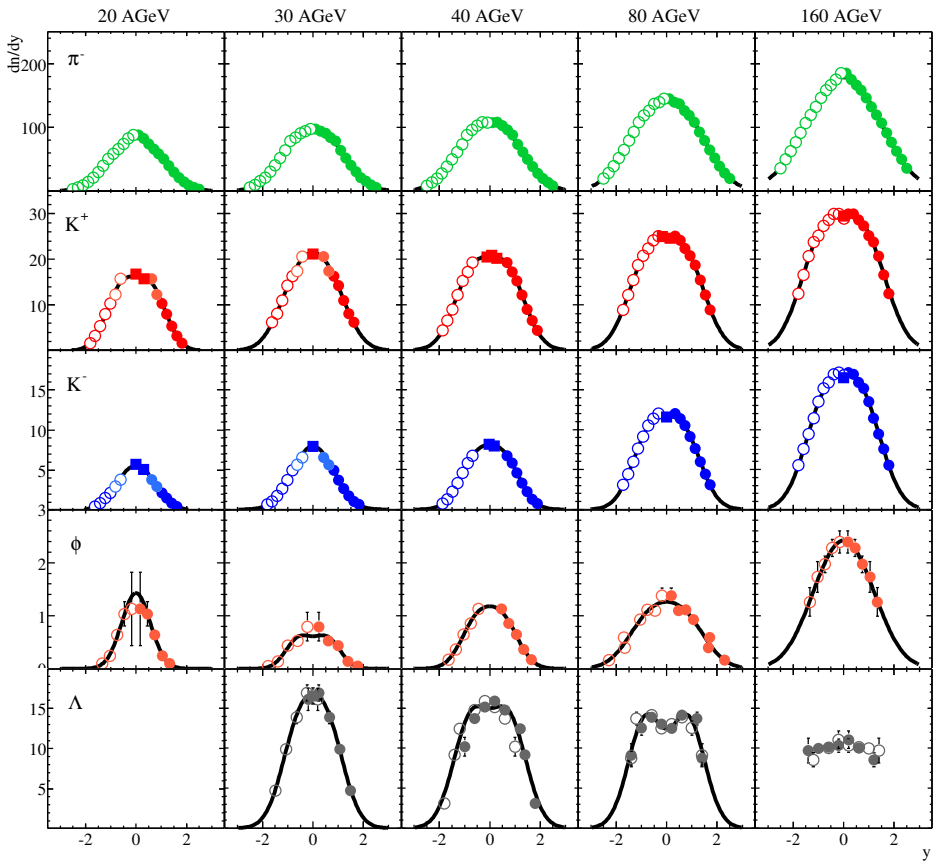

Figure 49: The rapidity spectra of identified hadrons produced in central Pb+Pb collisions at 20A, 30A, 40A, 80A and 158A GeV [103]. Only statistical errors are plotted, the systematic errors are in the range 5-10%.

5 Organization and Planning

This section presents the organization of the project, including the collaboration structure, the sharing of responsibilities, the cost estimate, the schedule of the future activities and the beam time request.

5.1 Structure of the project and responsibilities

An overview of the structure of the NA49-future collaboration and of the interim assignment of responsibilities is presented in Fig. 50. If and when the experiment is approved, a collaboration agreement will be drafted and adopted by the collaboration board and a formal election of the collaboration officers will take place.

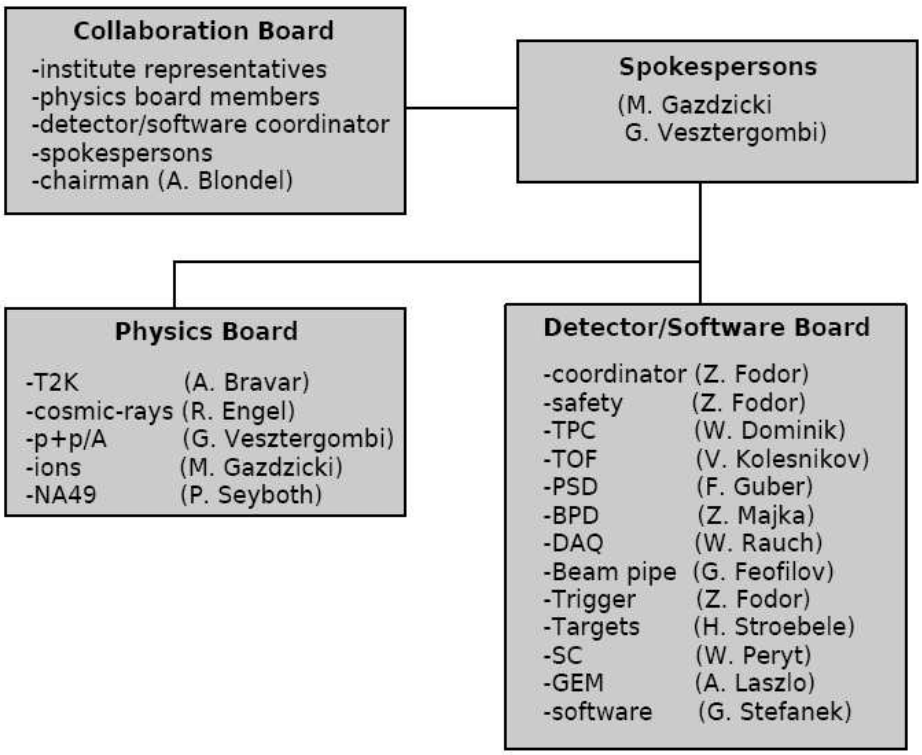

Figure 50: Interim structure of the NA49-future collaboration.

In the following the involvement of the NA49-future groups in the key hardware projects is given:

- maintenance and operation of TPCs and their infrastructure: Universities of Warsaw, Frankfurt and Pusan,
- maintenance and operation of TOFs and their infrastructure: Dubna,
- maintenance, operation and upgrade of Beam Position Detectors: University of Cracow,
- targets: University of Frankfurt,
- TPC DAQ upgrade: Budapest, Swiss groups and Fachhochschule Frankfurt,
- beam pipe construction and installation: St. Petersburg University,
- slow control and monitoring upgrade: Warsaw University of Technology and Zagreb,

- R&D and construction of the Projectile Spectator Detector: INP Moscow and University of Bergen.

The off-line software will be maintained by the groups from Swietokrzyska Academy and Warsaw University of Technology.

All institutes will jointly participate in the data taking activities. The analysis of the data taken for T2K and cosmic-ray experiments will be done by the groups from Swiss groups, Karlsruhe, Paris, Sofia and University of Warsaw. The remaining groups will focus on the analysis of the data taken within p+p/p+A and A+A programs.

5.2 Cost estimate and financial plan

An estimate of the cost of upgrades, maintenance and running for the first 3 years is given below. All numbers are in SFR and the cost does not include the cost of travel and manpower of NA49-future participants. During the last two years of operation no upgrades are foreseen. The cost of running and maintenance will be about 100 kSFR per year.

About 70 % of the expenses forseen for the 2006/2007 period (see Table 5) will be covered by the T2K and cosmic-ray related groups: CERN, Swiss groups, Karlsruhe, Paris, Sofia and Valencia. The remaining groups will cover the rest of the cost. The cost of TPC DAQ upgrade for 2008 will be covered jointly by KFKI Budapest and Geneva University groups. In order to cover costs of the R&D and production of the PSD it is planned to apply for European and national grants in Norway and Poland. The rest of the costs will be covered from the common fund contributions of the collaborating institutes.

5.3 Work schedule

- **2006/2007:** preparation of the detector for the 2007 physics run (p+C at 30 GeV/c), production of one PSD super-module and the prototype of the new DAQ,
- **2007 run:** data on p+C at 30 GeV/c for T2K, test data on p+p interactions at 30 GeV/c, test of the PSD super-module, test of the new DAQ,
- **2007/2008:** production and installation of the new DAQ electronics, production of PSD modules,
- **2008 run:** high statistics run for T2K and cosmic-ray experiments,
- **2008/2009:** production and installation of the PSD and the He beam pipe,
- **2009 ion run:** data on In+In collisions at $10A$, $20A$, $30A$, $40A$, $80A$ and $158A$ GeV,
- **2009 proton run:** data on p+p interactions at $10A$, $20A$, $30A$, $40A$, $80A$ and $158A$ GeV,

Item	Cost (kSFR)
2006/2007	
pool electronics	70
TPC maintenance and gas	30
upgrade of the cooling system	20
upgrade of the TOF read-out	30
slow control and monitoring	33
DAQ+CDR upgrade	5
BPDs	10
PSD super-module	70
Safety	10
technician (500h)	30
total	308
2007/2008	
TPC DAQ upgrade	440
TPC gas	30
PSD production	350
technician (500h)	30
total	850
2008/2009	
TPC gas	30
PSD production	350
He beam pipe	30
technician (500h)	30
total	440

Table 5: Estimate of the cost of upgrades, maintenance and running for the first 3 years of the NA49-future operation.

- **2010 ion run:** data on Si+Si collisions at 10A, 20A, 30A, 40A, 80A and 158A GeV,
- **2010 proton run:** high statistics data on p+p interactions at 158A GeV,
- **2011 ion run:** data on C+C collisions at 10A, 20A, 30A, 40A, 80A and 158A GeV,
- **2011 proton run:** data on p+Pb interactions at 10A, 20A, 30A, 40A, 80A and 158A GeV.

5.4 Beam requirements and expected event numbers

The beam requirements and the expected event numbers needed to reach the physics goals of the program presented in this document are summarized below:

- 2007: 30 days of proton beam at 30 GeV/c;
  $3 \cdot 10^6$ p+C events,
- 2008: 45 days of proton and pion beams at 30-400 GeV/c;
  $75 \cdot 10^6$ p+p, p+C and π+C events,
- 2009: 30 days of indium beam at 10A, 20A, 30A, 40A 80A, 158A GeV;
  $6 \cdot 10^6$ In+In events at each energy,
- 2009: 30 days of proton beam at 10A, 20A, 30A, 40A 80A, 158A GeV;
  $6 \cdot 10^6$ p+p events at each energy,
- 2010: 30 days of silicon beam at 10A, 20A, 30A, 40A 80A, 158A GeV;
  $6 \cdot 10^6$ Si+Si events at each energy,
- 2010: 30 days of proton beam at 158A GeV;
  $60 \cdot 10^6$ p+p events at 158A GeV,
- 2011: 30 days of carbon beam at 10A, 20A, 30A, 40A 80A, 158A GeV;
  $6 \cdot 10^6$ C+C events at each energy.
- 2011: 30 days of proton beam at 10A, 20A, 30A, 40A 80A, 158A GeV;
  $6 \cdot 10^6$ p+Pb events at each energy.

6 Appendix: Supporting documents

6.1 Frank Wilczek

From wilczek@MIT.EDU Thu Oct 19 18:10:30 2006
Date: Thu, 19 Oct 2006 11:45:48 -0400
From: Frank Wilczek <wilczek@MIT.EDU>
To: j.b.dainton@dl.ac.uk
Subject: NA49 scan for critical point

Dear John,

In considering the NA49 proposal to do a systematic scan to find the QCD critical point, I think it is appropriate to emphasize that the existence of this critical point is a major prediction of QCD, and that learning its location will give us very valuable guidance in formulating the phase diagram. Besides its intrinsic interest, the result would stimulate research both in lattice gauge theory and in neutron star astrophysics. I realize there are many important, sometimes conflicting priorities for using the valuable resources at CERN, of course, so it's important that the motivations for each proposal are clear and significant -- all I want to do here is to emphasize that the NA49 proposal meets high standards by those measures.

All best wishes,
Frank W.
--
Frank Wilczek
Herman Feshbach Professor of Physics
ADDRESS for U.S. POST:
Massachusetts Institute of Technology
Building NE25 4-039
5 Cambridge Center
Cambridge, MA 02139

6.2 International Board of Representatives of T2K

Statement from T2K
International Board of Representatives (IBR)

The T2K collaboration would like to stress the importance of the measurement of particle production from 30-50 GeV protons on carbon, as the available data are not of sufficient precision.
We support the NA49/T2K proposal very strongly.

Work on NA49/T2K which leads to successful data-taking and analysis needed to produce hadron production data for the T2K flux calculation, would be considered a sufficient contribution to the T2K experiment to qualify as a T2K collaborator. Members of NA49 who would thus contribute will be encouraged to apply to become members of T2K.

By following the same obligations, such as participation to data taking, common fund contribution, attending collaboration meetings, etc. they will have the same rights as all T2K members.

6.3 Pierre Auger Observatory and KASCADE spokespersons

To: **Professor John B. Dainton (j.b.dainton@dl.ac.uk)**
Chairman of SPS and PS Experiments Committee
Cockcroft Institute, Daresbury Laboratory
University of Liverpool
Warrington, WA4 4AD (GB)

26 April 2006

Dear Professor Dainton,

Recently a fixed target experiment has been proposed for the CERN SPS. This would make use of the existing NA49 detector set-up to measure proton and pion interactions with carbon nuclei (see CERN-SPSC-2003-038), in addition to other reactions. Through this letter we would like to express the great interest of the Pierre Auger Collaboration in the measurement of secondary pion and kaon spectra with these projectile/target combinations.

The investigation of flux and composition of ultra-high energy cosmic rays (above ~ 10^{19} eV) can only be carried out by studying the extensive air showers initiated by these particles in the atmosphere. Due to the indirect character of the measurement, the interpretation of the data in terms of the cosmic ray mass composition relies strongly upon realistic simulations of air showers. Pions are the most frequent created secondary hadrons created in air showers and also are the major source of the muon component of showers. Many observables that are sensitive to the mass composition are directly or indirectly related to the number of muons produced in air showers. Consequently, it is expected that the uncertainty in the simulation of hadronic interactions will become one of the dominating sources of systematic uncertainties in cosmic ray mass composition measurements.

Simulation studies show that pion interactions with light nuclear targets in the energy range between 50 and 200 GeV are of particular importance (see, for example, astro-ph/0512536). As almost no data on pion interactions with light nuclei exist, any minimum-bias measurement would be extremely important for tuning hadronic interaction models and, in turn, reducing systematic uncertainties of the interpretation of air shower data.

We very much hope that NA49 extension experiment will be carried out.

Yours sincerely,

Giorgio Matthiae and Alan Watson

Spokespersons for the Pierre Auger Observatory

KASCADE-Grande Experiment

http://www-ik.fzk.de/KASCADE/

Dr. Andreas Haungs
Spokesperson

John B. Dainton
Chairman of SPS and PS Experiments Committee

Cockcroft Institute, Daresbury Laboratory
University of Liverpool
Warrington, WA4 4AD
UK

Dr. Andreas Haungs
Forschungszentrum Karlsruhe
Institut für Kernphysik
Postfach 3640
D-76021 Karlsruhe

Telefon: 07247-82-3310
Telefax: 07247-82-3321
E-Mail: haungs@ik.fzk.de
Date: **27.04.2006**

LoI: Study of Hadron Production in Collisions of Proton and Nuclei at the CERN SPS

Dear John B. Dainton,

A newly formed collaboration has recently stated its interest to use the CERN NA49 apparatus for measurements at the SPS by a detailed LoI to the Experiments Committee. I am writing to you to support this plan from the perspective of cosmic ray research, in particular for the KASCADE-Grande experiment in Karlsruhe.

The analysis and interpretation of cosmic ray air shower data makes heavy use of simulations. Here, the program package CORSIKA has become the standard tool worldwide and is used by more than 40 groups. The Karlsruhe team (KASCADE-Grande and Pierre-Auger Observatory groups) is constantly developing and optimizing the physics as well as programming techniques in CORSIKA. We have realized that measurements of particle production in the very forward region, in particular also in the lower energy range are needed for further improve of the hadronic interaction models embedded in CORSIKA. An international workshop series is meanwhile established to foster a closer cooperation between cosmic ray and particle accelerator experiments (see e.g. CERN COURIER 46/3 for a résumé).

We, the KASCADE-Grande collaboration, wish to express the strong interest in the continuation of the measurements with the NA49 apparatus at the CERN SPS. A modest investment will yield a significant return.

Sincerely yours,

Andreas Haungs, KASCADE-Grande spokesperson

References

[1] J. Bartke *et al.* [NA49-future Collaboration], *A new experimental programme with nuclei and proton beams at the CERN SPS*, CERN-SPSC-2003-038(SPSC-EOI-01) and presentations at the Villars workshop 2004.

[2] N. Antoniou *et al.* [NA49-future Collaboration], *Study of hadron production in collisions of protons and nuclei at the CERN SPS*, CERN-SPSC-2006-001, CERN-SPSC-I-235.

[3] S. Afanasev *et al.* [NA49 Collaboration], Nucl. Instrum. Meth. A **430**, 210 (1999).

[4] C. Alt *et al.* [NA49 Collaboration], Phys. Rev. Lett. **94**, 052301 (2005) [arXiv:nucl-ex/0406031] and P. Dinkelaker [NA49 Collaboration], J. Phys. G **31**, S1131 (2005).

[5] C. Alt *et al.* [NA49 Collaboration], Eur. Phys. J. C **45**, 343 (2006) [arXiv:hep-ex/0510009].

[6] S. V. Afanasiev *et al.* [The NA49 Collaboration], Phys. Rev. C **66**, 054902 (2002) [arXiv:nucl-ex/0205002].

[7] M. Gazdzicki *et al.* [NA49 Collaboration], J. Phys. G **30**, S701 (2004) [arXiv:nucl-ex/0403023].

[8] M. Gazdzicki and M. I. Gorenstein, Acta Phys. Polon. B **30**, 2705 (1999) [arXiv:hep-ph/9803462].

[9] G. S. F. Stephans, *critRHIC: The RHIC low energy program*, arXiv:nucl-ex/0607030.

[10] J. Dainton et al., [The CERN SPS and PS Committee], CERN–SPSC–2005–010, SPSC–M–730 (2005).

[11] T. Akesson *et al.*, "Towards the European strategy for particle physics: The briefing book," arXiv:hep-ph/0609216.

[12] N. Antoniou *et al.* [NA49-future Collaboration], *Report from tests of the NA49 experimental facility and the NA49-future detector prototypes*, CERN-SPSC-2006-023, CERN-SPSC-SR-010.

[13] M. C. Gonzalez-Garcia and Y. Nir, Rev. Mod. Phys. **75**, 345 (2003) [arXiv:hep-ph/0202058].

[14] Y. Itow *et al.*, KEK report 2001-4.

[15] D. Ayres *et al.*, FNAL-P-929 (2002).

[16] P. Zucchelli, Phys. Lett. B **532**, 166 (2002).

[17] T2K ND280 Conceptual Design Report.

[18] M.G. Catanesi *et al.*, [The HARP Collaboration], *Measurement of the production cross-section of positive pions in p–Al collisions at 12.9 GeV/c*, Nucl. Phys. B **732**, 1 (2006).

[19] J. R. Sanford and C. L. Wang, Brookhaven National Laboratory, AGS internal report, 1967 (unpublished); C. L. Wang, Phys. Rev. Lett. **25**, 1068 (1970); ibid. **25**, 1536(E) (1970).

[20] M.H. Ahn *et al.* [The K2K Collaboration], Phys. Rev. Lett. **90**, 041801 (2003);
M.H. Ahn *et al.* [The K2K Collaboration], Phys. Lett. B**511**, 178 (2001).

[21] E. Aliu *et al.* [The K2K Collaboration], Phys. Rev. Lett. **94**, 081802 (2005).

[22] M. H. Ahn *et al.* [The K2K Collaboration], Phys. Rev. D **74**, 072003 (2006) [arXiv:hep-ex/0606032].

[23] Y. Sugaya *et al.*, Nucl. Phys. A **634**, 115 (1998).

[24] I. A. Vorontsov *et al.*, ITEP-11-1988.

[25] I. A. Vorontsov *et al.*, ITEP-85-1983.

[26] T. Abbott *et al.* [The E-802 Collaboration], Phys. Rev. D **45**, 3906 (1992).

[27] Y. Cho *et al.*, Phys. Rev. D **4**, 1967 (1971).

[28] A. Haungs, H. Rebel, and M. Roth, Rept. Prog. Phys. **66**, 1145 (2003).

[29] M. Nagano and A.A. Watson, Rev. Mod. Phys. **72**, 689, 2000; R. Engel and H. Klages, Comptes Rendus Physique **5**, 505 (2004).

[30] A. Bhattacharjee and G. Sigl, Phys. Rep. **327**, 109 (2000).

[31] J. Knapp *et al.*, Astropart. Phys. **19**, 77 (2003); R. Engel, Nucl. Phys. B (Proc. Suppl.) **122**, 40 (2003).

[32] T. Antoni *et al.* (The KASCADE Collaboration),
Nucl. Instrum. Meth. A **513**, 490 (2003).

[33] J. Abraham *et al.* (The Pierre Auger Collaboration), Nucl. Instrum. Meth. A **523**, 50 (2004).

[34] T. Antoni *et al.* [The KASCADE Collaboration]), Astropart. Phys. **24**, 1 (2005) and astro-ph/0505413.

[35] A. Fasso *et al.*, Proceedings of the Workshop on Simulating Accelerator Radiation Environments, Los Alamos, p. 134, 1992.

[36] M. Bleicher *et al.*, J. Phys. G: Nucl. Part. Phys. **25**, 1859 (1999).

[37] H. Fesefeldt, preprint PITHA-85/02, RWTH Aachen, 1985.

[38] N. N. Kalmykov, S. Ostapchenko, and A. I. Pavlov, Nucl. Phys. B (Proc. Suppl.) **52**, 17 (1997).

[39] H.-J. Drescher, M. Bleicher, S. Soff, and H. Stoecker, Astropart. Phys. **21**, 87 (2004) [arXiv:astro-ph/0307453].

[40] P. Sommers (Pierre Auger Collab.), astro-ph/0507150 to appear in Proc. of 29th ICRC, Pune, India, 3-11 Aug 2005.

[41] J. Knapp, D. Heck, and G. Schatz, in report FZKA 5828, Forschungszentrum Karlsruhe, 1996.

[42] R. Engel, T. K. Gaisser, and T. Stanev, Proc of 29th International Symposium on Multiparticle Dynamics (ISMD 99), Providence, Rhode Island, 8-13 Aug 1999.

[43] H.-J. Drescher and G. R. Farrar, Astropart. Phys. **19**, 235 (2003) [arXiv:hep-ph/0206112].

[44] C. Meurer, J. Blumer, R. Engel, A. Haungs, and M. Roth, arXiv:astro-ph/0512536, Czech. J. Phys. 56 (2006) **A211**, Proc. of Int. Conference "From Colliders to Cosmic Rays" (C2CR 2005), Prague, Czech Rep., 7-13 Sep 2005.

[45] T. Eichten et al., Nucl. Phys. B **44**, 333 (1972); W.F. Baker et al., Phys. Rev. Lett. **7**, 101 (1961); D. Dekkers et al., Phys. Rev. B **137**, 962 (1965); R.A. Lundy et al., Phys. Rev. Lett. **14**, 504 (1965); J.V. Allaby et al., CERN Yellow Report 70-12 (1970); Y. Cho et al., Phys. Rev. D **4**, 1967 (1971); D. Antreasyan et al., Phys. Rev. D **19**, 764 (1979); D.S. Barton et al., Phys. Rev. D **27**, 2580 (1983); T. Abbott et al., Phys. Rev. D **45**, 3906 (1992).

[46] C. Meurer et al. and HARP Collab., to appear in Proc. of XIV ISVHECRI, Weihei, China, 15-22 Aug 2006.

[47] C. Alt et al. [NA49 Collaboration], *Inclusive production of charged pions in p + C collisions at 158-GeV/c beam momentum*, arXiv:hep-ex/0606028.

[48] S. Ostapchenko, Phys. Lett. B636, 40 (2006); Phys. Rev. **D74**, 014026 (2006)

[49] R.S. Fletcher et al., Phys. Rev. **D50**, 5710 (1994); R. Engel et al., in Proc. 26-th Int. Cosmic Ray Conf., Salt Lake City, 1999.

[50] C. Alt *et al.* [NA49 Collaboration], Nucl. Phys. A **774**, 473 (2006) [arXiv:nucl-ex/0510054].

[51] D. d'Enterria, Phys. Lett. B **596**, 32 (2004) [arXiv:nucl-ex/0403055].

[52] E. W. Beier *et al.*, Phys. Rev. D**18**, 2235 (1978).

[53] S. R. Blattnig *et al.*, Phys. Rev. D**62**, 094030 (2000).

[54] U. W. Heinz and M. Jacob, arXiv:nucl-th/0002042, J. Rafelski and B. Muller, Phys. Rev. Lett. **48**, 1066 (1982) [Erratum-ibid. **56**, 2334 (1986)], T. Matsui and H. Satz, Phys. Lett. B **178**, 416 (1986), F. Becattini, L. Maiani, F. Piccinini, A. D. Polosa and V. Riquer, Phys. Lett. B **632**, 233 (2006) [arXiv:hep-ph/0508188].

[55] I. Arsene *et al.* [The BRAHMS Collaboration], Nucl. Phys. A **757**, 1 (2005) [arXiv:nucl-ex/0410020], B. B. Back *et al.* [The PHOBOS Collaboration], Nucl. Phys. A **757**, 28 (2005) [arXiv:nucl-ex/0410022], J. Adams *et al.* [The STAR Collaboration], Nucl. Phys. A **757**, 102 (2005) [arXiv:nucl-ex/0501009], K. Adcox *et al.* [The PHENIX Collaboration], Nucl. Phys. A **757**, 184 (2005) [arXiv:nucl-ex/0410003],

[56] J. Cleymans and K. Redlich, Phys. Rev. C **60**, 054908 (1999) [arXiv:nucl-th/9903063].

[57] H. Sorge, H. Stocker and W. Greiner, Nucl. Phys. A **498** (1989) 567C.

[58] S. A. Bass *et al.*, Prog. Part. Nucl. Phys. **41**, 225 (1998) [arXiv:nucl-th/9803035],

[59] W. Cassing, E. L. Bratkovskaya and S. Juchem, Nucl. Phys. A **674**, 249 (2000) [arXiv:nucl-th/0001024].

[60] M. I. Gorenstein, M. Gazdzicki and K. A. Bugaev, Phys. Lett. B **567**, 175 (2003) [arXiv:hep-ph/0303041].

[61] M. Gazdzicki, M. I. Gorenstein, F. Grassi, Y. Hama, T. Kodama and O. J. Socolowski, Braz. J. Phys. **34**, 322 (2004) [arXiv:hep-ph/0309192].

[62] H. G. Fischer, slides from the open 74th Meeting of the SPSC, November 15, 2005, http://indico.cern.ch/conferenceDisplay.py?confId=a057199.

[63] B. A. Cole *et al.*, Phys. Lett. B **639**, 210 (2006) [arXiv:nucl-ex/0503009].

[64] A. Bialas and W. Czyz, Acta Phys. Polon. B **36**, 905 (2005) [arXiv:hep-ph/0410265].

[65] M. Gazdzicki and M. Gorenstein, "Transparency, mixing and reflection of initial flows in relativistic Phys. Lett. B **640**, 155 (2006) [arXiv:hep-ph/0511058].

[66] H. Bialkowska, M. Gazdzicki, W. Retyk and E. Skrzypczak, Z. Phys. C **55**, 491 (1992).

[67] Y. Hama, F. Grassi, O. Socolowski, T. Kodama, M. Gazdzicki and M. Gorenstein, Acta Phys. Polon. B **35**, 179 (2004).

[68] E. L. Bratkovskaya *et al.*, Phys. Rev. C **69**, 054907 (2004) [arXiv:nucl-th/0402026], J. Cleymans and K. Redlich, Phys. Rev. C **60**, 054908 (1999) [arXiv:nucl-th/9903063].

[69] M. Gazdzicki, M. I. Gorenstein and S. Mrowczynski, Phys. Lett. B **585**, 115 (2004) [arXiv:hep-ph/0304052] and M. I. Gorenstein, M. Gazdzicki and O. S. Zozulya, Phys. Lett. B **585**, 237 (2004) [arXiv:hep-ph/0309142].

[70] J.-Y. Ollitrault, Phys. Rev. D **46**, 229 (1992), P. F. Kolb, J. Sollfrank and U. W. Heinz, Phys. Rev. C **62**, 054909 (2000) [arXiv:hep-ph/0006129].

[71] J. Cleymans and K. Redlich, Nucl. Phys. A **661**, 379 (1999) [arXiv:nucl-th/9906065].

[72] P. Braun-Munzinger, K. Redlich and J. Stachel, arXiv:nucl-th/0304013.

[73] F. Becattini and U. W. Heinz, Z. Phys. C **76**, 269 (1997) [Erratum-ibid. C **76**, 578 (1997)] [arXiv:hep-ph/9702274] and F. Becattini, M. Gazdzicki and J. Sollfrank, Eur. Phys. J. C **5**, 143 (1998) [arXiv:hep-ph/9710529].

[74] M. A. Stephanov, K. Rajagopal and E. V. Shuryak, Phys. Rev. D **60**, 114028 (1999) [arXiv:hep-ph/9903292].

[75] K. Rajagopal and F. Wilczek, arXiv:hep-ph/0011333.

[76] M. A. Stephanov, Prog. Theor. Phys. Suppl. **153**, 139 (2004) [Int. J. Mod. Phys. A **20**, 4387 (2005)] [arXiv:hep-ph/0402115].

[77] F. Karsch, J. Phys. G **31**, S633 (2005) [arXiv:hep-lat/0412038].

[78] S. D. Katz, Nucl. Phys. A **774**, 159 (2006) [arXiv:hep-ph/0511166].

[79] F. Becattini, J. Manninen and M. Gazdzicki, Phys. Rev. C **73**, 044905 (2006) [arXiv:hep-ph/0511092].

[80] M. I. Gorenstein, M. Gazdzicki and W. Greiner, Phys. Rev. C **72**, 024909 (2005) [arXiv:nucl-th/0505050].

[81] N. G. Antoniou, Y. F. Contoyiannis, F. K. Diakonos, A. I. Karanikas, C. N. Ktorides, Nucl. Phys. A **693**, 799 (2001), N. G. Antoniou, F. K. Diakonos, G. Mavromanolakis, Nucl. Phys. A **761**, 149 (2005)

[82] Y. Hatta and T. Ikeda, Phys. Rev. D **67**, 014028 (2003) [arXiv:hep-ph/0210284].

[83] Z. Fodor and S. D. Katz, JHEP **0404**, 050 (2004) [arXiv:hep-lat/0402006].

[84] C. R. Allton *et al.*, Phys. Rev. D **71**, 054508 (2005) [arXiv:hep-lat/0501030].

[85] T. Anticic *et al.* [The NA49 Collaboration], Phys. Rev. C **70**, 034902 (2004) [arXiv:hep-ex/0311009].

[86] D. Adamova *et al.* [CERES Collaboration], Nucl. Phys. A **727**, 97 (2003) [arXiv:nucl-ex/0305002].

[87] M. A. Stephanov, Phys. Rev. D **65**, 096008 (2002) [arXiv:hep-ph/0110077].

[88] V. P. Konchakovski, S. Haussler, M. I. Gorenstein, E. L. Bratkovskaya, M. Bleicher and H. Stoecker, Phys. Rev. C **73**, 034902 (2006) [arXiv:nucl-th/0511083].

[89] M. Gazdzicki and M. Gorenstein, Phys. Lett. B **640**, 155 (2006) [arXiv:hep-ph/0511058].

[90] E. Shuryak, arXiv:hep-ph/0504048.

[91] E. L. Bratkovskaya *et al.*, arXiv:nucl-th/0401031.

[92] C. Alt *et al.* [The NA49 Collaboration], Phys. Rev. C **68**, 034903 (2003) [arXiv:nucl-ex/0303001].

[93] M. Rybczynski *et al.* [The NA49 Collaboration], J. Phys. Conf. Ser. **5**, 74 (2005) [arXiv:nucl-ex/0409009].

[94] C. Roland *et al.* [The NA49 Collaboration], J. Phys. G **30**, S1381 (2004) [arXiv:nucl-ex/0403035].

[95] W. Rauch *et al.* [The NA49 Collaboration], *The NA49 Data Acquistion System*, IEEE Trans. Nucl. Sci., Vol. 41, No. 1, 1994.

[96] G. Pala *et al.*, Nucl. Instrum. Meth. **A451**, 416 (2000).

[97] ALICE Collaboration, *Trigger, Data Acquisition, High Level Trigger and Control System Technical Design Report*, CERN/LHCC-2003-062, ALICE TDR 010, January 2004

[98] R. Wigmans, Nucl. Instrum. Meth. **A259**, 389 (1987).

[99] G. A. Alekseev, *et al.*, Nucl. Instrum. Meth. **A461**, 381 (2001).

[100] Y. Fujii, Nucl. Instrum. Meth. **A453**, 237 (2000).

[101] I. Britvitch, *et al.*, Nucl. Instrum. Meth. **A535**, 523 (2004).

[102] A. Akindinov, *et al.*, Nucl. Instrum. Meth. **A539**, 172 (2005).

[103] S. V. Afanasiev *et al.*, Nucl. Phys. A **715**, 161 (2003) [arXiv:nucl-ex/0208014].